STRUCTURE-PROPERTY RELATIONSHIP OF HYDROGEL:

MOLECULAR DYNAMICS SIMULATION APPROACH

A Dissertation
Presented to
The Academic Faculty

by

Seung Geol Lee

In Partial Fulfillment
of the Requirements for the Degree
DOCTOR OF PHILOSOPHY in the
School of MATERIALS SCIENCE AND ENGINEERING
COLLEGE OF ENGINEERING

Georgia Institute of Technology
AUGUST 2011

STRUCTURE-PROPERTY RELATIONSHIP OF HYDROGEL:

MOLECULAR DYNAMICS SIMULATION APPROACH

Approved by:

Dr. Jang, Seung Soon, Advisor
School of Materials Science and Engineering
Georgia Institute of Technology

Dr. Bucknall, David G., Co-Advisor
School of Materials Science and Engineering
Georgia Institute of Technology

Dr. Brédas, Jean-Luc
School of Chemistry and Biochemistry
Georgia Institute of Technology

Dr. Tsukruk, Vladimir V.
School of Materials Science and Engineering
Georgia Institute of Technology

Dr. Thio, Yonathan S.
School of Materials Science and Engineering
Georgia Institute of Technology

Date Approved: June 06, 2011

ACKNOWLEDGEMENTS

The author would like to thank Dr. Seung Soon Jang, Chairman of his advisory committee, for his advice, support, and guidance throughout this study. It was his confidence in the author and continuous encouragement that made this work possible. Dr. David Bucknall, Co-Chairman of his advisory committee, contributed much to the author's understanding of the hydrogel system as a biomedical material. Appreciation is also extended to Dr. Jean-Luc Brédas, Dr. Vladimir Tsukruk, and Dr. Yonathan Thio, members of the advisory committee, for their valuable advice, suggestions, and encouragement.

The author would also like to thank Dr. Ji Il Choi for his valuable comments and management of the computational resources, Wonsang Koh and Giuseppe Brunello for their help with the analysis of the data and the discussion of the results, Dr. Hannah Lee for her valuable comments on the VP-*co*-HEMA hydrogel system, and Grace Kim and Ngoc Nhi Le for their help with data analysis. The author also appreciates working with Dr. Jong-Beom Baek, Dr. Mahan Srinivasarao, Dr. Satish Kumar, Dr. Han Gi Chae, Dr. Cantwell Carson, Dr. Soonchul Kwon, Dr. Joonseok Koh, and Hyerim Kim during his Ph.D. The author is also grateful to all MSE people, especially to my classmates Minsang Park, Il Tae Kim, Jung Hwa Park, Wei Lin, and Michelle Schlea for their encouragement. The author would also like to thank the School of Materials Science and Engineering, the Georgia Institute of Technology, the IPST (Institute of Paper Science and Technology), and the ACS (American Chemical Society) for providing financial support for this project.

Finally, thanks to all members of my family, especially my parents, my wife Jung Hyun and my daughter Jaeyoung, for their continued love, support and encouragement throughout this study.

TABLE OF CONTENTS

LIST OF TABLES

Page

LIST OF FIGURES

Page

LIST OF SYMBOLS AND ABBREVIATIONS

QM	Quantum Mechanics
MM	Molecular Mechanics
MD	Molecular Dynamics
FEM	Finite Element Method
DP	Degree of Polymerization
P(VP-*co*-HEMA)	poly(N-vinyl-2-pyrrolidone-*co*-2-hydroxyethyl methacrylate)
P(NIPAAm)	poly(N-isopropylacrylamide)
NVE	microcanonical
NVT	canonical
NPT	isothermal-isobaric
VP	N-vinyl-2-pyrrolidone
HEMA	2-hydroxyethyl methacrylate
PVP	poly(N-vinyl-2-pyrrolidone)
PHEMA	poly(2-hydroxyethyl methacrylate)
DR	Degree of Randomness
MBA	N,N´-methylenebisacrylamide
LAMMPS	Large-scale Atomic/Molecular Massively Parallel Simulator
PCF	Pair Correlation Function
CN	Coordination Number
SASA	Solvent Accessible Surface Area
LCST	Lower Critical Solution Temperature
MSD	Mean Square Displacement

DLS	Dynamic Light Scattering
SPR	Surface Plasmon Resonance spectroscopy
NR	Neutron Reflectivity
QCM	Quartz Crystal Microbalance measurement
AFM	Atomic Force Microscope
NMR	Nuclear Magnetic Resonance
ATRP	Atom Transfer Radical Polymerization
RAFT	Reversible Addition-Fragmentation chain Transfer
P(AAm)	poly(acrylamide)
UCST	Upper Critical Solution Temperature

SUMMARY

We have used a molecular modeling of both random and blocky sequence hydrogel networks of poly(N-vinyl-2-pyrrolidone-*co*-2-hydroxyethyl methacrylate) (P(VP-*co*-HEMA)) with a composition of VP:HEMA = 37:13 to investigate the effect of the monomeric sequence and the water content on the equilibrium structures and the mechanical and transport properties by full-atomistic molecular dynamics (MD) simulations. The degree of randomness of the monomer sequence for the random and the blocky copolymers, were 1.170 and 0.104, respectively, and the degree of polymerization was fixed at 50. The equilibrated density of the hydrogel was found to be larger for the random sequence than for the blocky sequence at low water contents (< 40 wt %), but this density difference decreased with increasing water content. The pair correlation function analysis shows that VP is more hydrophilic than HEMA and that the random sequence hydrogel is solvated more than the blocky sequence hydrogel at low water content, which disappears with increasing water content. Correspondingly, the water structure is more disrupted by the random sequence hydrogel at low water content but eventually develops the expected bulk-water-like structure with increasing water content. From mechanical deformation simulations, the stress-strain analysis showed that the VP is found to relax more efficiently, especially in the blocky sequence, so that the blocky sequence hydrogel shows less stress levels compared to the random sequence hydrogel. As the water content increases, the stress level becomes identical for both sequences. The elastic moduli of the hydrogels calculated from the constant strain energy minimization show the same trend with the stress-strain analysis. Ascorbic acid and D-glucose were used to study the effect of the monomeric sequence on the diffusion of small guest molecules within the hydrogels. By analyzing the pair correlation functions,

it was found that the guest molecule has greater accessibility to the VP units than to the HEMA units with both monomeric sequences due to its higher hydrophilicity compared to the HEMA units. The monomeric sequence effect on the P(VP-*co*-HEMA) hydrogel is clearly observed with 20 wt % water content, but the monomeric sequence effect is significantly reduced with 40 wt % water content and disappears with 80 wt % water content. This is because the hydrophilic guest molecules are more likely to be associated with water molecules than with the polymer network at the high water content. By analyzing the mean square displacement, the displacement of the guest molecules and the inner surface area, it is also found that the guest molecule is confined in the system at 20 wt % water content, resulting in highly anomalous subdiffusion. Therefore, the diffusion of the guest molecules is directly affected by their interaction with the monomer units, the monomeric sequence and the geometrical confinement in the hydrogel at a low water content, but the monomeric sequence effect and the restriction on the diffusion of the guest molecule are significantly decreased with increasing the water content.

We also investigated the de-swelling mechanisms of the surface-grafted poly(N-isopropylacrylamide) (P(NIPAAm)) brushes containing 1300 water molecules at 275 K, 290 K, 320 K, 345 K, and 370 K. We clearly observed the de-swelling of the water molecules for P(NIPAAm) above the lower critical solution temperature (LCST) (~305 K). Below the LCST, we did not observe the de-swelling of water molecules. Using the upper critical solution temperature (UCST) systems (poly(acrylamide) brushes) for comparison purposes, we did not observe the de-swelling of water molecules at a given range of temperatures. By analyzing the pair correlation functions and the coordination numbers, the de-swelling of the water molecules occurred distinctly around the isopropyl group of the P(NIPAAm) brush above the LCST because $C_{(NIPAAm)}$ does not offer sufficient interaction with the water molecules via the hydrogen bonding type of secondary interaction. We also found that the contribution of the $N_{(NIPAAm)}$-$O_{(water)}$ pair is quite small because of the steric hindrance of the isopropyl group. By analyzing the

change in the hydrogen bonds, the hydrogen bonds between polar groups and water molecules in the P(NIPAAm) brushes weaken with increasing temperature, which leads to the de-swelling of the water molecules out of the brushes above the LCST. Below the LCST, the change in the hydrogen bonds is not significant. Again, the contribution of the NH(NIPAAm)-water pairs is insignificant; the total number of hydrogen bonds is ~20, indicating that the interaction between the NH group and the water molecules is not significant due to steric hindrances. Lastly, we observed that the total surface area of the P(NIPAAm) brushes that is accessible to water molecules is decreased by collapsing the brushes followed by the de-swelling of water molecules above the LCST.

CHAPTER 1: INTRODUCTION

Hydrogel

By definition, a hydrogel is a three-dimensionally cross-linked polymeric network that is capable of absorbing and retaining huge amounts of water or biological fluids [1]. Since Wichterle and Lim [2] introduced the hydrophilic gels for biological use in the early 1960s, significant efforts have been devoted to use the hydrogels in the biomedical and pharmaceutical applications [3-10] , especially for drug delivery and tissue engineering applications due to an excellent biocompatibility and smart stimulus-response properties. Indeed, in order to comply with rapidly increasing demands in medical treatment and health care, a large variety of hydrogels have been made and tested so far on the basis of recent progresses in organic synthesis techniques that can realize exactly-tailored molecular architectures according to the suggested design [4, 11]. Although these given materials have helped a lot of people enjoy lives in a better state, there are still strong demands for better materials which have better properties such as biocompatibility, mechanical properties, sensitivity, and smart responsiveness and so on. For example, relatively good mechanical stability and high oxygen permeability is required for applications in contact lenses which is one of the earliest biomedical applications of hydrogels [12-16]. This approach is also critical to design the hydrogel for other promising applications such as artificial tendon materials, wound-healing bioadhesives, artificial kidney membranes, artificial cartilage, artificial skin, maxillofacial and sexual organ reconstruction materials, vocal cord replacement materials, and drug delivery vehicles [3, 6, 17, 18]. In order to obtain better materials, we may think various ways to do: to redesign given synthetic materials, to hybridize synthetic materials with biomaterials, and to modify given biomaterials. For this purpose, we need to understand the detailed information on the molecular mechanisms behind the physical

properties for each class of biomaterial as well as principles behind events that determined excellent or poor biomaterials. Thus, we will focus on the understanding of the molecular mechanisms at an atomic/molecular level to provide valuable information to design new materials using computational approaches to obtain any desirable properties.

Computer Simulation

By definition, simulation is a process that can mimic the relevant features of a physical process [19]. Except in a few very special simple cases, most interesting molecular systems contain many atoms or molecules so there is no hope of finding the exact solution for even simple governing equation or equation of motion using only pencil and paper. Prior to use computer simulation, desirable properties could only be predicted using theory that provided a crude description of materials of interest. Using a computer, we try to obtain answers to some desired accuracy. Indeed, the computer simulation has provided useful information for problems in various field such as biology, chemistry, and physics, as well as economics and psychology since it played a essential role in developing nuclear weapons and code breaking in the early 1950s [20]. Recently, the usefulness of the computer simulation has been accelerated tremendously with rapid evolution of high performance computers, so that the application of the computer simulation grow continuously in almost every science and technology field.

Molecular Simulation

Among various computer simulation methods such as molecular simulation and finite element method (FEM), especially the molecular simulation methods have provided direct routes from the microscopic structural details of materials to the

macroscopic properties of interest. So far, lots of molecular simulation methods have been developed and validated in many fields of physics and chemistry. As shown in Figure 1.1, it should be noted, however, that the use of molecular simulation methods should be dependent on the properties of interest due to the multi-scale characteristics of material systems for given distance and time scale.

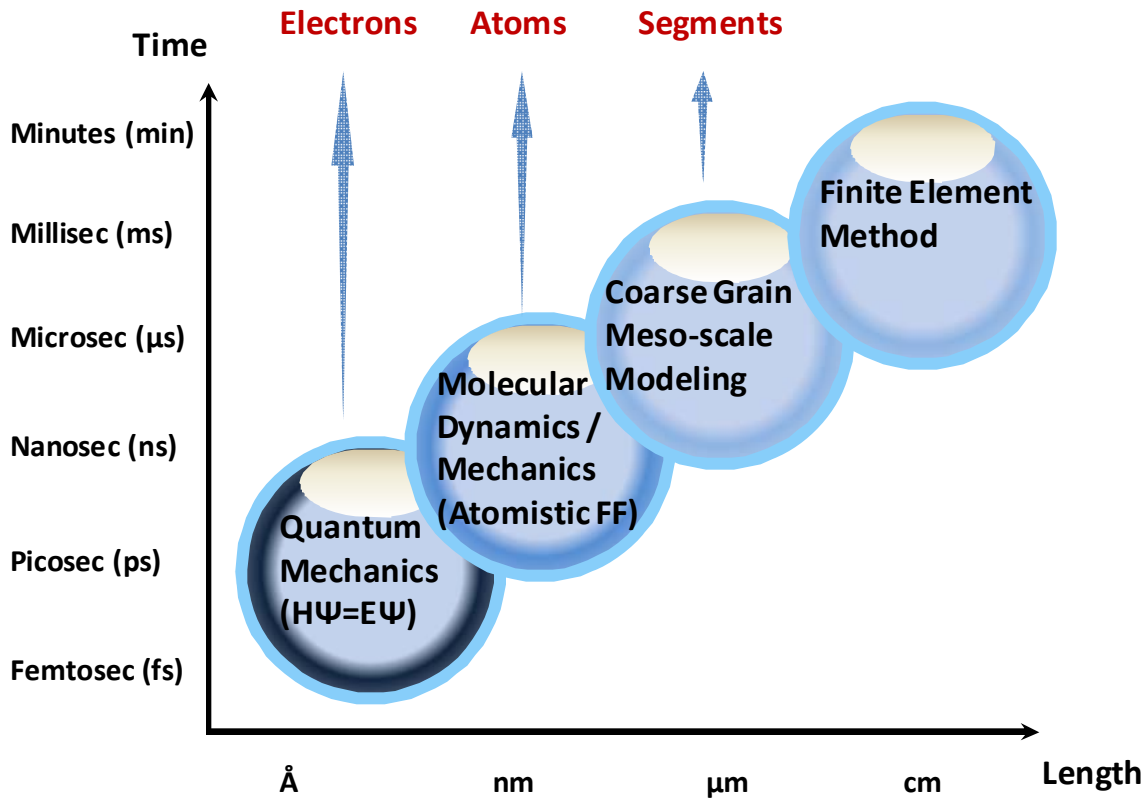

Figure 1.1: The hierarchical multi-scale paradigm in molecular simulation

In other words, in order to investigate the electronic structures and properties of materials for which atomic dimension is the characteristic length scale, the quantum mechanics (QM) simulation should be used to obtain useful information for electronic properties of material of our interest by calculating electron wave functions up to several Angstroms and picoseconds. Since QM methods determine state of all electrons, the results from QM show very accurate geometries and energies of the system. However,

the computational cost of QM calculations beyond 100 atoms range is very high. If the simulation of over several hundreds and thousands of atoms is required, a different approach must be used.

By averaging over the electron wave functions, QM can be approximated with molecular mechanics (MM) and molecular dynamics (MD) which allows us to investigate the structure and energetic of larger system with up to hundred nanometer or even micrometer scale dimension. At this stage, electrons and nuclei are represented by atoms and bonding schemes in a classical dynamical manner. In MM or MD, the atoms are considered as a soft sphere bonded to each other with springs, so that energies and forces derived from this approximation can be plugged into classical physics formulas to obtain dynamic trajectories or optimized geometries.

For this study, we will build the model that consists of several thousand atoms and need to simulate up to 50 nanoseconds to obtain the equilibrated structure and any desirable properties from the simulation. MD simulations allow for the study of comparatively large systems and have emerged as an effective tool for the characterization of the mechanical and thermal behaviors of nanostructure. Thus, we will use the molecular simulation techniques of MD in order to complete the investigation using a reasonable amount of time and resources. Further up in the hierarchy lie simulation methods requiring ever more crude approximations to maintain computational feasibility for systems operating on longer time and distance. While our system is based on full atomistic models, the methods beyond MD/MM in the hierarchy will not be discussed. Since polymeric systems are complex, it is still not feasible to completely describe all aspects of a system using MD technique. However, using accurate and robust MD simulations on polymeric models, we can obtain reliable results to analyze the systems. This data can be used to build high quality atomistic models to design the polymeric materials for any practical applications. Chapter 2 discuss about MD in more detail.

Motivations

Computational studies for hydrogel

With recent advanced in computing power, MD simulation technique has been widely used to characterize the molecular structure and properties of various materials systems including bio-systems since it can provide detailed information on structures and behaviors of systems at the molecular level [20-25]. It should be noted, however, that there have been only a limited number of MD simulation studies on hydrogel systems.

Tamai and Tanaka carried out MD simulations for hydrogel models of poly(vinyl alcohol), poly(vinyl methyl ether), and poly(N-isopropylacrylamide) hydrogels to study polymer-water interaction in hydrogels by analyzing the hydrogen bond structure and dynamics [26, 27]. The range for degree of polymerization (DP) of the polymer chain is 11-161 and the range for number of water molecules is 5 to 215. They have also performed MD simulations of poly(vinyl alcohol) with 81 or 161 DP and pure water over a wide temperature range 150-400 K to study effects of polymer chains on structure and dynamics of supercooled water in hydrogels [28, 29]. They used 150 to 216 water molecules and the simulation time range was 1 to 40 ns.

Oldiges et al. have simulated poly(acrylamide) hydrogels to investigate the local structural, mobility effects between dilute aqueous acetonitrile solution, water, and crosslinked poly(acrylamide) [30-32]. They used 12 to 59 DP of acrylamide molecules with the range for 300 to 390 water molecules.

Recently, Jang et al. have also applied full-atomistic simulations to hydrogel systems made of poly(ethylene glycol) and poly(acrylic acid) double network to investigate its structure and mechanical properties [33, 34]. They built a three-dimensional nanostructured interpenetrating network of poly(ethylene glycol) and

poly(acrylic acid) in presence of water molecules to study what kind of network structure can achieve the excellent mechanical strength for replacing human cornea.

The knowledge from these studies can be used to determine the structure-property relationships that will be valuable in developing novel hydrogels. However, as I mentioned before, there are only a limited number of systematic investigation available. Thus, it is critical to study the equilibrated structure, mechanical properties, and transport properties of hydrogels with various water contents or small guest molecules such as nutritious molecules or anti-cancer drugs. Among various hydrogels, we are particularly interested on poly(N-vinyl-2-pyrrolidone-*co*-2-hydroxyethyl methacrylate) hydrogel and poly(N-isopropylacrylamide) hydrogel as shown in Figure 1.2:

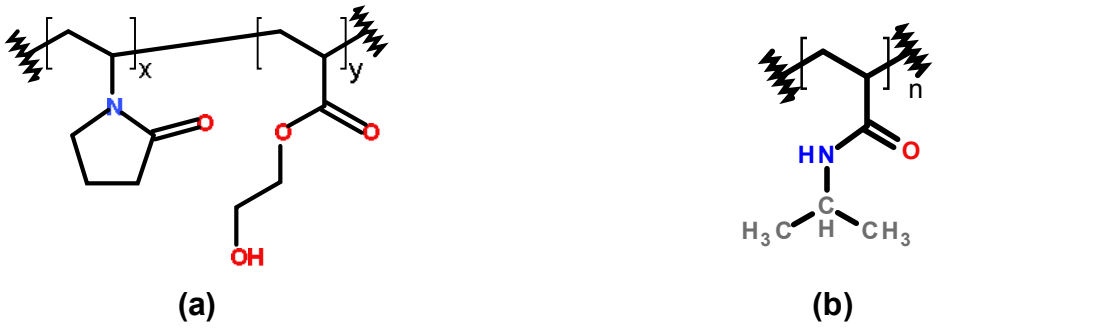

Figure 1.2: Chemical structures of (a) poly(N-vinyl-2-pyrrolidone-*co*-2-hydroxyethyl methacrylate), x and y indicate the units of N-vinyl-2-pyrrolidone and 2-hydroxyethyl methacrylate, respectively; (b) poly(N-isopropylacrylamide).

Monomeric sequence effect on poly(N-vinyl-2-pyrrolidone-*co*-2-hydroxyethyl methacrylate) hydrogel

Poly(2-hydroxyethyl methacrylate) (PHEMA) is one of the most important synthetic hydrogels; it has been extensively developed in biomedical applications [35] due to its non-toxicity, hydrophilicity, biocompatibility, thermal stability, inertness toward many chemicals, high resistance to degradation, and adequate mechanical strength [36-46]. In addition, PHEMA can be easily polymerized and cross-linked for the fabrication of various architectures [37, 38, 47, 48]. Such properties make PHEMA gels

suitable materials for controlled drug release systems [44, 45, 49-69] and for other biomedical and pharmaceutical applications, such as post-surgical reconstruction [70, 71], artificial skin [72, 73], wound dressing [51, 74-77], ocular biomaterials [78-82], enzyme immobilization [41-43, 83], cell culture [84-89], microcapsules [90], and biosensors [41].

HEMA monomers can be copolymerized with a wide range of other monomers to manipulate their properties. Copolymerization provides an excellent way to control physical properties, such as hydrophilicity, solubility, and mechanical strength. Of the various monomers, we are specifically interested in the copolymerized hydrogels of N-vinyl-2-pyrrolidone (VP) and HEMA because poly(N-vinyl-2-pyrrolidone-*co*-2-hydroxyethyl methacrylate) (P(VP-*co*-HEMA)) is a well-known, biocompatible hydrogel with a broad range of applications in the biomedical field [91-93] . Although poly(N-vinyl-2-pyrrolidone) (PVP) has also been individually used in biomedical and pharmaceutical applications, such as blood volume expanders [94], drug binders [95], vitreous substitutes [46, 96-100], DNA isolation [101], and even cosmetic and food additives [95] due to its exceptional solubility in water, inertness, non-toxicity, and biocompatibility [96, 102], PVP has a very limited applicability due to its poor mechanical properties [103]. Because PHEMA is known to have better mechanical properties than PVP, but less swelling, mechanical strength of PVP can be enhanced by copolymerization with PHEMA. Additionally, the overall properties of P(VP-*co*-HEMA) can be controlled for particular applications with various VP:HEMA compositions [103-106]. Thus, the composition of the copolymeric system determines the swelling behavior and the mechanical strength [107], and this composition can be changed to obtain suitable devices for particular applications [58, 108]. Moreover, P(VP-*co*-HEMA) hydrogels are some of the major synthetic polymers that are approved by federal agencies, including the U.S. Food and Drug Administration (FDA) [109], for medical and pharmaceutical applications. Thus, P(VP-*co*-HEMA) has been extensively investigated in biomedical and pharmaceutical applications, such as implants for bone substitutes [110] and bone

tissue regeneration [111], controlled drug delivery [58, 103, 104, 112-119], enzyme immobilization [120-122], contact lenses [123, 124], and tissue expanders for reconstructive plastic surgery [125-138].

The water content of a hydrogel can be described as a percentage of the weight of water: water content (%) = (weight of water/(weight of water + weight of dry gel)) × 100 [139]. The water content of hydrogels plays an important role in the use of hydrogels in biomedical applications, because it affects the solute diffusion and the optical and mechanical properties of the hydrogels. In general, the low water content of the hydrogel ranged from 20 to 50%. A hydrogel with over 90% water content is considered a super-adsorbent hydrogel [139]. For instance, the U.S. Food and Drug Administration (FDA) classified the water content of the hydrogel contact lenses as low water content (>50%) and high water content (<50%). The water content of the PHEMA hydrogel contact lenses is ~40% [2], and that of the VP-HEMA-based contact lenses is 40–70% [124, 139, 140].

The physical properties of a copolymer hydrogel system correspond to the distribution and length of monomer units in the copolymer chain [104, 141]. In other words, the physical properties can be regulated by the microstructural distribution of the sequences of the monomeric units along the copolymer chains, which depend mainly upon the initial composition of the reaction medium and the reactivity ratio of the monomers participating in the copolymerization reactions [142-144]. Different reactivity ratios of the participating monomers could also affect the formation of the microstructural distribution of the sequences of the monomeric units during the reaction. In a limiting case, the formation of blocks of the monomer could be expected [145-148].
The reactivity ratios (Equation 23) of VP and HEMA monomers have been well described by several experimental groups [141, 149-151]: 2.97 – 8.18 for HEMA and 0.02 – 0.10 for VP. Because the reactivity ratio of the VP and HEMA comonomeric pair is very different, the consumption of HEMA is faster than that of VP, which leads to

compositional heterogeneity in the copolymer chains [150] and a broad microstructural distribution [104]. Surprisingly, despite the intensive effort spent on the P(VP-*co*-HEMA) hydrogel, there has been no systematic study to understand the effect of the monomeric sequence on the properties of the hydrogel at a molecular level. Therefore, our primary objective is to elucidate the effect of the monomeric sequence on the equilibrated structures (Chapter 3) and the mechanical (Chapter 4) and transport (Chapter 5) properties of P(VP-*co*-HEMA) hydrogel with various water contents.

De-swelling mechanisms of poly(N-isopropylacrylamide) hydrogel

Secondly, poly(N-isopropylacrylamide), P(NIPAAm), is one of the most widely studied temperature-sensitive polymers. Aqueous solutions of P(NIPAAm) exhibit a lower critical solution temperature (LCST) of approximately 305 K (32 C°) [152-155]. Gels of P(NIPAAm) can swell at below the critical temperatures and collapse to form a separate phase above the critical temperature. Due to the unique and novel characteristics of their thermal responses, P(NIPAAm) hydrogels have been extensively studied for pharmaceutical applications, such as drug delivery systems [156-169], detachment of cultured cells [170, 171], surface-properties control [172-181], concentrating dilute solutions [182], bioconjugation [183-185], solute separation [186], drug barrier membranes [187], tissue cultures [188], and nanocomposites [189, 190]. The volume phase transition behavior of P(NIPAAm) has been investigated by many research groups using various experimental tools, such as FT-IR spectroscopy [191-198], Raman spectroscopy [195, 199-202], laser light scattering [194], differential scanning calorimetry [191, 197, 203-206], temperature-jump apparatus [207-211], nuclear magnetic resonance [212, 213], and atomic force microscopy [214].

It should be noted, however, there have been only a few systematic studies on the detailed mechanisms of the swelling/de-swelling of the P(NIPAAm) hydrogel at a molecular level that utilized full atomistic molecular dynamics simulation. Tamai and

Tanaka carried out MD simulations for P(NIPAAm) hydrogel models to study polymer-water interactions by analyzing the hydrogen bond structure and dynamics [26, 27, 215]. The range for the degree of polymerization (DP) of the polymer chain is from 4 to 81, and the range for the number of water molecules is from 150 to 215 with 23, 44, and 75 wt % water content. They simulated a single chain of P(NIPAAm) in water at a temperature range of 200 – 400 K. The distributions and dynamics of the hydrogen-bonds, the translational diffusion of the water, and the orientational relaxation of the water were analyzed to investigate the properties of the water that are influenced by the surrounding polymer chains. Tonsing et al. [216] simulated P(NIPAAm) hydrogel models at three different temperatures (285, 300 and 325 K) using 15 to 33 NIPAAm units with 2 to 4 cross-linkers and 227 to 317 water molecules. The simulations were used for the analysis of the polymer-water structure and for the determination of the diffusion coefficients. Longhi et al. [217] performed MD simulation with 50 units of NIPAAm at 300 and 310 K. They found that the equilibrated chain configurations have a more compact conformation at 310 K than they do at 300 K. Correspondingly, the number of water molecules within the first hydration shell is smaller (~6%) at 310 K than it is at 300 K. Recently, Gangemi et al. [218] performed MD simulations on a single NIPAAm chain (26 units) with 3560 water molecules to study the mechanisms of LCST at 302 K and 315 K. They also showed that at 315 K, the NIPAAm chain assumes a compact form, while it maintains a more extended form at 302 K. They found that the formation of intramolecular hydrogen bonds and water-bridges between distant units of the solute play an important role in this transition.

One major disadvantage of these studies is that only a single chain of NIPAAm was considered for the investigation. For a more realistic model, we must build a new P(NIPAAm) hydrogel model to investigate the polymer-water interaction and the intermolecular polymer-polymer interaction in the model structure. Therefore, the

development of protocols to build a sound P(NIPAAm) hydrogel model is one of our primary goals in this investigation.

Thus, in our study, we simulated temperature-dependent volumetric changes of P(NIPAAm) hydrogel at the atomic level to pursue the fundamental understanding of the interaction between P(NIPAAm) and water molecules using newly developed models. We expect that the building protocols, the analyzing methodologies, and the understanding of such water-polymer interactions can be extended to other polymeric hydrogels, which will contribute to developing new polymer hydrogels with finely tuned characteristics.

Objectives

The focus of this research is to understand the structure-property relationships of hydrogels using MD simulations with the goal of creating new material design guidelines for the construction of fine-tuned nanostructured hydrogel systems. Pursuing these objectives, full-atomistic MD simulations have been employed to provide a fundamental understanding of the effect of the monomeric sequence on the equilibrated structure (Chapter 3), mechanical properties (Chapter 4), and transport properties (Chapter 5) of poly(N-vinyl-2-pyrrolidone-*co*-2-hydroxyethyl methacrylate) (P(VP-*co*-HEMA)) hydrogels at various water contents (0, 20, 40 and 80 wt %). The detailed research objectives are as follow:

1. To characterize the role of water molecules in determining the equilibrated structures (Chapter 3);
2. To investigate the effect of structural variables, such as the monomeric sequence, on the mechanical properties (Chapter 4);
3. To investigate the effect of water molecules on the mechanical properties (Chapter 4);

4. To investigate the effect of structural variables, such as the monomeric sequence, on the transport properties of guest molecules (Chapter 5);
5. To investigate the effect of water content on the transport properties of guest molecules (Chapter 5).

The hydrogel should meet various requirements depending on the detailed purposes of the individual application; therefore, research into the abovementioned objectives will shed light on the deformation mechanism of hydrogels at the molecular level. The investigation of the transport properties of P(VP-*co*-HEMA) hydrogels with respect to nutritious molecules and drug molecules will provide important knowledge to develop artificial materials for bio-applications, such as tissue engineering and drug delivery.

In Chapter 6, we study the temperature-dependent volumetric change of poly(N-isopropylacrylamide), P(NIPAAm), hydrogel to elucidate the interaction between P(NIPAAm) and water molecules at the atomic level. The detailed molecular mechanism between the water molecules and the NIPAAm chains as a function of temperature is described in Chapter 6. The detailed research objectives are as follow:

6. To develop modeling protocols to build a reasonable P(NIPAAm) hydrogel system to investigate temperature-dependent volumetric change behavior (Chapter 6);
7. To investigate the interaction and the mechanisms between the water-polymer chains of the temperature-sensitive P(NIPAAm) hydrogel (Chapter 6);
8. To investigate the exact molecular de-swelling mechanisms of the hydrogel as a function of temperature (Chapter 6).

CHAPTER 2: COMPUTATIONAL BACKGROUNDS

Force Field

Force field plays one of the most important roles for MD simulations. It contains the main set of parameters (approximations) used to represent the molecular system examined. Once a find quality force field is prepared for a system, the application of classical physical principle is enough to derive high quality information about the system. Since many researchers put their significant efforts to develop high quality force fields, accurate force fields are available for many organic, inorganic and biological systems. For instance, DREIDING [219] or UFF [220] is well known generic force field and CHARMM [221] or AMBER [222, 223] is well developed force field to describe biological systems.

The total energy is expressed by force field for a molecular system as a sum of valance (or bonded) interactions and nonbonded interactions (Equation 1).

$$E_{Total} = E_{valence} + E_{nonbond} \qquad \textbf{(1)}$$

The valence interactions can be broken down into bond stretch, bond angle bending, dihedral angle torsion, and inversion term (Equation 2).

$$E_{valence} = E_{bond} + E_{angle} + E_{torsion} + E_{inversion} \qquad \textbf{(2)}$$

The first valence term in a force field is a bond stretch term. The simplest bond stretch term is harmonic bond potential (Equation 3).

$$E_b = \frac{1}{2} K_b (R - R_0)^2 \qquad \textbf{(3)}$$

where R is the bond distance in units of Å, R_0 is the equilibrium bond distance in units of Å and K_b is the force constant in units of (kcal/mol)/Å^2. In harmonic bond potential, the bond is considered like a spring with an equilibrium bond length of R_0 and spring constant of K_b. This expression is very economical to compute and most commonly used in all standard force field. For distance R = ∞, like breaking a chemical bond, a Morse potential (Equation 4) for bonding is used for systems where a covalent bond is allowed to break.

$$E_b = D_o[e^{-\alpha(R-R_0)} - 1]^2 \text{ , } \alpha = \sqrt{K_b / 2D_0} \qquad \textbf{(4)}$$

where D_0 is the bond energy in units of kcal/mol and α is the Morse scaling parameter. R_0 and K_b are same term from harmonic bond potential. This Morse scaling parameter allows the bond energy to go to zero for large R.

The second valence term in a force field is a bond angle bend. Given any two bonds to an atom, the bond angle interaction is a function of the angle θ between them as shown in Figure 2.1.

The most basic and common bond angle bend term is again a harmonic potential (Equation 5).

$$E_a = \frac{1}{2} K_\theta (\theta - \theta_0)^2 \qquad \textbf{(5)}$$

where θ is the bond angle, θ_0 is the equilibrium bond angle and K_θ is the force constant in units of (kcal/mol)/Å^2. For an accurate description of the three-body terms which required for good vibrational frequencies, bond angle term can also include angle-stretch term (Equation 6).

$$E_\theta = K_{\theta,R_1}(R_1 - R_{10})(\theta - \theta_0) + K_{\theta,R_2}(R_2 - R_{20})(\theta - \theta_0) + K_{R_2,R_1}(R_1 - R_{10})(R_2 - R_{20}) \quad \textbf{(6)}$$

where R_1 and R_2 is the distance between atom i, j and j, k in units of Å, respectively; R_{10} and R_{20} is the equilibrium distance between atom i, j and j, k in units of Å, respectively; $K_{R1,R2}$ is the stretch-stretch factor in units of (kcal/mol)/Å^2.

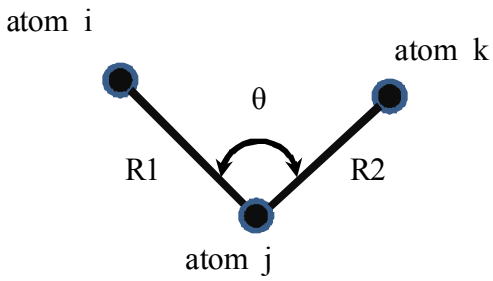

Figure 2.1: Scheme of bond angle bend

The third valence term in a force field is a dihedral angle torsion term. Given any two bonds ij and kl attached to a bond jk, the dihedral angle φ is defined as the angle between the ijk plane and the jkl plane as shown in Figure 2.2.

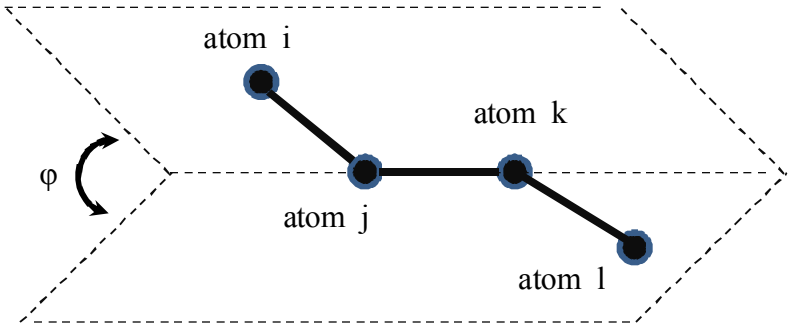

Figure 2.2: Scheme of torsion angle

The torsional energy is expressed as (Equation 7)

$$E_\theta = \sum_{n=1}^{p} \frac{1}{2} K_{\theta,n}[1 - d\cos(n\phi)] \qquad \textbf{(7)}$$

where each $K_{\theta,n}$ is one half the rotational barrier in unit of kcal/mol, n=1,2,3,4,5,6 is the periodicity (p) of the potential and d = ±1 is the phase factor. For d = +1, the cis conformation is the minimum while for d = -1 the cis conformation is the maximum.

The last valence term in a force field is inversion term. Given an atom i having three distinct bonds ij, ik, and il, the force field may contain terms affecting the energy involved in planarizing the center atom I as shown in Figure 2.3.

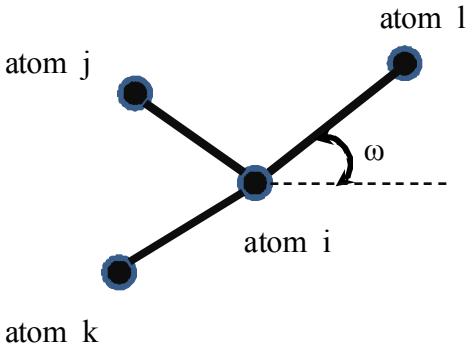

Figure 2.3: Scheme of inversion

The inversion term (or umbrella term) can be expressed by simple harmonic term (Equation 8).

$$E_\theta = \frac{1}{2} C(\cos\omega - \cos\omega_0)^2, \; K_\omega = C\sin^2\omega_0 \qquad \textbf{(8)}$$

where K_ω is the force constant in unit of kcal/mol and ω is the angle between the il axis and the ijk plane. If $\omega_0 = 0°$, the potential term has a minimum for the planar structure.

The nonbonded interactions consist of electrostatic, van der Waals and hydrogen bond term (Equation 9).

$$E_{nonbond} = E_{electrostatic} + E_{vdW} + E_{hbond} \qquad \textbf{(9)}$$

The first nonbonded term in a force field is electrostatic interaction. The electrostatic interactions are important to describe the packing of organic molecules and in the structure of inorganic systems. The total electrostatic interaction energy can be calculated by evaluating the Columbic interaction between each pair of atoms in the system (Equation 10).

$$E_{electrostatic} = C_0 \sum \frac{q_i q_j}{\varepsilon r_{ij}} \qquad \textbf{(10)}$$

where $C_0 = 332.0637$ is the conversion factor to take care of the units, giving $E_{electrostatic}$ in kcal/mol, q_i and q_j are the charges (in electron units), ε is the dielectric constant (ε = 1 for a vacuum), r_{ij} is the distance between atom i and j in unit of Å.

The second nonbonded term in a force field is van der Waals interactions. The van der Waals interaction also plays fundamental role in structural biology, surface science, nanotechnology, polymer science, and condensed matter physics. The van der Waals energy contains the attractive and repulsive force between molecules. The most common form is the Lennard-Jones 12- 6 potential (Equation 11).

$$E_{vdW(LJ12-6)} = D_0 \left[\left(\frac{R_0}{R} \right)^{12} - 2 \left(\frac{R_0}{R} \right)^{6} \right] \qquad \textbf{(11)}$$

where D_0 is well depth and R_0 is an equilibrium distance in unit of Å. The main drawback of this form is that it required only two parameters, D_0 and R_0. For R is less

than R_0, the Lennard-Jones 12-6 potential may be too repulsive at short ranges. To have a more reasonable form, the exponential-6 potential (Equation 12) and Morse potential (Equation 13) allows three parameters to describe the inner wall (short ranges) more realistically.

$$E_{vdW(\exp-6)} = D_0\left\{\left[\left(\frac{6}{\xi-6}\right)\exp^{\xi\left(1-\frac{R}{R_0}\right)}\right]-\left[\left(\frac{6}{\xi-6}\right)\left(\frac{R_0}{R}\right)^6\right]\right\} \quad \textbf{(12)}$$

$$E_{vdW(Morse)} = D_0\left(\chi^2-2\chi\right),\ \chi = \exp\left[-\frac{\gamma}{2}\left(\frac{R}{R_0}-1\right)\right] \quad \textbf{(13)}$$

The last nonbonded term in a force field is hydrogen bond. Some force fields such as CHARMM and DREIDING use a hydrogen bond potential to describe the interactions between atoms involved in hydrogen bonds. The general form of hydrogen bond form is Lennard-Jones 12-10 potential (Equation 14).

$$E_{hbond(LJ12-10)} = D_0\left[5\left(\frac{R_0}{R}\right)^{12}-6\left(\frac{R_0}{R}\right)^{10}\right] \quad \textbf{(14)}$$

where D_0 is the hydrogen bond strength in kcal/mol and R_0 is an equilibrium distance in unit of Å.

Molecular Dynamics Simulation

Molecules in the real world are constantly fluctuating and changing its conformation to respond to external environment. Molecular dynamics (MD) simulations allow studying these moving molecules by time-dependent processes.

Equations of motion

MD simulations consist of the numerical solution of classical equations of motion to determine the positions and velocities of atoms at finite temperatures. At given temperature, initial velocity of a particle is usually determined by a random distribution (Maxwell-Boltzmann distribution). Once an initial velocity is determined, it is updated using the calculated accelerations. MD techniques usually use Cartesian coordinates, resulting in 3N degrees of freedom from N particles in the system. Thus, the forces, velocities, and accelerations are independently obtained to a specific particle for each degree of freedom. The total force, F_x, in the x direction is the opposite of the gradient (Equation 15).

$$F_x = -\frac{\partial}{\partial x} V \quad \textbf{(15)}$$

where V is potential energy and x is the coordination information in x direction.

Newton's equation of motion (Equation 16) id used to determine the accelerations

$$m_i \ddot{x} = F_x \quad \textbf{(16)}$$

where m_i is the mass of particle i.

Verlet Algorithm

Since we have computed all forces between the particles, we can update velocities from the accelerations by integrating Newton's equation of motion. Many numerical algorithms have been developed for integrating Newton's equation of motion, such as Verlet algorithm [224], leap-frog algorithm [225, 226], and velocity-Verlet algorithm [227]. Verlet [224] initially used method of integrating the equations of motion using Taylor series expansion which uses the positions r(t), accelerations a(t), and the previous

positions r(t-δt) to predict new positions r(t+δt). Modifications to the basic Verlet algorithm have been proposed by Hockney and Potter [225, 226]. In this scheme, so-called a leap frog scheme, the current position r(t) and accelerations a(t) with the mid-step velocities v(t-(δt/2)) were used to obtain the next mid-step velocities v(t+(δt/2)). The velocities leap over the positions and the positions leap over the velocities. Swope et al. introduced the velocity-Verlet algorithm, because both the basic Verlet and leap frog algorithms do not describe the velocities in a satisfactory manner. The velocity-Verlet algorithm needs to store positions, accelerations, and velocities at the same time to minimize round-off error. This algorithm takes the form as follows (Equation 17 and 18)

$$r(t+\delta t) = r(t) + \delta t v(t) + \frac{1}{2}\delta t^2 a(t) \qquad \textbf{(17)}$$

$$v(t+\delta t) = v(t) + \frac{1}{2}\delta t[a(t) + a(t+\delta(t)] \qquad \textbf{(18)}$$

The new position at time t+δ(t) are calculated using Equation 17 and 18, and the velocities at mid-step v(t+(δt/2)) are calculating using Equation 19.

$$v(t+\frac{1}{2}\delta t) = v(t) + \frac{1}{2}\delta t a(t) \qquad \textbf{(19)}$$

The forces and accelerations at time t+δ(t) are then calculated, and the velocity move is completed as follows (Equation 20)

$$v(t+\delta t) = v(t)\left(t+\frac{1}{2}\delta t\right) + \frac{1}{2}\delta t a(t+\delta t) \qquad \textbf{(20)}$$

Ensembles

Ensemble is assembly of all possible microstates, defined by given constraints. For example, a simple way to create a thermodynamic ensemble is to maintain a constant total energy, volume, and number of particles in a system to produce a microcanonical (NVE) ensemble of conformations. In the same way, canonical (NVT) ensemble assembly of all states with fixed number of particles, volume, and temperature and isobaric-isothermal (NPT) ensemble fixed number of particles, pressure, and temperature. Once ensemble is formed, relative free energies, average densities, and other thermodynamic properties can be calculated.

Energy Minimization

Energy minimization is typically performed by perturbing atoms in order to reduce the net force applied to atoms by the force field potentials. Since a minimized structure usually has a well-mannered geometry and rarely has large forces on any atom, it is preferred to start a molecular dynamics simulation with a minimized structure.

Energy minimization can be carried out in Cartesian coordinates by optimizing in 3N-dimensional space where N is the number of particles in the system. The path chosen is the gradient, ∇, as follows (Equation 21)

$$\nabla_x = \frac{\partial}{\partial x} V \qquad \textbf{(21)}$$

Each Cartesian component, x, of the gradient is the derivative of the potential energy of the force field with respect to that component.

CHAPTER 3: EQUILIBRATED STRUCTURE OF P(VP-*co*-HEMA) HYDROGEL

Introduction

In our study, we are particularly interested in the poly(N-vinyl-2-pyrrolidone-*co*-2-hydroxyethyl methacrylate) (P(VP-*co*-HEMA)), which is a network copolymer composed of various compositions of N-vinyl-2-pyrrolidone (VP) and 2-hydroxyethyl methacrylate (HEMA) monomers as shown in Figure 3.1. Poly(N-vinyl-2-pyrrolidone) (PVP) and poly(2-hydroxyethyl methacrylate) (PHEMA) homopolymers have individually been used as biomedical materials for artificial skin [72, 73], drug release [49, 52, 55], microcapsules [90] and DNA isolation [101].

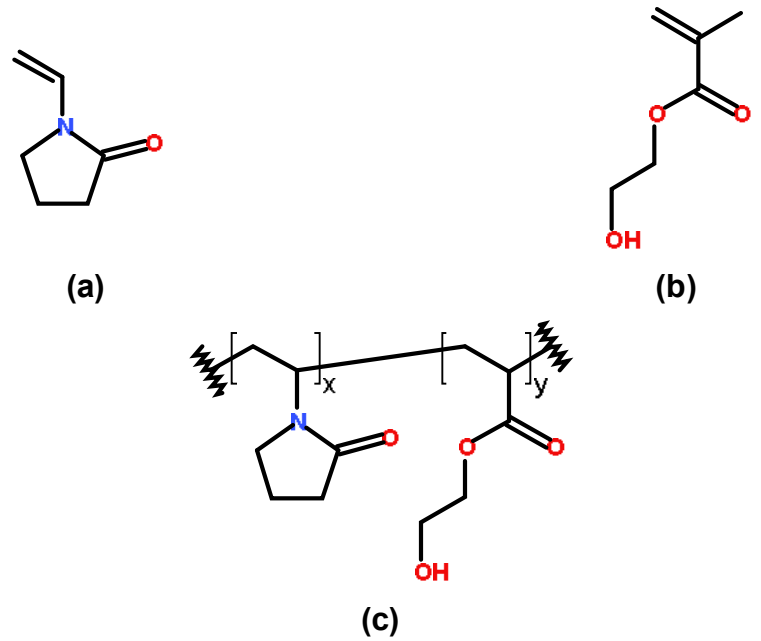

Figure 3.1: Chemical structures of (a) VP; (b) HEMA; and (c) P(VP-*co*-HEMA)

P(VP-*co*-HEMA) provides a way to control the properties of interest since PVP is more hydrophilic and therefore swells the most, but PHEMA has a higher mechanical strength [46, 103, 105, 110, 228]. Thus, the hydrophilicity and swelling behavior of P(VP-*co*-HEMA) hydrogel can be controlled as a function of VP:HEMA composition at various temperatures and pH conditions [46, 103-106, 111, 115, 116, 141, 149, 229]. Surprisingly, despite all these intensive efforts on the P(VP-*co*-HEMA) hydrogel, there has been no systematic study and therefore understanding on the properties of the P(VP-*co*-HEMA) hydrogel at a molecular level. Thus, in this study, we describe the use of full-atomistic MD simulations, to determine the equilibrated structure of P(VP-*co*-HEMA) hydrogels at various water contents (0, 20, 40 and 80 wt %). Our primary objective in this simulation study is to model the equilibrium structures of P(VP-*co*-HEMA) hydrogels at various water contents, and to elucidate the role of water molecules in determining the equilibrated structures.

Models and Simulation Details

Model Constructions

Many factors in the molecular architecture can be explored, but we focus herein on the monomeric sequence effect on the equilibrium structure of P(VP-*co*-HEMA) using full-atomistic MD simulations.

Monomeric Sequence of P(VP-co-HEMA)

All simulations were performed using full atomistic models. Figure 3.2 (a) and (b) show two types of model P(VP-*co*-HEMA) chains used in our simulations. While the model chains have the same degree of polymerization (DP=50) and the same composition (VP:HEMA=37:13), our interest here is to determine how the monomeric sequence affects the equilibrated structure of the copolymer network. The monomeric composition

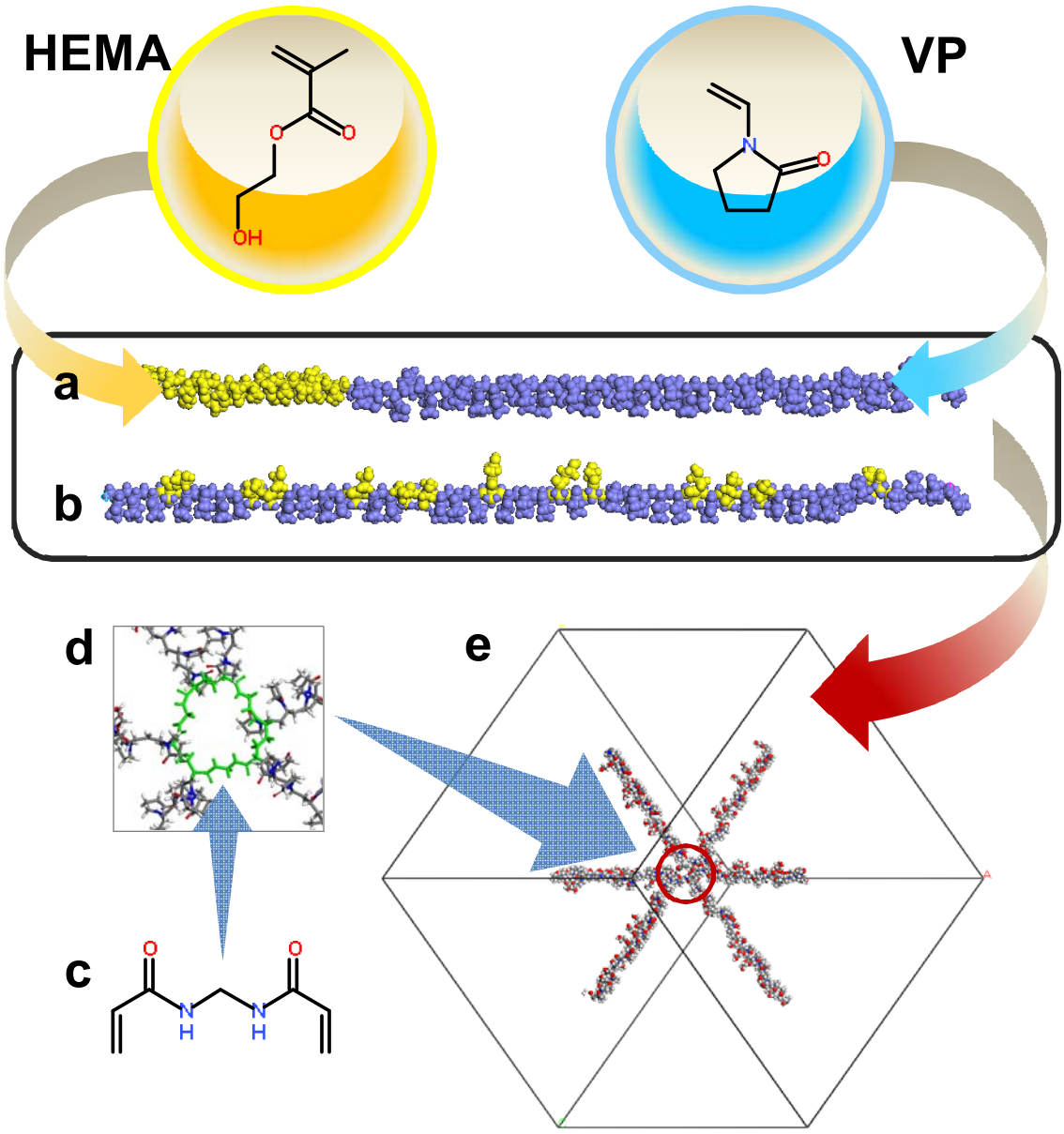

Figure 3.2: The scheme of the preparation of P(VP-*co*-HEMA) hydrogel; (a) single chain of the blocky sequence with DP=50; (b) single chain of the random sequence with DP=50; (c) N,N´-methylenebisacrylamide (cross-linker); (d) configuration of cross-linking point; (e) connected network through the periodic box

was chosen to match that used experimentally [230]. The monomer sequences in our model P(VP-*co*-HEMA) chain are intentionally designed to have either a blocky sequence with 0.104 of the degree of randomness (DR) where the HEMA monomers are gathered at one chain end (Figure 3.2 (a)), a random sequence with 1.170 of DR, so that HEMA monomers are randomly distributed along the chain (Figure 3.2 (b)). Here the value of DR is calculated by

$$DR = \frac{1}{\bar{L}_A} + \frac{1}{\bar{L}_B} \qquad \textbf{(22)}$$

where $\bar{L}_A$ and $\bar{L}_B$ are the average number of subsequent monomers within one block for monomeric species A and B, respectively. From this definition, we notice that the value of DR is 0, 1, and 2 for the case of homopolymers, random copolymer, and alternating copolymer, respectively.

According to the experimental condition of synthesis, UV-initiated free radical polymerization was used for synthesis [46, 103-106, 111, 115, 116, 141, 149, 229, 230]. As a results, the monomeric sequence is determined by the reactivity ratio [142]. Thus, it is possible to statistically predict the monomeric sequence of copolymer as a function of comonomer feed ratio. If VP and HEMA are denoted as monomers 1 and 2, respectively, the monomer reactivity ratios are defined as

$$r_1 = k_{11}/k_{12} \text{ and } r_2 = k_{22}/k_{21} \qquad \textbf{(23)}$$

where k_{11} and k_{22} are the rate constant that a polymer chain with a certain type of terminal monomer attacks the same type of monomer for polymerization, and k_{12} and k_{21} are the rate constant that a polymer chain with a certain type of terminal monomer attacks another type of monomer (comonomer). The reactivity ratios of the VP and HEMA

comonomer pair was reported by several groups: r_{HEMA} = 2.97 – 3.40 and r_{VP} = 0.02 – 0.09 (in ethanol, Al-Issa et al. [150]); r_{HEMA} = 4.35 – 4.50 and r_{VP} = 0.02 – 0.06 (in methanol, Reddy et al. [151]); r_{HEMA} = 6.77 – 7.97 and r_{VP} = 0.017 – 0.077 (in water/ethanol, Gallardo et al. [141]). Most recently Faragalla et al. [149] determined r_{HEMA} = 8.18 and r_{VP} = 0.097 using the bulk copolymerization of the VP and HEMA system. However, it should also be pointed out that in order to satisfy the statistical nature of the reactivity ratio describing the monomeric sequence, the molecular weight needs to be sufficiently large (DP > ~1000). Considering the DP of our model chain is 50 which might be too small to meet true statistical requirements, consequently we intentionally designed the monomeric sequence to have two extremes (random and blocky sequences). It is assumed that the realistic sequence would lie somewhere between these two extremes.

Establishing the Polymeric Network

The three-dimensional network structure is constructed from the random or blocky copolymer chains using a cross linker, N,N′-methylenebisacrylamide (MBA) (Figure 3.2 (c)). To simplify the model, the MBA molecules are located at end of each P(VP-co-HEMA) chain (Figure 3.2 (d)), with all the chains arranged so that they participate in the network structure through periodic boundary conditions as shown in Figure 3.2 (e). Although experimental samples potentially have structural variations such as free dangling chain ends and self-looping [230], we assumed a perfect model network structure leaving no free dangling chain ends or self-loops. Here, it should be noticed that the topology of our model network is purely theoretical in terms of the number of chain ends at the cross-linking junction. Although the usual number of junctions in experiments involves 3~4 chain ends, we deliberately chose the current junction connecting 6 chain ends to build a three-dimensional grid structure, which was used in the previous study by Jang, et al [33, 34]. This is supposed to have an identical

equilibrated behavior along each axis direction. Once the polymer network system was constructed, water molecules are added to hydrate the system to a water content equivalent to 20, 40, and 80 wt %. The characteristics of the hydrogels are described in Table 3.1.

Table 3.1: Characteristics of the hydrogels from 5 ns of NPT MD Simulations

Monomeric sequence	Random				Blocky			
Number of monomer per chain	VP=37 and HEMA=13				VP=37 and HEMA=13			
Number of chains per system	3				3			
Cross-linking molecular weight, M_c	5804.16				5804.16			
Degree of randomness	1.17				0.10			
Water content	0 wt %	20 wt %	40 wt %	80 wt %	0 wt %	20 wt %	40 wt %	80 wt %
Density at 300K (g/cm^3)	0.97 ± 0.01	1.06 ± 0.01 (1.06 ± 0.00(3))[a]	1.07 ± 0.01	1.02 ± 0.00(3)	0.91 ± 0.01	1.02 ± 0.01 (1.02 ± 0.00(3))[a]	1.06 ± 0.01	1.02 ± 0.00(3)
Simulated cell Size (Å)	31.30 ± 0.08	32.73 ± 0.06 (65.43 ± 0.06)[a]	35.94 ± 0.07	52.60 ± 0.06	31.94 ± 0.08	33.09 ± 0.08 (66.17 ± 0.07)[a]	35.96 ± 0.06	52.60 ± 0.06
Number of water molecule	0	248 (1984)[a]	661	3969	0	248 (1984)[a]	661	3969
Mesh size, (ξ) (Å, simulation)	31.30 ± 0.08	32.73 ± 0.06	35.94 ± 0.07	52.60 ± 0.06	31.94 ± 0.08	33.09 ± 0.08	35.96 ± 0.06	52.60 ± 0.06

a The values are obtained from the 8 times larger systems.

Model Equilibration

It should be emphasized that generally the initial structures prepared by molecular mechanics (energy minimization) have highly strained local configurations with unstable

energies. However, the time scales for relaxation of polymers are very slow for standard equilibrium MD simulations to evolve to the equilibrium state. In order to obtain well equilibrated structures for complex amorphous polymers with a minimum of effort, we applied an annealing procedure that accelerates the equilibration by driving the system repeatedly through sequential thermal (between 300 and 600 K) and pressure (between densities of 0.5 to 1.1 times the expected density) annealing cycles. This procedure aims to help the system quickly escape from various local minima and thereby efficiently reach an equilibrated structure.

The steps in the annealing procedure are summarized below:

a. Starting from the initial structure, gradually expand the initial cell by 100 % over a period of 30 ps while the temperature is simultaneously increased from 300 K to 600 K.

b. Equilibrate at 600 K for 30 ps at a half density of the original target density ($\rho = 0.5\rho_0$, $\rho_0 = 1.1$ g/cm^3) using NVT MD.

c. Gradually compress the system back to the original target density over 30 ps while cooling the temperature down to the target temperature (T=300 K).

d. Repeat steps **a** to **c** four times.

e. At the original target density, we equilibrate for 100 ps NVT MD at 300K

f. Finalize the equilibration by running a NPT MD for 10 ns at 1 atm and 300 K.

During this step, the density of the system is optimized by changing the simulation cell parameters.

This annealing equilibration procedure has been used successfully in the studies of polymer membrane for fuel cell [231-233] to achieve equilibrated systems at the target temperature and pressure. After completing the building and equilibration steps described above, data collection from all the systems were obtained by running a 5 ns NPT MD simulation.

Force Field and MD Parameters

In this investigation, we employed the generic DREIDING force field [219], which has been well tested in various organic systems, such as polymer electrolyte membranes [231-234], the self-assemblies of organic molecules [235-237] and hydrogels [33, 34]. The F3C force field [238] is also used to describe water molecules in the hydrogel systems. Although various water models, such as SPC and TIP3P, produce high quality simulations for water and hydrated macromolecules, we think that the undeniable advantage of the F3C water model is it can be easily combined with any full atomistic models in classical MD simulations because of its fully flexible nature. Indeed, we have used the F3C water model successfully in various studies of hydrogels [33, 34] and hydrated polymer electrolyte membranes for fuel cells [231-234]. Thus, the total potential energy is given as follows:

$$E_{total} = E_{vdW} + E_{electostatic} + E_{bond} + E_{angle} + E_{torsion} + E_{inversion} \quad \textbf{(24)}$$

where E_{total}, E_{vdW}, $E_{electrostatic}$, E_{bond}, E_{angle}, $E_{torsion}$ and $E_{inversion}$ are the energies for the total, van der Waals, electrostatic, bond stretching, angle bending, torsion and inversion components, respectively. The details of the force field parameters have already been described [219, 238]. For MD simulations, the velocity-Verlet algorithm [227] method was used to integrate the equations of motion with a time step of 1.0 fs. A Nose-Hoover thermostat [239-241] and Andersen-Hoover barostat [239, 242] were used with a damping relaxation time of 0.1 ps and a dimensionless cell mass factor of 1.0, respectively. During simulation, all of the valence parameters were fully unconstrained. The time interval between samplings was 5 ps. The atomic charges of the polymers were assigned using the charge equilibration (QEq) method [243], and the atomic charges of water molecules were the outputs of the F3C water model [238]. The Lennard-Jones (LJ)

potential was smoothly shifted to zero between 1.2 and 1.5 nm. A Particle-Particle Particle-Mesh (PPPM) method [244] is used to calculate the electrostatic interactions. The MD simulation code used in this study is the Large-scale Atomic/Molecular Massively Parallel Simulator (LAMMPS) MD simulator that was developed by S. Plimpton at Sandia National Laboratories [245, 246].

Results and Discussion

Equilibrated Structure

The snapshots of the equilibrated structures resulting from the final 5 ns NPT MD simulations are shown in Figure 3.3. The spatial distribution of the VP (blue) and HEMA (yellow) monomers as well as the MBA (green) and water molecules can be seen. The differences in the random and blocky hydrogels are clearly observed.

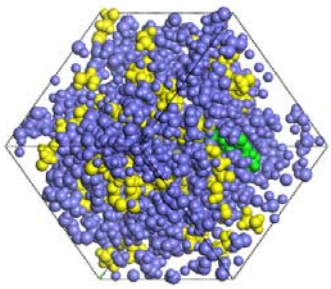

(a) Random (0 wt %)

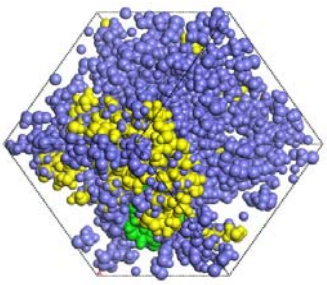

(b) Blocky (0 wt %)

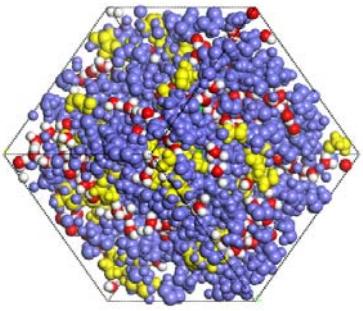

(c) Random (20 wt %)

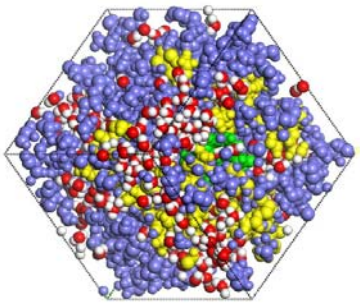

(d) Blocky (20 wt %)

Figure 3.3: (Continued on next page.)

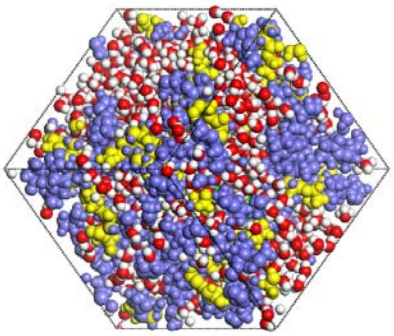

(e) Random (40 wt %)

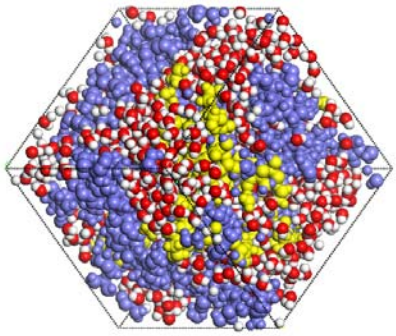

(f) Blocky (40 wt %)

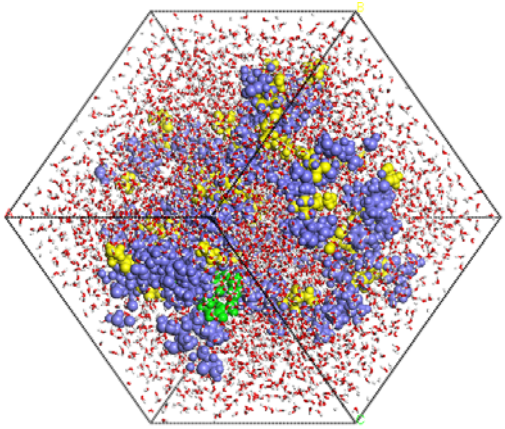

(g) Random (80 wt %)

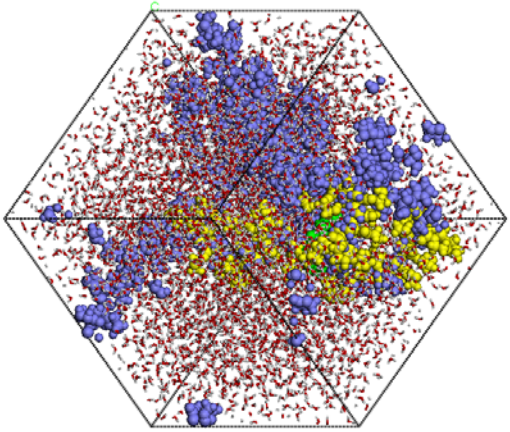

(h) Blocky (80 wt %)

Figure 3.3: Equilibrated random sequence P(VP-*co*-HEMA) networks with (a) 0 wt % of water content; (c) 20 wt % of water content; (e) 40 wt % of water content; (g) 80 wt % of water content, and equilibrated blocky sequence P(VP-*co*-HEMA) networks with (b) 0 wt % of water content; (d) 20 wt % of water content; (f) 40 wt % of water content; (h) 80 wt % of water content. Blue, yellow, and green color denote VP, HEMA, and MBA, respectively. The oxygen of water molecule is represented by red color. The ball size of water molecules with 80 wt % water content is reduced for clarity.

Density

In Figure 3.4, it was observed that the density depends on the monomeric sequence at low water content (0 and 20 wt %), with the random sequence showing a ~6.3% higher density than the blocky sequence. We think that this is mainly because of the steric interaction between the bulky branches in HEMA is relatively more significant in blocky sequences due to the spatial proximity of the branches in a block. The blocky sequence therefore can have a more expanded chain conformation compared to the random sequence.

To investigate this density difference further, a 5 ns MD simulation was run for a single isolated P(VP-*co*-HEMA) chain in vacuum for each monomeric sequence. Each simulated single chain has the same degree of polymerization (DP=50) and the same composition (VP:HEMA=37:13) as shown in Figure 3.2 (a) and (b). It was found that the root-mean-square radius of gyration of a single P(VP-*co*-HEMA) chain is 10.92±0.33 Å for the random and 12.03±0.08 Å for the blocky sequences, indicating that the blocky sequence chains have a larger dimension than the random sequence by ~10 %. This can be understood by considering steric interactions between the bulky branches made up from large blocks of HEMA (Figure 3.2 (a)), which makes the blocky sequence P(VP-*co*-HEMA) chains more expanded than those with random sequences. Therefore, the sequence-dependent chain dimension would be a reason for the density difference between the two monomeric sequences.

However, with increasing water content, this density difference between random and blocky sequence decreases and eventually the densities of both sequence become identical at 80 wt % water content because the copolymer chains are similarly expanded when highly solvated by water molecules. The details regarding the solvation of polymer by water are discussed in the next section.

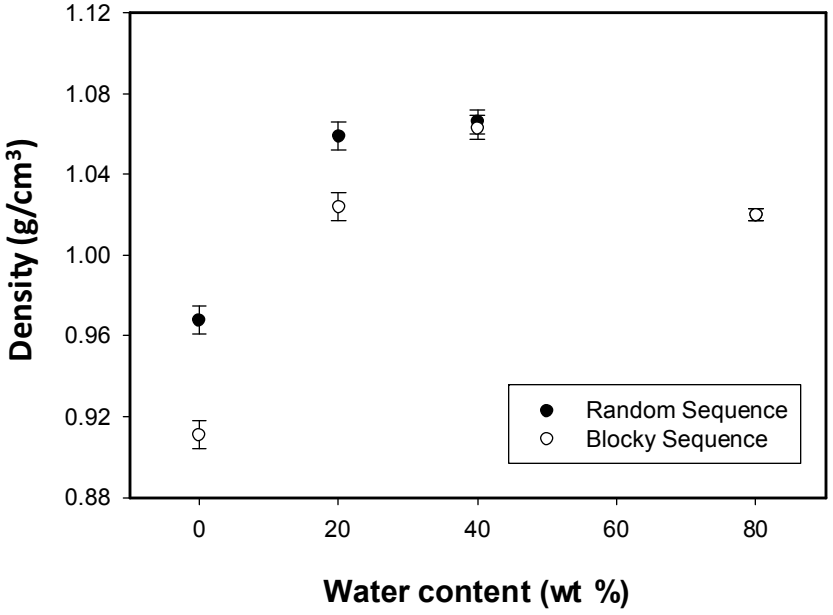

Figure 3.4: Change of density as a function of water content

"Reprinted from Biomaterials, Vol. 30, Seung G. Lee, Giuseppe F. Brunello, Seung S. Jang and David G. Bucknall, Molecular dynamics simulation study of P (VP-*co*-HEMA) hydrogels: Effect of water content on equilibrium structures and mechanical properties, 6130-6141, Copyright 2009, with permission from Elsevier."

Distribution of water molecules

Experimental studies using small-angle neutron scattering of in-situ swelling of PVP-*co*-PMMA hydrogels have shown that the distribution of water in the early stages of swelling are non-uniform in the hydrated regions [126]. This is thought to be due a non-uniform distribution of the two monomers, which have different hydrophilicity.

The water structures in the hydrogels are analyzed by the pair correlation function (PCF), $g_{A-B}(r)$ which is the probability density of finding atoms *A* and *B* at a distance *r* averaged over the equilibrium trajectory, so that:

$$g_{A-B}(r) = \left(\frac{n_B}{4\pi r^2 dr}\right) / \left(\frac{N_B}{V}\right) \qquad \textbf{(25)}$$

where n_B is the number of B particles located at a distance r in a shell of thickness dr from on A particle, N_B is the number of B particles in the system, and V is the total volume of the system. Using this pair correlation function, it is possible to determine what environment the water molecules are located in.

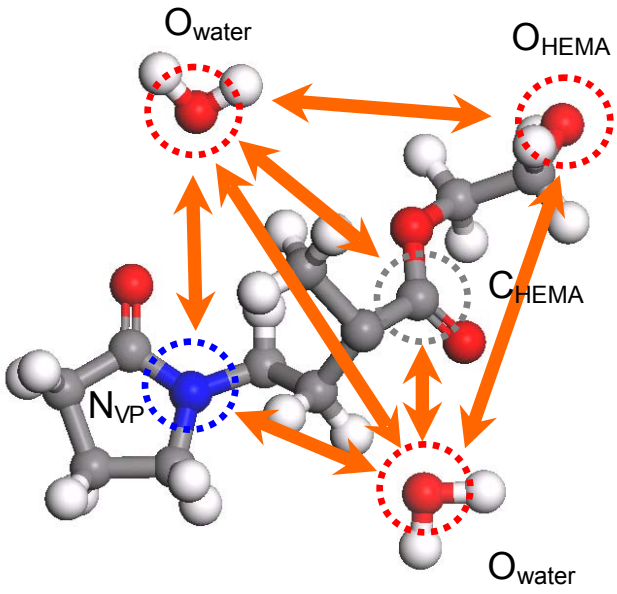

Figure 3.5: The concept of the pair correlation function; the change of ρg(r) as a function of the distance between oxygen and other atoms from our simulations.

Pair Correlation Functions of Polymer-Water Molecules

As shown in Figure 3.5, $g_{N(VP)-O(water)}(r)$, $g_{C(HEMA)-O(water)}(r)$, $g_{O(HEMA)-O(water)}(r)$ and $g_{O(water)-O(water)}(r)$ are defined by the N (VP) – O (water), C (HEMA) – O (water), O (HEMA) – O (water) and O (water) – O (water) pairs, respectively. In order to directly compare intensities, the product of the pair correlation and the number density ($\rho g(r)$) is used instead of $g(r)$. The $\rho g_{N(VP)-O(water)}(r)$, $\rho g_{C(HEMA)-O(water)}(r)$ and $\rho g_{O(HEMA)-O(water)}(r)$ as a function of water content (see Figure 3.6) show that the intensity of $\rho g(r)$ increases with increasing water content.

This occurs because the monomer units in the polymer chains are surrounded by increasing amounts of water molecules as the water content increases. This is quantitatively evaluated from the water coordination number of the monomer, CN, which is the average number of water molecules in the first solvation shell surrounding each monomer. As shown in Table 3.2, the water CNs for N (VP) is larger than these for C (HEMA) and O (HEMA), by 2.3 ~ 2.9 times and 1.3 ~ 2.2 times, respectively, indicating that the VP is more hydrophilic than the HEMA. These results are entirely consistent with experimental results [46, 103, 105, 110, 228] which have also shown the increased hydrophilicity of VP compared to HEMA.

(a)

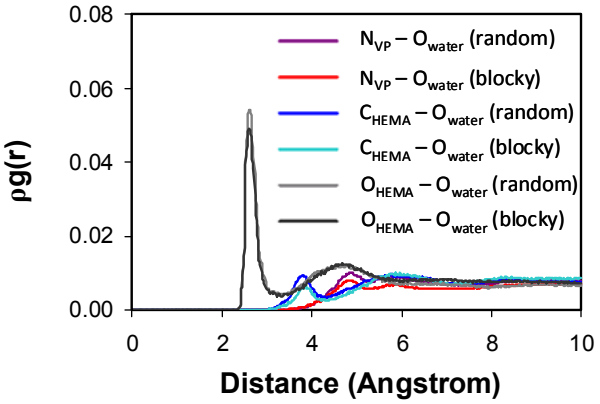

(b)

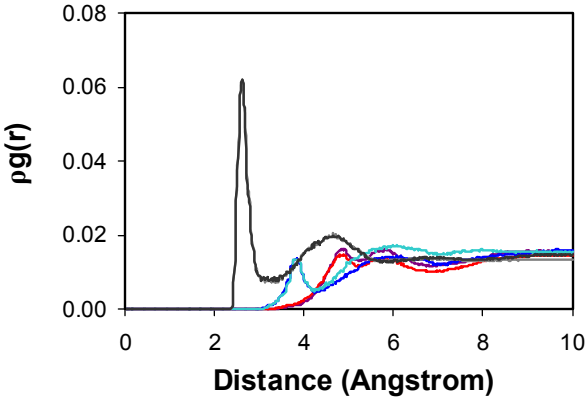

(c)

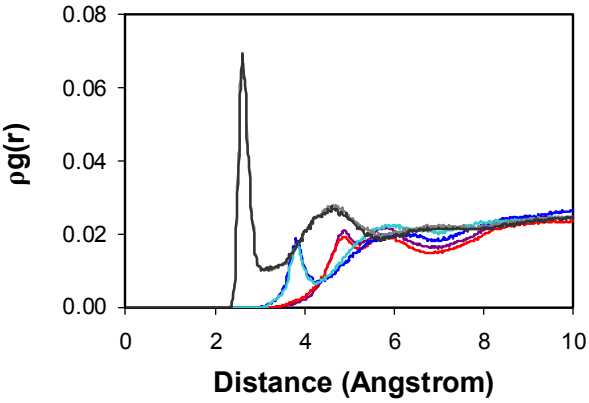

Figure 3.6: Pair correlation function of the N (VP) – O (water) pair, the C (HEMA) – O (water) and the O (HEMA) – O(water) with various water contents: (a) 20 wt %; (b) 40 wt %; (c) 80 wt %.

"Reprinted from Biomaterials, Vol. 30, Seung G. Lee, Giuseppe F. Brunello, Seung S. Jang and David G. Bucknall, Molecular dynamics simulation study of P (VP-*co*-HEMA) hydrogels: Effect of water content on equilibrium structures and mechanical properties, 6130-6141, Copyright 2009, with permission from Elsevier."

Table 3.2: Water coordination number (CN) from X – O (water) pair

X	Water content (wt %)		
	20	40	80
N_{VP} (random)	2.13 (2.12) [a]	3.35	4.21
N_{VP} (blocky)	1.74 (1.74) [a]	3.28	4.14
C_{HEMA} (random)	0.93 (0.96) [a]	1.26	1.65
C_{HEMA} (blocky)	0.61 (0.63) [a]	1.24	1.52
O_{HEMA} (random)	1.47 (1.43) [a]	1.72	1.95
O_{HEMA} (blocky)	1.31 (1.32) [a]	1.69	1.91
O_{water} (random)	2.42 (2.42) [a]	3.37	4.19
O_{water} (blocky)	2.62 (2.62) [a]	3.37	4.20
Bulk Water	4.50 (exp.) [b], 4.59 (simul.) [c]		

a The values are obtained from the 8 times larger systems.
b The values are from references. [247, 248]
c The values are from reference. [232]

Solvation Free Energies of VP and HEMA

To quantify the differences in hydrophilicity between the VP and the HEMA moieties, the water solvation free energies were calculated using the Poisson-Boltzmann self-consistent reaction field model [249-251] with Jaguar quantum chemical software [252]. The solvation free energy is defined as the energy required to move a specific molecule in vacuum into a specific solvent medium [253]. The elements in the solvation free energy are shown in the following equation [254]:

$$\Delta G_{sol} = \Delta G_{ele} + \Delta G_{disp} + \Delta G_{cav} \qquad \textbf{(26)}$$

where ΔG_{ele} is the electrostatic solvation free energy; ΔG_{disp}, the dispersive solvation free energy; and ΔG_{cav}, the cavity formation free energy of the solute in the solvent.

First, long-range electrostatic forces play a dominant role in molecular interactions. When a solute is immersed in a solvent, the charge distribution of the solute interacts with that of the solvent. The charge of the solute polarizes the solvent. In a continuum model, the charge distribution of the solvent is represented by a continuous electric field as a layer of charges at the solute surface rather than by an explicit solvent model. This field is typically called the reaction field, and it is determined by numerically solving the Poisson-Boltzmann (PB) equation in the regions of space occupied by the solute. The reaction field acts back on the solute, which in turn changes the electric field on the solute. This process is iterated until self-consistency is achieved. The Poisson equation describes the electrostatic potential between the charge of the solute and the continuum dielectric solvent as follows:

$$-\nabla \cdot [\varepsilon(r)\nabla\Phi(r)] = 4\pi\rho(r) \qquad \textbf{(27)}$$

where $\varepsilon(r)$ is the dielectric constant at position r; $\Phi(r)$, the electrostatic potential at position r; and $\rho(r)$, the charge density of the solute at position r. When the solute is dissolved, the distribution of the mobile electrolytes in the solvent is given by the Boltzmann distribution. Thus, the Poison-Boltzmann equation applies instead of the Poisson equation:

$$-\nabla \cdot [\varepsilon(r)\nabla\Phi(r)] + \kappa(r)^2 \sinh\left(\frac{e_c\Phi(r)}{k_B T}\right) = 4\pi\rho(r) \qquad \textbf{(28)}$$

where κ is the Debye-Huckel parameter; e_c, the absolute charge of the electrolyte ions; k_B, Boltzmann's constant; and T, the absolute temperature. The Debye-Huckel parameter is given by the following equation:

$$\kappa(r) = \sqrt{\frac{8\pi N_A e_c^2 I}{1000\varepsilon(r)k_B T}} \qquad \textbf{(29)}$$

where N_A is Avogadro's number and I, the ionic strength. The electrostatic solvation free energy, ΔG_{ele}, can be described by solving the PB equation in the solvent dielectric with the solute and in vacuum with the solute as follows:

$$\Delta G_{ele} = \frac{1}{2}\sum_{i=0}^{N} q_i(\Phi_{solvent}(r_i) - \Phi_{vacuum}(r_i)) \qquad \textbf{(30)}$$

where q_i is a set of point charges of the solute at positions r_i. The dispersive and cavity effects are calculated as follows:

$$\Delta G_{disp} + \Delta G_{cav} = \sum_{i=0}^{N} \sigma_i A_i \qquad \textbf{(31)}$$

where A is the solvent accessible surface area (SASA) and σ_i, the surface tension parameter for an atom i of the solute. The contributions from the dispersive and cavity effects are proportional to SASA.

For the calculation conditions, we used the 6-31G** basis set, which is one of the most widely used Gaussian-type basis sets [255-260]. A basis set is a fixed finite set of mathematical functions from which the wave function is constructed. With a 6-31G** level of basis set, the B3LYP exchange correlation functional was used to describe the

many-electron exchange and the correlation effects. The B3LYP functional is the most popular and most widely used functional [261] and was suggested by P. J. Stephen et al., 1994 [262]. The B3LYP functional with the 6-31G** basis set shows good performance in many chemistry fields [261], including the solvation of various molecules in water [263-268]. We also carried out the calculation using the M06 and M06-2X functionals [269] due to the lack of accuracy of the B3LYP functional to describe the dispersion-like interaction of organic molecules [270-277], organometallic catalytic systems [278, 279], and transition metals [280-283]. The M06 and M06-2X functionals were recently developed by D. G. Truhlar's group at the University of Minnesota, and they give good performance for noncovalent interactions [284]. The calculated solvation free energies of the PVP and PHEMA unit are shown in Table 3.3.

Table 3.3: Solvation free energy of PVP and PHEMA unit

	Solvation Free Energy (kcal/mol)		
	B3LYP/6-31G**	M06/6-31G**	M06-2X/6-31G**
VP	-8.56	-8.84	-9.27
HEMA	-8.22	-8.64	-8.72

A negative energy indicates that the solvation of the solute is favorable for that particular solvent [285, 286]. From these calculations, it was found that the solvation free energy of the PVP unit is lower (more favorable in water) than that of the PHEMA unit. The M06-2X functional shows the lowest solvation free energy for both the PVP and the PHEMA unit, but we observed that the solvation free energy of the PVP unit was always lower than the PHEMA unit in any functional. These QM computations of the water solvation free energies are consistent with the experimental observations [46, 103, 105, 110, 228], which show that VP is more hydrophilic than HEMA.

Pair Correlation Functions of Water-Water Molecules

The water CN for water molecules was also analyzed (Figure 3.7). From the previous simulation study [232] reporting that the water CN for the bulk water, 4.59 is in a good agreement with the experimental value, 4.50 [247, 248], we think that the water molecules in the hydrogel system are described well in our simulation. First, the water CN for water is also increased up to 4.2 as the water content increases, similar to the water CN for the monomers. In addition, the water CN for water is larger in the blocky sequence hydrogel than in the random sequence although that difference reduces with increasing water content and are the same beyond 40 wt % water content. From Table 3.2, it is noted that the water CN for N (VP), C (HEMA) and O (HEMA) is larger in the random sequence hydrogel than in the blocky sequence one, meaning that the monomers in the random sequence are more solvated by water compared to those in the blocky sequence. From this result, therefore, it is inferred that the water structure is more disturbed in order to solvate the monomers in the random sequence hydrogel.

Solvent Accessible Surface Area

To understand this behavior, it is necessary to consider the packing of the monomers in the systems. As the monomers in the blocky sequence are close together, it is possible that the monomers segregate together to form their own phase in which a certain number of monomers are buried inside the phase. Those buried monomers do not provide accessible sites to the water molecules. This explanation has been confirmed by checking the solvent accessible surface area (SASA) of the monomers. The calculated SASA values for the VP and HEMA in the random sequence hydrogel are 8905 ± 45 Å^2 and 4557 ± 37 Å^2, respectively, and 7590 ± 99 Å^2 for VP and 3628 ± 32 Å^2 for HEMA in the blocky sequence hydrogel, clearly indicating that both VP and HEMA segments have a smaller SASA in the blocky sequence compared to the random sequence hydrogel.

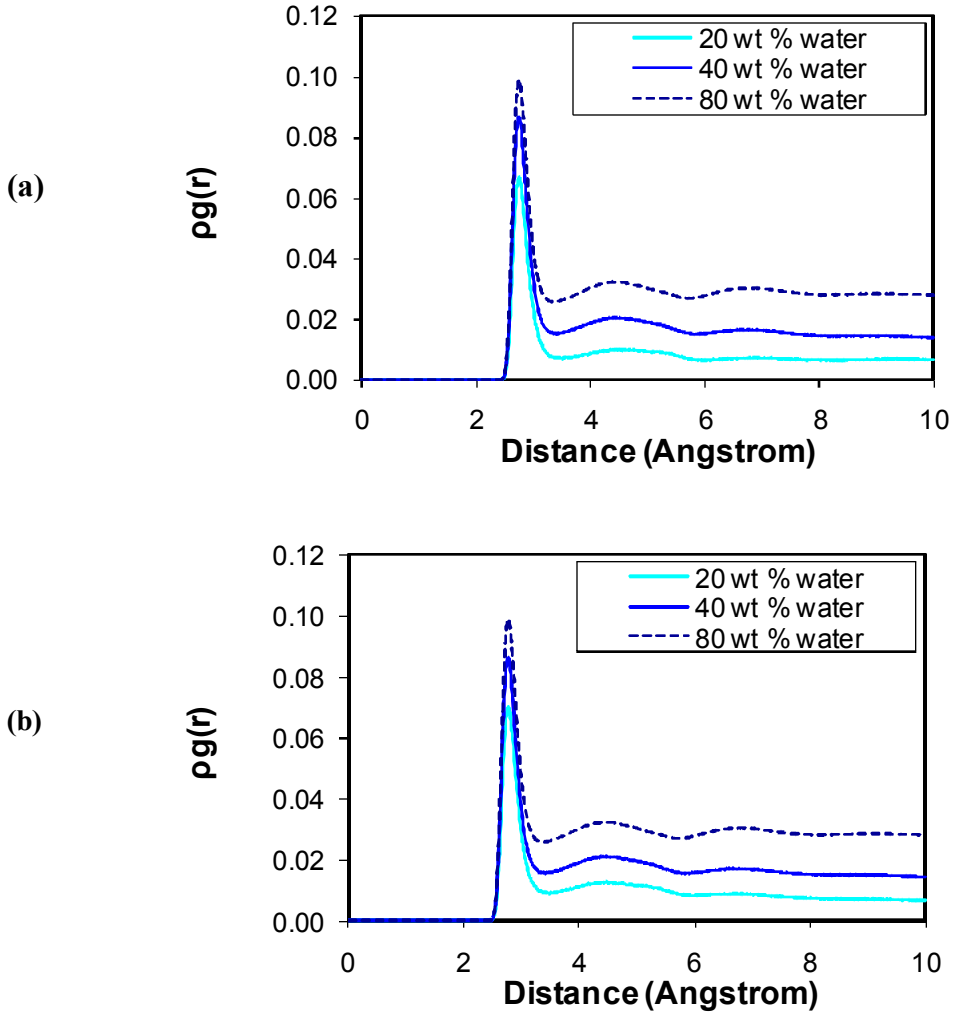

Figure 3.7: Pair correlation function of the O (water) – O (water) pairs: (a) random monomeric sequence; (b) blocky monomeric sequence.

"Reprinted from Biomaterials, Vol. 30, Seung G. Lee, Giuseppe F. Brunello, Seung S. Jang and David G. Bucknall, Molecular dynamics simulation study of P (VP-*co*-HEMA) hydrogels: Effect of water content on equilibrium structures and mechanical properties, 6130-6141, Copyright 2009, with permission from Elsevier."

Finite Size Effect

We performed independent simulations using 8 times larger systems with 20 wt % water content for the random and the blocky sequence in order to check the size effect on the structures of the hydrogel. We found the average densities of 1.059 ± 0.003 and

1.024 ± 0.003 for the random and the blocky sequence system, respectively. The results are identical to those reported in Table 3.1 for the original models. We also investigated the local structures by analyzing the pair correlation function and the coordination number for the larger systems as summarized in Table 3.2, showing that the local structures within the hydrogels are not affected by the varied size in our study. We think that this result support the validity of our simulations.

Conclusions

MD simulations were performed to study the effect of water content on the equilibrated structure of the poly(N-vinyl-2-pyrrolidone-*co*-2-hydroxyethyl methacrylate) (P(VP-*co*-HEMA)) hydrogels with two different monomeric sequences; a random sequence (DR=1.170) and a blocky sequence (DR=0.104). By analyzing the pair correlation functions, it is found that VP has more hydrophilic character compared to the HEMA. The water structure in the hydrogel also shows a consistent feature with the solvation of monomeric units: at low water content, relatively more water molecules participate in solvating monomeric units in the random sequence hydrogel than those in the blocky sequence hydrogel, and thereby the water CN for the water is smaller in the former than in the latter. As the water content increases, however, such differences disappear since the solvation of P(VP-*co*-HEMA) chains are enhanced with dominant water composition.

CHAPTER 4: MECHANICAL PROPERTIES OF P(VP-*co*-HEMA) HYDROGEL

Introduction

Among the many characteristics of hydrogels, we are interested in the mechanical properties which are macroscopic and easily measurable experimentally. The importance of such mechanical properties is particularly important in the use of hydrogels in the field of tissue engineering where the hydrogel should meet various requirements depending on the detailed purpose of individual application. In this context, in order to achieve such specific requirements, the molecular simulations, can be used to characterize the effect of structural variables such as monomeric sequence and composition on the macroscopic properties of interest, and thereby establish the structure-property relationship for rational design of new hydrogels. Implementation of mechanical deformation simulations has therefore been utilized in order to discover the relationship of molecular structure variables such as monomeric sequence of copolymer with mechanical properties.

For the mechanical simulation of polymers, the use of a molecular mechanics technique such as the quasi-static method is advantageous in that the simulation requires less computing time relative to other simulation techniques, and therefore, the use of more complex and sophisticated potential functions for energy calculations is allowed. However, it is disadvantageous in that the chain conformation has a large probability of falling in local energy minima. The entropic contribution in the deformation process of the polymers may play an important role and provide essential clues for understanding the origin of the deformation; however, it has not been focused on in molecular mechanics simulation techniques. This is because the molecular mechanics simulation is carried out without considering any thermal motion of the atoms, which is normally

regarded as the 0 K condition in classical mechanics. In contrast, the molecular dynamics simulation allows the chain conformation to change in the configurational space at real temperature. In this study, we performed molecular dynamics simulations.

Models and Simulation Details

We adopted same models of P(VP-*co*-HEMA) from previous chapter to study the mechanical properties. To assess the mechanical properties of the hydrogels, the hydrogels were deformed by uniaxial compression up to 80 % strain over a period of 2 ns at 300 K. The scheme of initial and deformed structures for random and blocky sequence hydrogels are shown in Figure 4.1. The deformation was performed by continuous application of strain of 4.0×10^{-5} % per simulation step (1 fs) uniformly across the simulation box by rescaling all atom coordinates to the new box dimensions.

The stress (σ_{xx}) was calculated from the uniaxial compression in the x-axis direction using the virial equation:

$$\sigma_{xx} = \frac{1}{V}\sum_{i=1}^{N-1}\sum_{j=i+1}^{N}\mathbf{r}_{x,ij}\mathbf{f}_{x,ij} \qquad \textbf{(32)}$$

where V, $\mathbf{r}_{x,ij}$ and $\mathbf{f}_{x,ij}$ are the volume, the position vector between atom i and j (x component), and the force (x component) on the atom i exerted by j, respectively. The engineering strain is also represented by following equation:

$$\varepsilon = \frac{\Delta L}{L_0} \qquad \textbf{(33)}$$

where ΔL and L_0 are the deformed length and the original length of material, respectively. The y- and z-axis directional compressions were also carried out independently and averaged statistically.

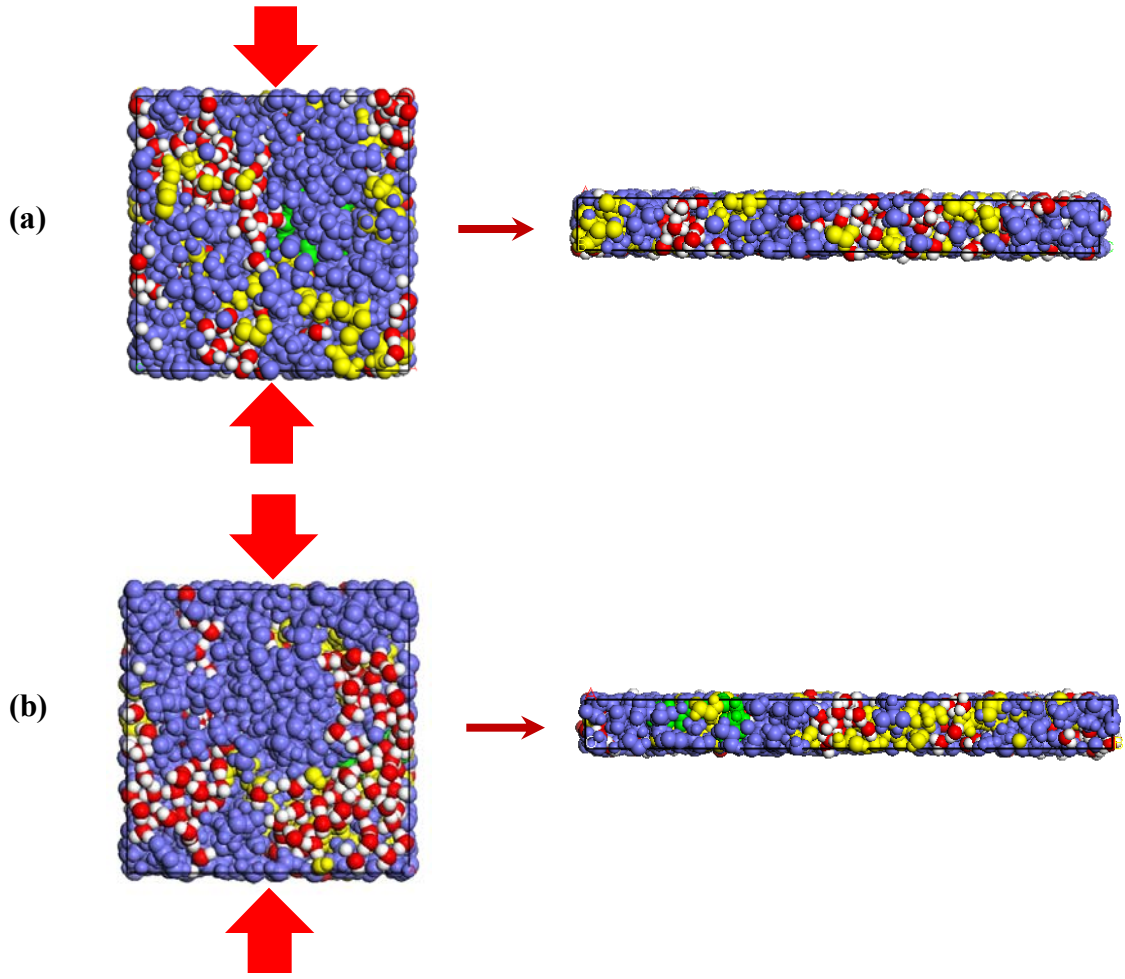

Figure 4.1: Compression of hydrogels up to 80%: (a) random P(VP-*co*-HEMA) with 20 wt % of water content; (b) blocky P(VP-*co*-HEMA) with 20 wt % of water content. We observed the same features from the compression of the 0, 40 and 80 wt % of water content P(VP-*co*-HEMA) system.

Results and Discussion

Stress-Strain Curves

The stress-strain curves obtained from our simulations are presented in Figure 4.2.

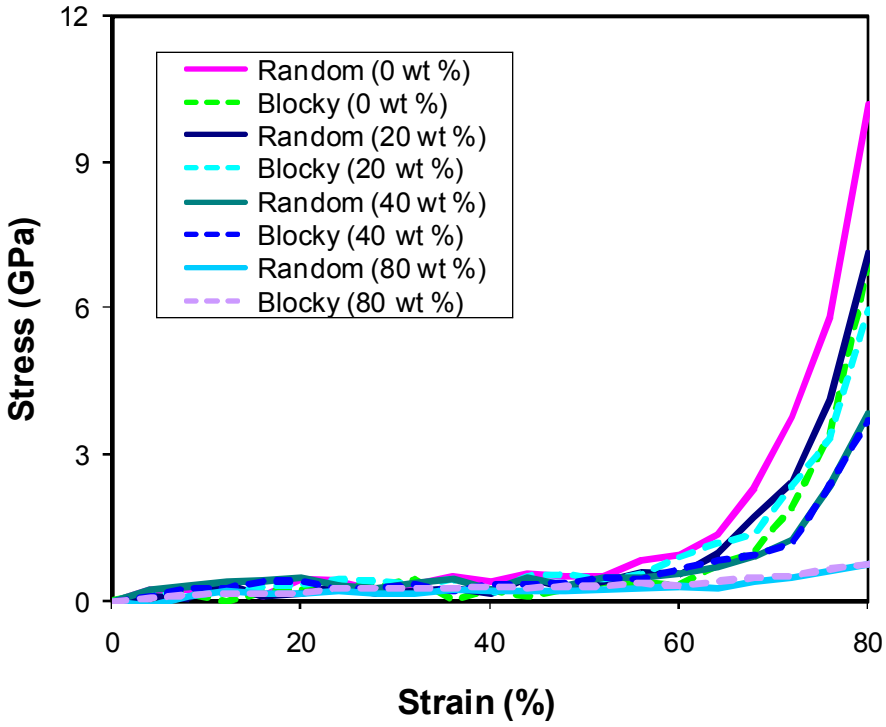

Figure 4.2: Change of stress as a function of strain.

"Reprinted from Biomaterials, Vol. 30, Seung G. Lee, Giuseppe F. Brunello, Seung S. Jang and David G. Bucknall, Molecular dynamics simulation study of P (VP-*co*-HEMA) hydrogels: Effect of water content on equilibrium structures and mechanical properties, 6130-6141, Copyright 2009, with permission from Elsevier."

The stress levels in this investigation are unusually higher than the typical stresses of 1–100 MPa for polymers observed in experiments [287]. This may be attributable to two factors. One is that the model structure used in this simulation does not have any micro- and macro-structural defects, the presence of which affects the mechanical response of the polymers by orders of magnitude [288]. Another is the very high strain rate relative to that in experimental conditions. Because most MD simulations are generally

performed up to 1-10 ns, the stresses are not sufficiently relaxed during the deformation process. Thus, rather than comparing with experimental results, we attempted to compare the mechanical response of the systems under the same simulation condition. The stress was observed to decrease with increasing water content for both monomeric sequences. We think that this is due to the water molecules acting to lubricate the segmental relaxation in the polymeric network of the P(VP-*co*-HEMA) hydrogels to help them respond the stress with respect to the imposed strain. It should be noticed though that at low water content (< 40 wt %), the random sequence hydrogel exhibits a higher stress than the blocky sequence. This behavior disappears at high water content.

Pair Correlation Function during the Deformation

To understand such stress relaxation of the hydrogel during the deformation, we analyzed the change of the pair correlation function between monomeric units, $\rho g_{N(VP)-N(VP)}(r)$, $\rho g_{C(HEMA)-C(HEMA)}(r)$ and $\rho g_{N(VP)-C(HEMA)}(r)$ during compression. For this, the 2ns MD simulation trajectory file was divided into four 500ps long trajectory files and then the pair correlation function was calculated from each divided section. Thus, information about the strain dependence in the four strain regime of 0 – 20 %, 20 – 40 %, 40 – 60 %, and 60 – 80 %, were obtained.

Figure 4.3 shows the evolution of $\rho g_{N(VP)-N(VP)}(r)$. As the compression proceeds, the intensity in the first peak increases while the second peak intensity decreases. We believe that the growth of the first peak is due to the enhancement of structural packing in the compression direction while the decrease of the second peak is due to the increasing dimension of the structure perpendicular to the compression direction. This means that the polymer networks are undergoing dynamic rearrangement during compression. For the structural relaxation, the VP monomers for both monomeric sequences are deformed regardless of the presence of water. However as Figure 4.4 reveals, the behavior of $\rho g_{C(HEMA)-C(HEMA)}(r)$ does not seem to show any systematic change but remains similar,

meaning that the short range order between HEMA monomers is not significantly affected by the compressive deformation. From these results from Figure 4.3 and Figure 4.4, we think that VP monomers are more effectively relaxed with respect to the strain in comparison with the HEMA monomers. A more significant relaxation of the VP in the blocky sequence hydrogel seems to be responsible for its lower stress level compared to that in the random sequence hydrogel although such differences are observed by the dominating contribution of water at high water content. From Figure 4.5, the behavior of $\rho g_{N(VP)-C(HEMA)}(r)$ also shows the dynamic rearrangement of VP and HEMA within the blocky sequence at 60 -80 % strain for 0 and 20 wt % water content: the intensity of the peaks at about 3 to 6 Å distance increases while the intensity at about 8 to 10 Å distance decreases. We think this is due to the structural relaxation of VP units as discussed for Figure 4.3, which is more distinct in the blocky sequence. On the contrary, we do not see any significant systematic change from other blocky sequence with high water content (40 wt and 80 wt %) as well as the random sequence. This agrees well with the stress-strain curve (Figure 4.2), showing the difference in stress between the random and the blocky sequence hydrogel with the low water contents (0 and 20 wt %) at the strain regime of 60 -80 %.

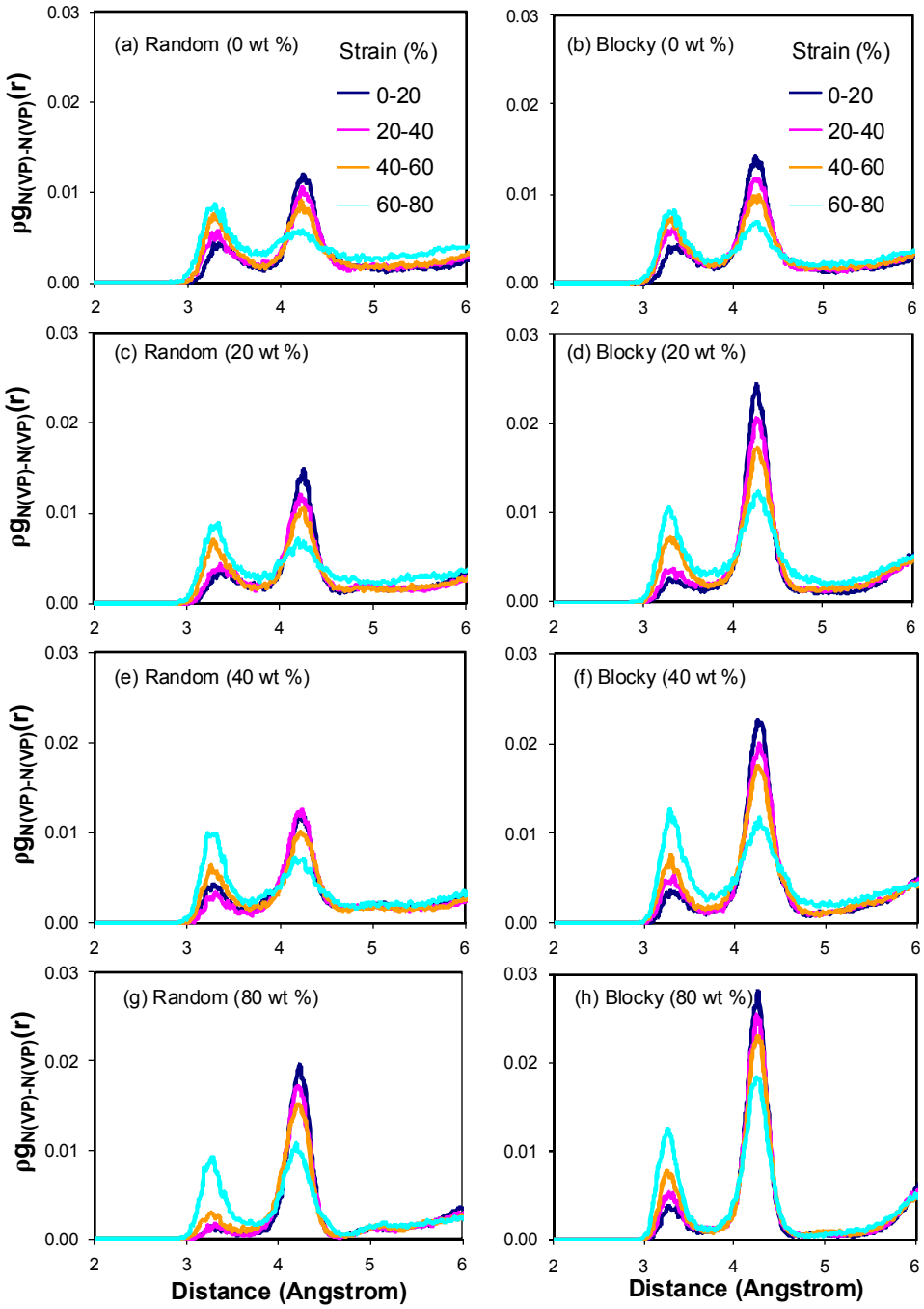

Figure 4.3: Pair correlation function of the N (VP) – N (VP) pair. The blue, magenta, orange, and cyan color denote the deformation of 0-20 %, 20-40%, 40-60%, and 60-80% of strain, respectively.

"Reprinted from Biomaterials, Vol. 30, Seung G. Lee, Giuseppe F. Brunello, Seung S. Jang and David G. Bucknall, Molecular dynamics simulation study of P (VP-*co*-HEMA) hydrogels: Effect of water content on equilibrium structures and mechanical properties, 6130-6141, Copyright 2009, with permission from Elsevier."

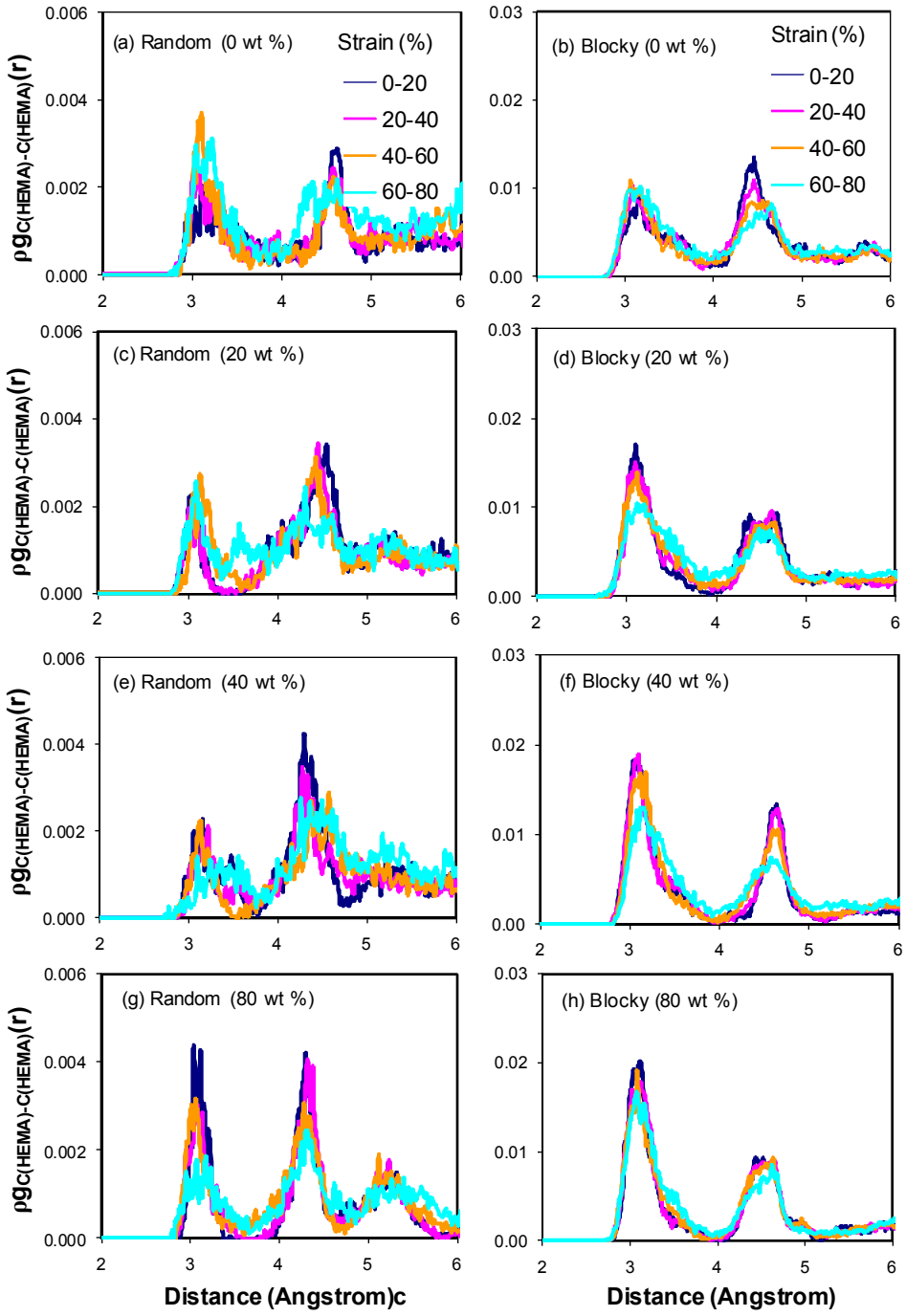

Figure 4.4: Pair correlation function of the C (HEMA) – C (HEMA) pair. The blue, magenta, orange, and cyan color denote the deformation of 0-20 %, 20-40%, 40-60%, and 60-80% of strain, respectively.

"Reprinted from Biomaterials, Vol. 30, Seung G. Lee, Giuseppe F. Brunello, Seung S. Jang and David G. Bucknall, Molecular dynamics simulation study of P (VP-*co*-HEMA) hydrogels: Effect of water content on equilibrium structures and mechanical properties, 6130-6141, Copyright 2009, with permission from Elsevier."

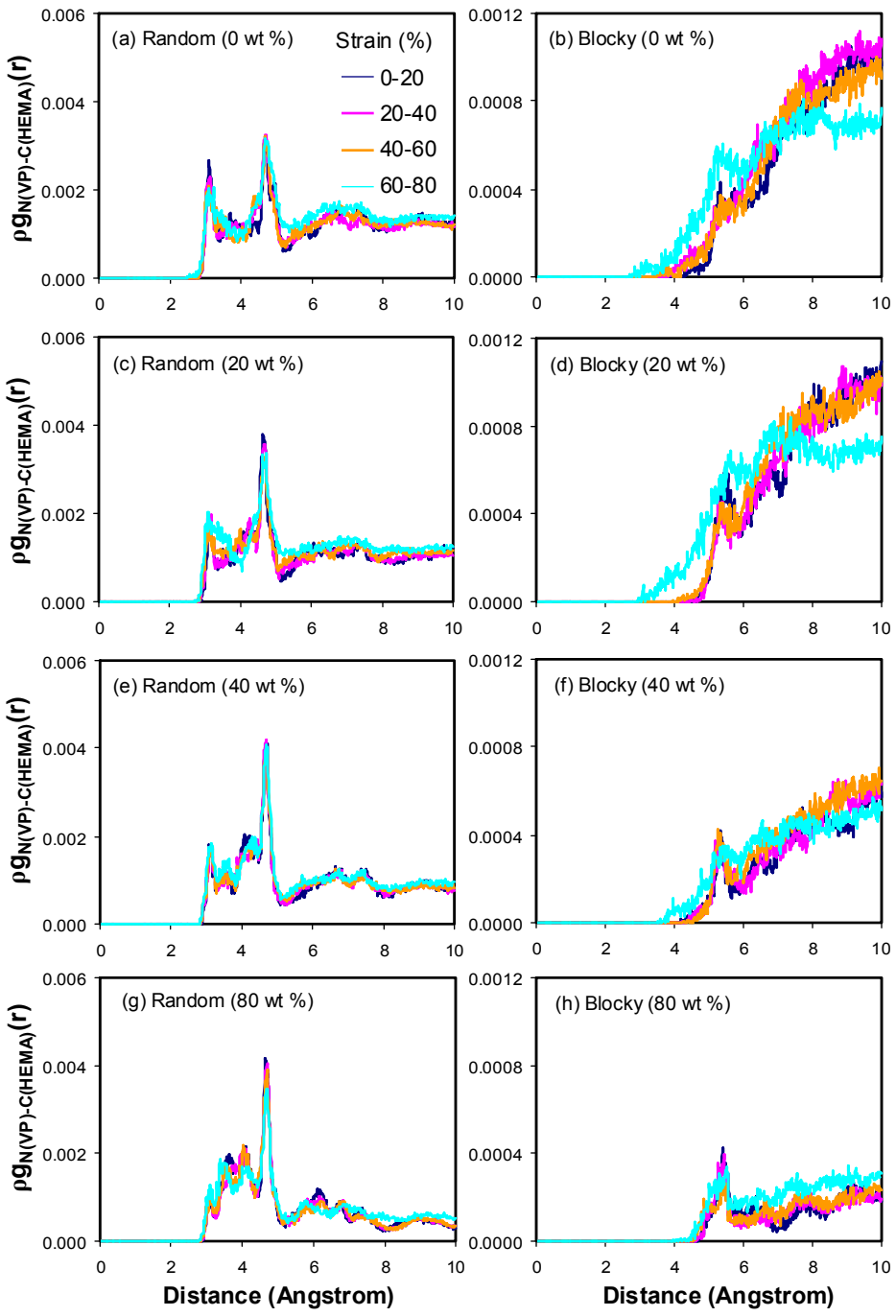

Figure 4.5: Pair correlation function of the N (VP) – C (HEMA) pair. The blue, magenta, orange, and cyan color denote the deformation of 0-20 %, 20-40%, 40-60%, and 60-80% of strain, respectively.

"Reprinted from Biomaterials, Vol. 30, Seung G. Lee, Giuseppe F. Brunello, Seung S. Jang and David G. Bucknall, Molecular dynamics simulation study of P (VP-*co*-HEMA) hydrogels: Effect of water content on equilibrium structures and mechanical properties, 6130-6141, Copyright 2009, with permission from Elsevier."

Elastic Modulus

Elastic moduli were also calculated using a constant strain minimization method [289]. In this method, a small strain ($\varepsilon = \pm 0.01$ %) is applied to the hydrogel in the direction of x, y and z axis, independently, and a subsequent energy minimization is performed. The resulting elastic moduli are summarized in Table 4.1.

As shown in Figure 4.6, at low water content (< 40 wt %), the elastic modulus of the random sequence hydrogel is larger than that of the blocky sequence hydrogel. However, this difference in the elastic modulus disappears as the water content increases, which is the same observation as the stress response at large deformation (Figure 4.2).

Table 4.1: Elastic Moduli of the hydrogels

Monomeric sequence	Random				Blocky			
Water content	0 wt %	20 wt %	40 wt %	80 wt %	0 wt %	20 wt %	40 wt %	80 wt %
Elastic Modulus (GPa)	14.59 ± 0.49	12.79 ± 0.37	11.22 ± 0.44	9.45 ± 0.18	12.74 ± 0.24	11.81 ± 0.13	11.25 ± 0.27	9.33 ± 0.25

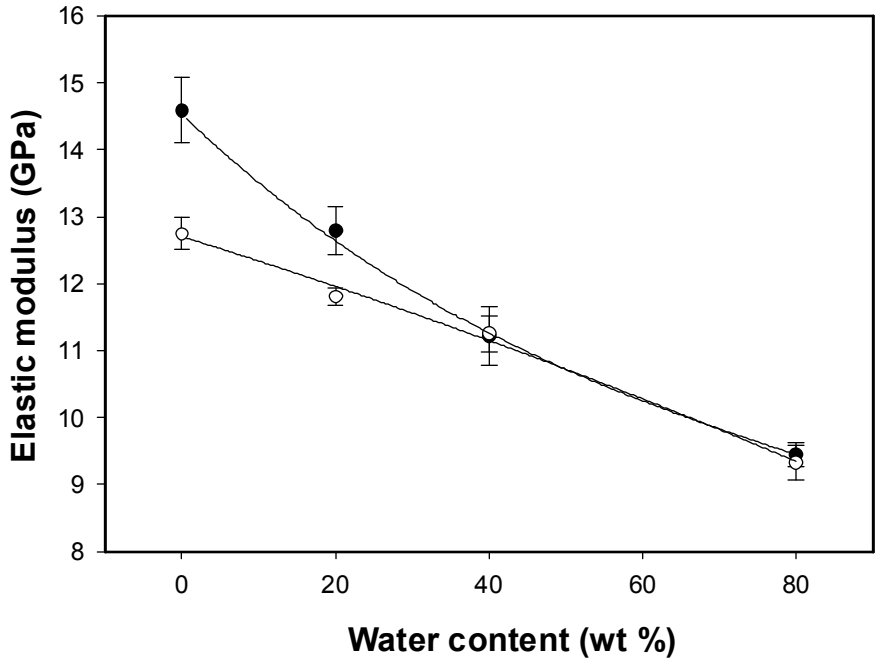

Figure 4.6: Change of elastic modulus as a function of water content.

Conclusion

Uniaxial compression MD simulations proved that the stress level is decreased with increasing water content due to the lubricating role of water molecules. By analyzing the change of the pair correlation function between the monomeric units, it was found that the structural relaxation takes place mainly through the response of VP monomers, especially in the blocky sequence. The dependence of the stress on the monomeric sequence, however, disappears with increasing water content. From this study, the properties of the P(VP-*co*-HEMA) hydrogels were shown to depend on the

monomeric sequence at low water content, whilst the water dominates all the structural and mechanical properties at high water content.

CHAPTER 5: TRANSPORT PROPERTIES OF P(VP-*co*-HEMA) HYDROGEL

Introduction

The previous chapter showed the dependence of the mechanical properties of P(VP-*co*-HEMA) on the monomeric sequence at low water contents using MD simulations, showing that the VP monomers (especially in a blocky sequence) are responsible for stress relaxation.

Here, we raise a question regarding the effect of the monomeric sequence of the P(VP-*co*-HEMA) on the transport properties of small guest molecules through the hydrogels at various water contents. At a low water content (< 40 wt %), small guest molecules are expected to be localized and isolated within the polymer network, so that the transport properties of the hydrogel would be mostly determined by the interaction of the polymer and the guest molecules. Based on our previous simulation results showing that the monomeric sequence determines the spatial distribution of the monomers, it is inferred that the guest molecules could experience different interactions with the monomeric units in hydrogels that are distributed heterogeneously, which affects the diffusion of the guest molecules. Because such effects of the monomer sequence on the diffusion of guest molecules in P(VP-*co*-HEMA) hydrogels have not yet been fully studied using a full-atomistic modeling approach, we have investigated the diffusion of two guest molecules, D-glucose and ascorbic acid (Figure 5.1), through P(VP-*co*-HEMA) hydrogels with two different monomeric sequences, one blocky and one random. In this study, the D-glucose and the ascorbic acid are chosen as model guest molecules not only because they are important molecules for essential body functionality but also because they have very similar size and constituents. Thus, we expect that studying the diffusion

of these two similar guest molecules will shed light on our understanding of how the diffusion of guest molecules in hydrogels is affected by the guest-hydrogel molecular interaction that is specified by the structures. For this, full-atomistic MD simulations have been performed to investigate the detailed structure and transport property of guest molecules through the sequence-dependent structures of the hydrogel.

(a) 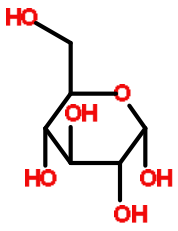

(b) 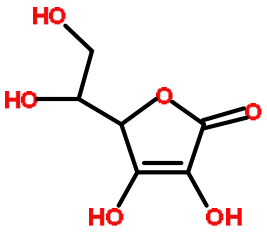

Figure 5.1: Chemical structures of (a) D-glucose and (b) ascorbic acid

Models and Simulation Details

We adopted two different structural models of P(VP-*co*-HEMA) hydrogels, consisting of a blocky sequence and a random sequence, from Chapter 3 as an initial structure to prepare the model for the study of the transport properties. In this investigation, we employed same conditions for force field and MD parameters from Chapter 3. Following the system construction, sequential canonical (NVT) and isothermal-isobaric (NPT) MD simulations were carried out to equilibrate the system for 200 ps and 16 ns, respectively, at 310.15 K. After equilibration, the guest molecules, D-glucose or ascorbic acid were added to the system with the random and the blocky sequence, respectively. The positions of each guest molecule were randomly selected in the model system. All of the systems were equilibrated by running 10 – 40 ns NPT MD simulations at 310.15 K. Data collection for the analyses was performed during a subsequent 10 - 20 ns NPT MD simulation.

Results and Discussion

Equilibrated Structure

The last snapshots from the final MD simulations are shown in Figure 5.2, in which the differences in the monomeric sequences of the hydrogels are clearly observed: the random P(VP-*co*-HEMA) presents more dispersed monomeric units (left side of Figure 5.2), while the blocky P(VP-*co*-HEMA) has a more segregated presentation (right side of Figure 5.2). Two independent hydrogel models for each monomer sequence were prepared that contained three molecules of either D-glucose or ascorbic acid, corresponding to a concentration of 0.03 ~ 0.14 M. The characteristics of the equilibrated P(VP-*co*-HEMA) hydrogels are shown in Table 5.1.

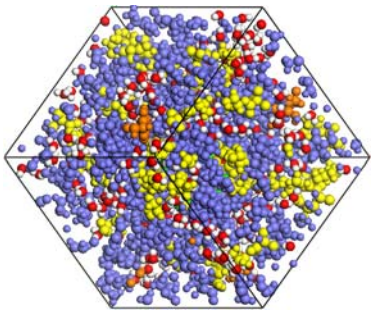

(a) Random (20 wt %, ascorbic acid)

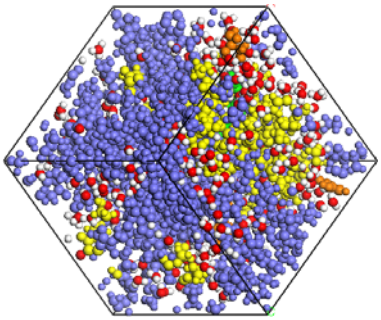

(b) Blocky (20 wt %, ascorbic acid)

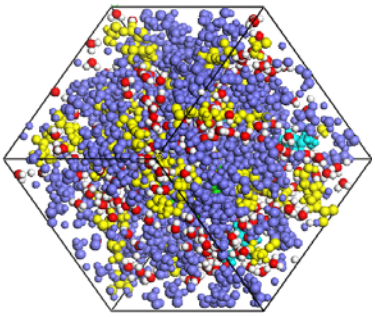

(c) Random (20 wt %, D-glucose)

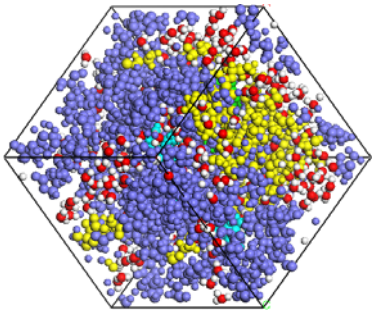

(d) Blocky (20 wt %, D-glucose)

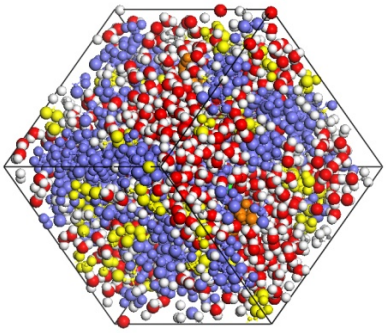

(e) Random (40 wt %, ascorbic acid)

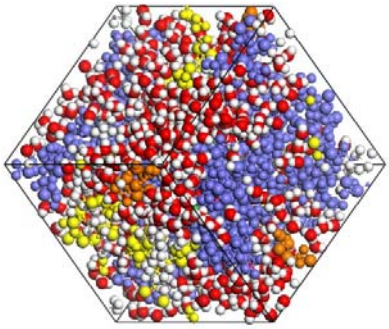

(f) Blocky (40 wt %, ascorbic acid)

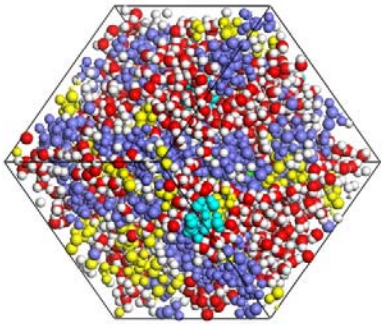

(g) Random (40 wt %, D-glucose)

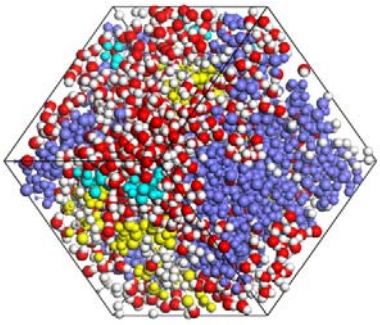

(h) Blocky (40 wt %, D-glucose)

Figure 5.2: (Continued on next page.)

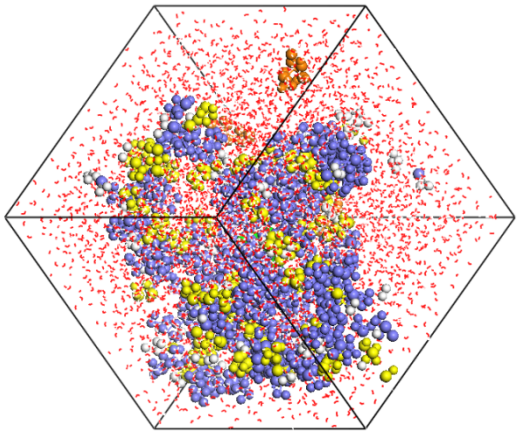

(i) Random (80 wt %, ascorbic acid)

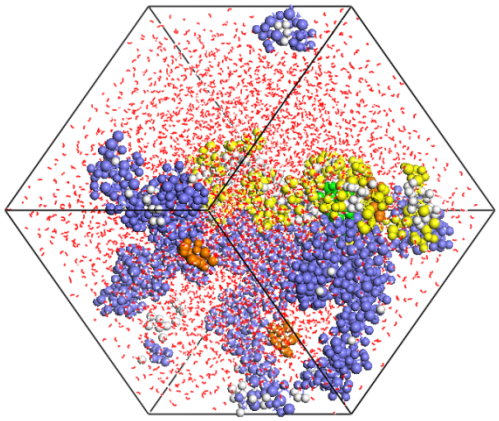

(j) Blocky (80 wt %, ascorbic acid)

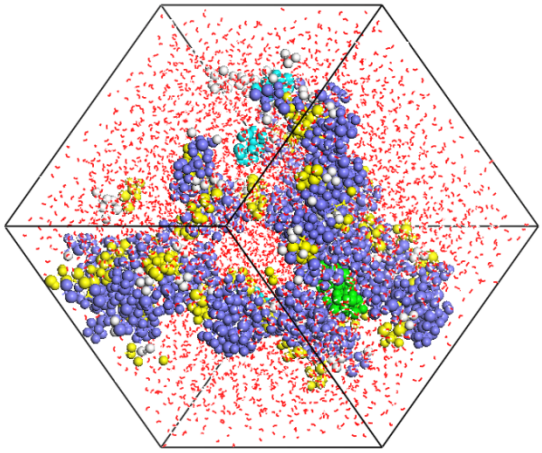

(k) Random (80 wt %, D-glucose)

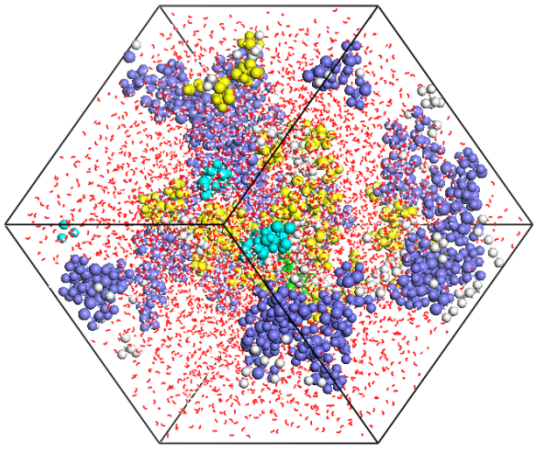

(l) Blocky (80 wt %, D-glucose)

Figure 5.2: Equilibrated *random* P(VP-*co*-HEMA) hydrogels with (a) ascorbic acid and (c) D-glucose with 20 wt % water content, (e) ascorbic acid and (g) D-glucose with 40 wt % water content, and (i) ascorbic acid and (k) D-glucose with 80 wt % water content; equilibrated *blocky* P(VP-*co*-HEMA) hydrogels with (b) ascorbic acid and (d) D-glucose with 20 wt % water content, (f) ascorbic acid and (h) D-glucose with 40 wt % water content, and (j) ascorbic acid and (l) D-glucose with 80 wt % water content. Blue, yellow, green, orange, and cyan color denotes VP, HEMA, MBA, ascorbic acid, and D-glucose, respectively. The oxygen and hydrogen of the water molecule are represented by red and white colors, respectively. The ball size of the water molecules with 80 wt % water content is reduced for clarity.

Table 5.1: Characteristics of the hydrogels

Monomeric sequence	Random						Blocky					
Monomer composition	VP: HEMA = 37: 13						VP=37 and HEMA=13					
Degree of randomness	1.17						0.10					
Cross-linking molecular weight, M_c	5804.16						5804.16					
Simulated temperature (K)	310.15						310.15					
Guest molecule	Ascorbic acid			D-glucose			Ascorbic acid			D-glucose		
Water content	20 wt %	40 wt %	80 wt %	20 wt %	40 wt %	80 wt %	20 wt %	40 wt %	80 wt %	20 wt %	40 wt %	80 wt %
Number of water molecule	248	661	3969	248	661	3969	248	661	3969	248	661	3969
Number of guest molecules (concentration, M)	3 (0.14)	3 (0.10)	3 (0.03)	3 (0.14)	3 (0.10)	3 (0.03)	3 (0.14)	3 (0.10)	3 (0.03)	3 (0.14)	3 (0.10)	3 (0.03)
Density (g/cm^3)	1.065 ± 0.007	1.034 ± 0.007	1.016 ± 0.004	1.058 ± 0.007	1.035 ± 0.007	1.016 ± 0.003	1.062 ± 0.007	1.032 ± 0.006	1.014 ± 0.004	1.046 ± 0.007	1.031 ± 0.007	1.014 ± 0.004
Simulated volume ($Å^3$)	35669 ± 226	48664 ± 329	146984 ± 518	35904 ± 226	48631 ± 326	147025 ± 504	35749 ± 221	48781 ± 307	147205 ± 508	36313 ± 243	48832 ± 339	147210 ± 514
Mesh size, ξ (Å)	32.92 ± 0.07	36.51 ± 0.08	52.77 ± 0.06	32.99 ± 0.07	36.50 ± 0.08	52.78 ± 0.06	32.94 ± 0.07	36.54 ± 0.08	52.80 ± 0.06	33.11 ± 0.07	36.55 ± 0.08	52.80 ± 0.06

Distribution of guest molecules

To check the distribution of the guest molecules, we analyzed the pair correlation function (PCF, see Equation 25) of the guest molecules with the P(VP-*co*-HEMA) hydrogels. Using this function, it is possible to determine in what environment the guest molecules are found. For this study, $\rho g(r)$, the product of $g(r)$ and the number density (ρ), is used instead of $g(r)$ to directly compare the absolute values between various systems. For quantitative analysis, the coordination number (CN) is calculated by integrating the first peak in the PCF. Figure 5.3 shows the three pairs of interest: *i)* $\rho g_{N(VP)-O(guest\ molecule)}$ for the nitrogen of the VP (N (VP)) and the oxygen of the guest molecule (O (guest molecule)); *ii)* $\rho g_{C(HEMA)-O(guest\ molecule)}$ for the alpha carbon of the HEMA (C (HEMA)) and O (guest molecule); and *iii)* $\rho g_{O(HEMA)-O(guest\ molecule)}$ for the oxygen of the hydroxyl group of the HEMA (O (HEMA)) and O (guest molecule).

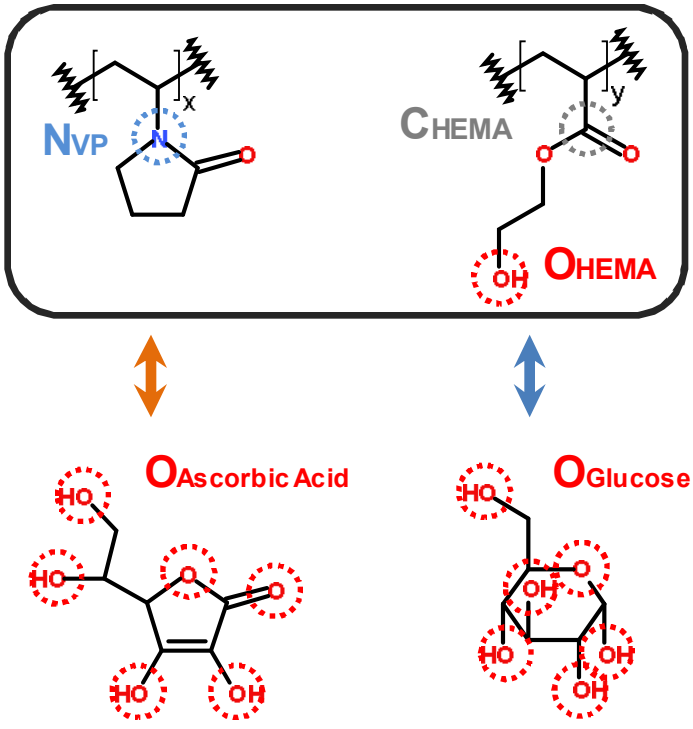

Figure 5.3: Atoms used to calculate the pair correlation function.

In Figure 5.4 and Figure 5.5, we show the $\rho g(r)$ values of the P(VP-*co*-HEMA) hydrogels with the random and blocky sequence with 20, 40 and 80 wt % water content.

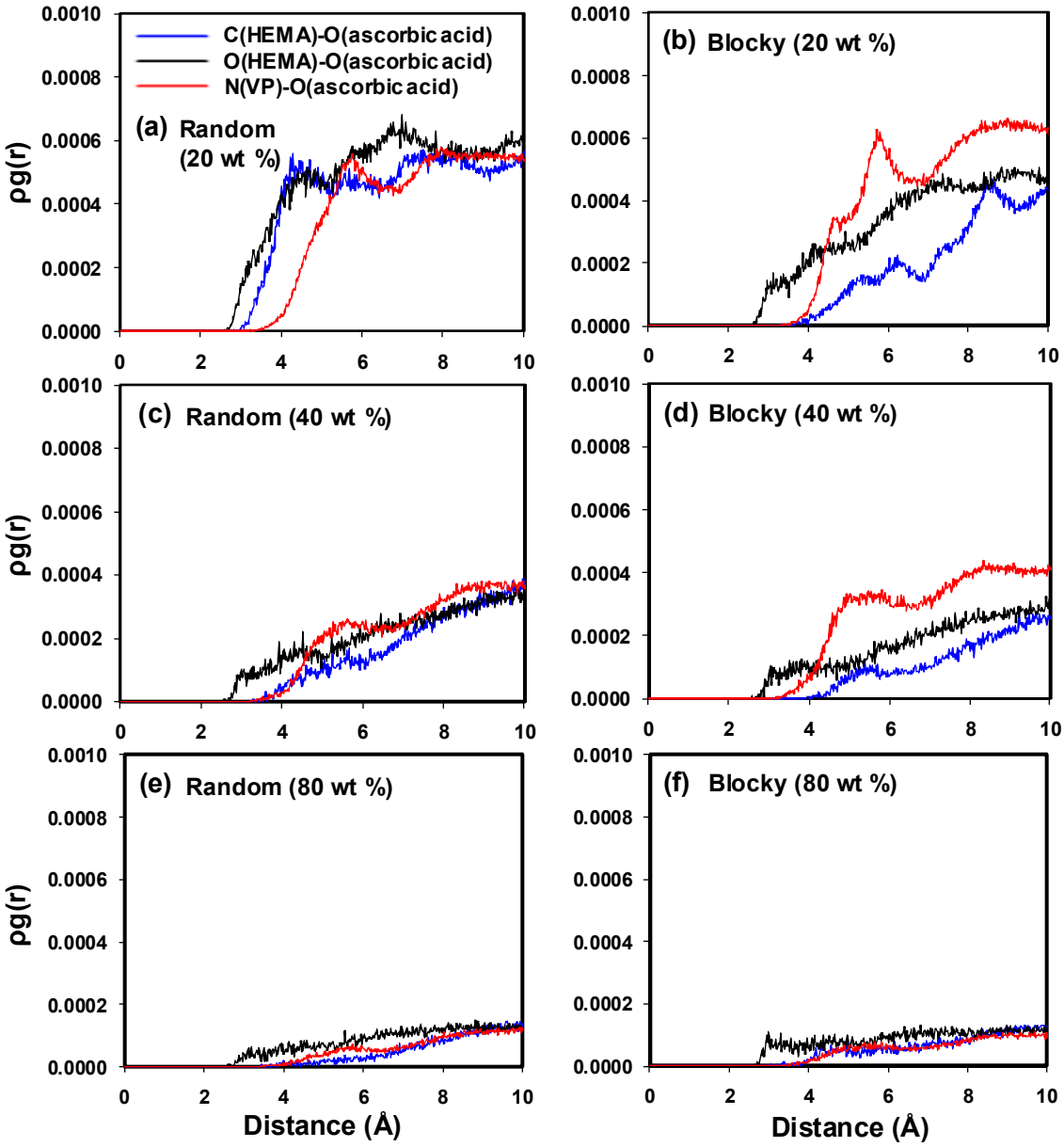

Figure 5.4: Pair correlation functions of ascorbic acid in the P(VP-*co*-HEMA) hydrogel: ascorbic acid in the random sequence with 20 wt % (a), 40 wt % (c), and 80 wt % water content (e) and in the blocky sequence with 20 wt % (b), 40 wt % (d), and 80 wt % water content (f).

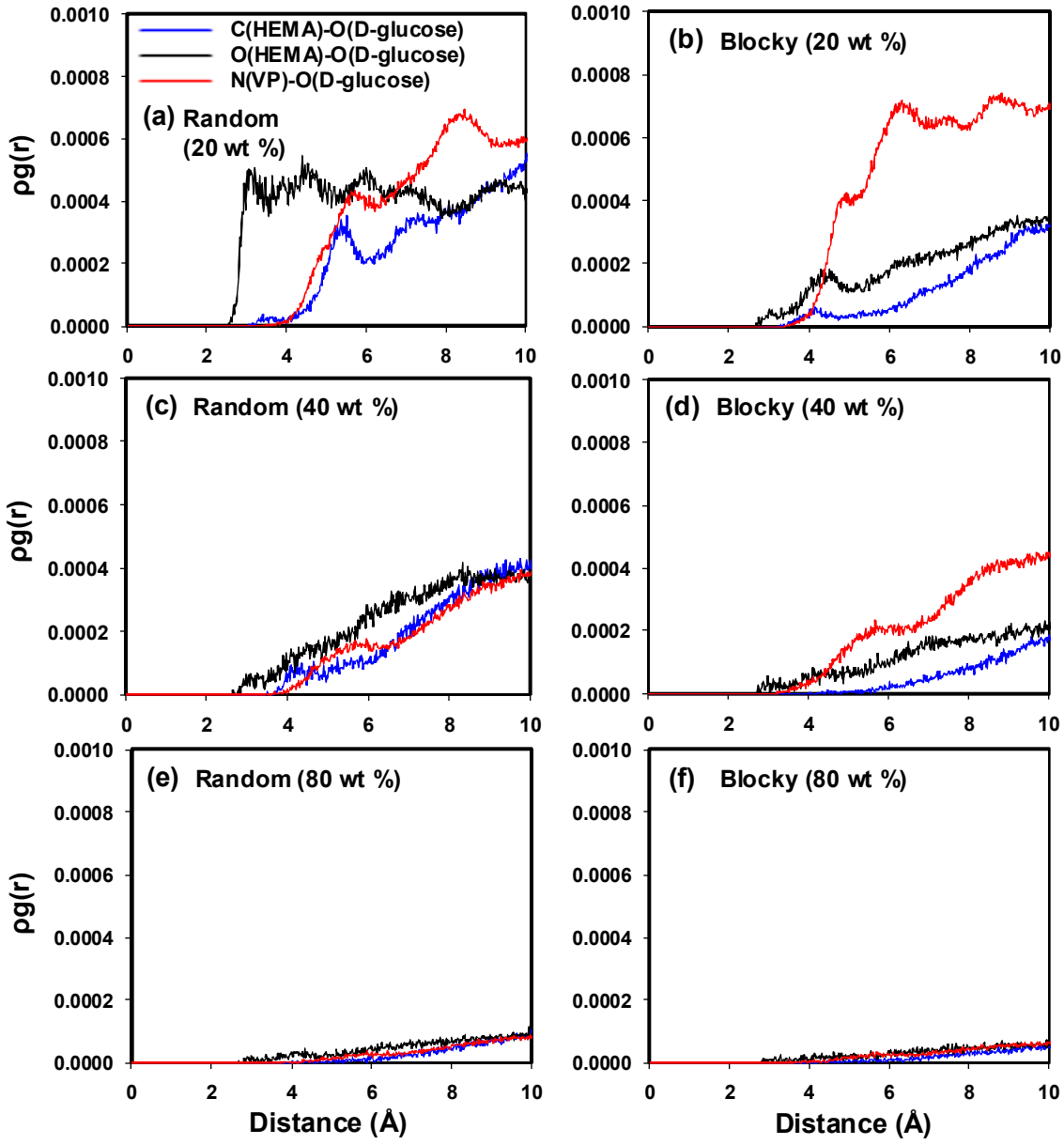

Figure 5.5: Pair correlation functions of D-glucose in P(VP-*co*-HEMA) hydrogel: ascorbic acid in the random sequence with 20 wt % (a), 40 wt % (c), and 80 wt % water content (e) and in the blocky sequence with 20 wt % (b), 40 wt % (d), and 80 wt % water content (f).

Figure 5.4 and Figure 5.5 show that the $\rho g_{O(HEMA)-O(guest\ molecule)}$ appears at ~ 2.5 Å, while the other $\rho g(r)$s appears at ~ 3.5 Å because of the location of O (HEMA) (the

oxygen of the terminal hydroxyl group in HEMA) unit is more accessible for the guest molecules in comparison with C (HEMA) and N (VP).

By comparing Figure 5.4 (a) and (b) for 20 wt % water content, we found that the peak intensities for the $\rho g_{C(HEMA)-O(ascorbic\ acid)}$ and the $\rho g_{O(HEMA)-O(ascorbic\ acid)}$ depend on the monomer sequence of P(VP-*co*-HEMA): $\rho g_{X(HEMA)-O(ascorbic\ acid)}$ (X=C or O) has a smaller intensity at ~5 Å for the blocky sequence hydrogel. As shown in Table 5.2, the calculated CNs for 20 wt % water content from the first peak of $\rho g_{C(HEMA)-O(ascorbic\ acid)}$ and $\rho g_{O(HEMA)-O(ascorbic\ acid)}$ for the blocky sequence are 2 ~ 4.3 times smaller than those for the random sequence.

Table 5.2: Guest molecule coordination number (CN) from the X-O (guest molecule) pair in the P(VP-*co*-HEMA) hydrogel

Guest molecule	X	CN			Range of pair correlation distance, r (Å)
		20 wt %	40 wt %	80 wt %	
Ascorbic Acid	C_{HEMA} (random)	0.17	0.03	0.00	< 5.1
	O_{HEMA} (random)	0.18	0.06	0.03	< 5.1
	N_{VP} (random)	0.43	0.22	0.05	< 6.8
	C_{HEMA} (blocky)	0.04	0.02	0.02	< 5.5
	O_{HEMA} (blocky)	0.09	0.04	0.03	< 5.1
	N_{VP} (blocky)	0.45	0.30	0.06	< 6.8
D-glucose	C_{HEMA} (random)	0.10	0.05	0.00	< 5.8
	O_{HEMA} (random)	0.20	0.05	0.01	< 5.1
	N_{VP} (random)	0.35	0.14	0.02	< 6.8
	C_{HEMA} (blocky)	0.01	0.00	0.00	< 4.7
	O_{HEMA} (blocky)	0.05	0.02	0.01	< 5.1
	N_{VP} (blocky)	0.55	0.19	0.02	< 6.8

The PCFs for D-glucose (Figure 5.5 (a) and (b)) also show dependency on the monomer sequence: the CN results for 20 wt % water content (Table 5.2) show that the CNs of the major peaks of the $\rho g_{C(HEMA)-O(D-glu\cos e)}$ and the $\rho g_{O(HEMA)-O(D-glu\cos e)}$ for the blocky sequence show smaller values than do those for the blocky sequence. The intensity of the first peak for $\rho g_{N(VP)-O(ascorbic\ acid)}$ and $\rho g_{N(VP)-O(D-glu\cos e)}$ is less affected by the monomer sequence of the hydrogel than are those of $\rho g_{X(HEMA)-O(guest\ molecule)}$, as shown in Figure 5.4 and Figure 5.5, but the CNs from the blocky sequence show higher values than do those from the random sequence, as shown in Table 5.2. The CNs from $\rho g_{N(VP)-O(ascorbic\ acid)}$ and $\rho g_{N(VP)-O(D-glu\cos e)}$ show larger values than do those of $\rho g_{X(HEMA)-O(ascorbic\ acid)}$ and $\rho g_{X(HEMA)-O(D-glu\cos e)}$ for both monomeric sequences, indicating that the guest molecule has a greater accessibility to the VP units than do the HEMA units in both monomeric sequences. We expect that hydrophilic guest molecules, such as ascorbic acid and D-glucose, may tend to be more associated with the VP units because the VP units are more hydrophilic than the HEMA units, as evaluated by previous experiments [46, 103, 105, 110, 228] and simulations [290, 291]. The guest molecules can be confined within the polymer network in low hydration conditions. This confinement can lead to the guest molecules having more interactions with the polymer network, especially with the more hydrophilic part, the VP units. Detailed discussion of the confinement will be shown in next section.

To explain this monomeric sequence effect on P(VP-*co*-HEMA) hydrogel with 20 wt % water content, we calculated the solvent accessible surface area (SASA) of the monomeric units to check the accessible surface for the guest molecule. The probe radius for calculating the SASA was set to be 2.78 Å and 2.71 Å, which are the hydrodynamic radii (r_h) [33] of D-glucose and ascorbic acid, respectively. It is shown in Table 5.3 that the SASA of the VP unit has a lager accessible area than the HEMA unit for the guest molecules, which agrees with the results of the PCFs and CNs. It is also observed that

the blocky sequence hydrogel is 29 – 37% and 4 - 15 % larger than those of the random sequence hydrogel for the VP units and the HEMA units, respectively. The SASA of the VP units is more sensitively affected by the monomeric sequence than is the SASA of the HEMA units. Because the HEMA units are randomly distributed among the VP units in the random sequence hydrogel, the HEMA units can hinder the probe in its detection of the VP units in the random sequence. As we mentioned above, the $\rho g_{O(HEMA)-O(guest\ molecule)}$ appears at ~ 2.5 Å, while the other $\rho g(r)$ s appear at ~ 3.5 Å, indicating that the O (HEMA) unit is more accessible to the probe, especially in the random sequence. It was also found that the root-mean-square radius of gyration is 1.92 ± 0.33 Å for the VP unit and 2.61 ± 0.01 Å for the HEMA unit at 310K, indicating that the HEMA unit is longer than the VP unit by ~ 36 %. Therefore, the guest molecules can be hindered in accessing the VP units by the HEMA units in the random sequence, which leads to smaller CNs for $\rho g_{N(VP)-O(guest\ molecule)}$ and higher CNs for $\rho g_{X(HEMA)-O(guest\ molecule)}$ in the random sequence than in the blocky sequence at the low water content.

Table 5.3: Solvent accessible surface area of VP units and HEMA units with respect to guest molecules

	Random Sequence		Blocky sequence	
	VP	**HEMA**	**VP**	**HEMA**
Ascorbic acid (Probe radius=2.71 Å^2)	1465 ± 75 Å^2	653 ± 66 Å^2	1893 ± 88 Å^2	678 ± 20 Å^2
D-glucose (Probe radius=2.78 Å^2)	1650 ± 109 Å^2	690 ± 56 Å^2	2253 ± 66 Å^2	796 ± 51 Å^2

However, this monomeric sequence effect is significantly reduced with 40 wt % water content (see (c), (d) of Figure 5.4 , Figure 5.5 and Table 5.2) and disappeared with 80 wt % water content (see (e), (f) of Figure 5.4 , Figure 5.5 and Table 5.2). This occurs

because the polymer chains are swelled by increasing the water content. Therefore, the hydrophilic guest molecules, such as ascorbic acid [292] and D-glucose [293], are more likely to be associated with water molecules than with the polymer network at the high water content. To determine in what environment the guest molecules are associated with the water molecules, we characterized the water distribution around the guest molecules by PCF of the oxygen of the guest molecule and the oxygen of the water molecule ($\rho g_{O(guest\ molecules)-O(water)}$), as shown in Figure 5.6. The water CN for the guest molecules was also analyzed in Table 5.4. It is clearly shown that the intensities of the PCFs and CNs are increased with increasing water content.

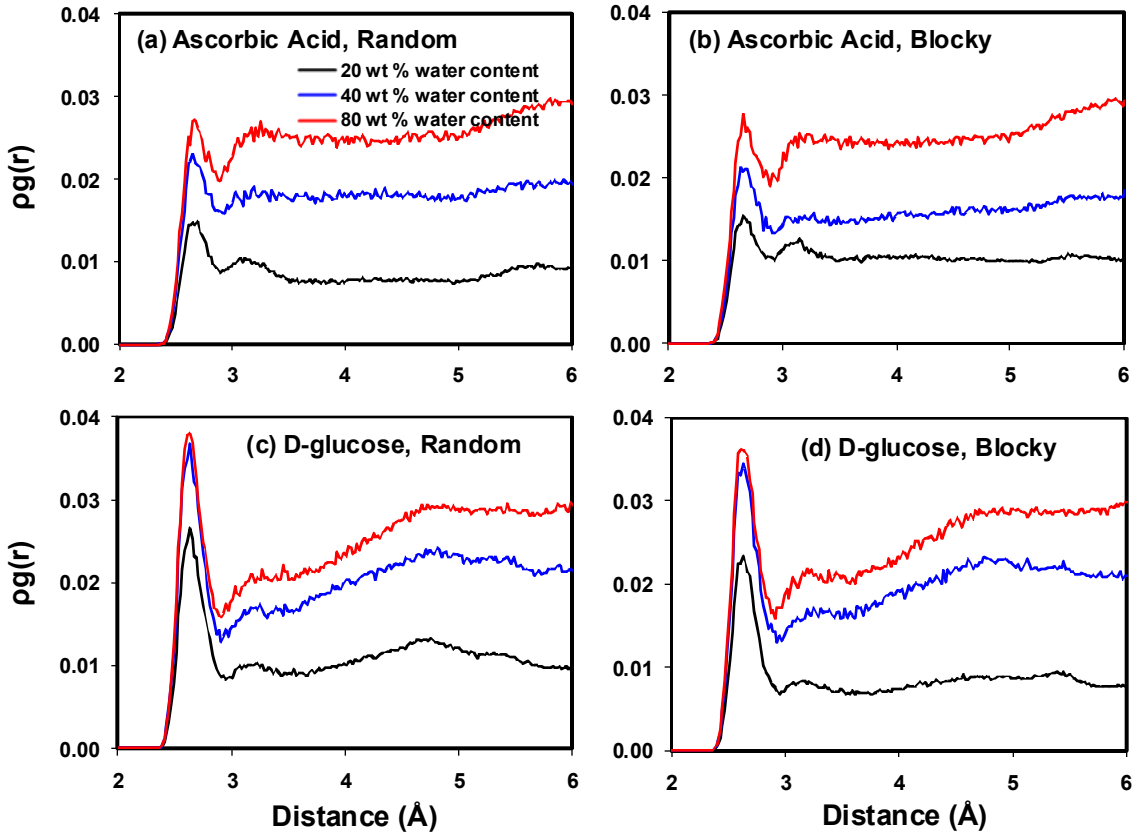

Figure 5.6: Pair correlation functions of O(ascorbic acid)-O(water) in random sequence (a) and in blocky sequence (b); pair correlation functions of O(D-glucose)-O(water) in random sequence (c) and in blocky sequence (d).

Table 5.4: Coordination number (CN) from the O(guest molecule)-O(water) pair in a P(VP-*co*-HEMA) hydrogel

		Random Sequence	Blocky sequence	Range of pair correlation distance, r (Å)
Ascorbic acids	20 wt %	0.45	0.48	< 2.9
	40 wt %	0.72	0.66	< 2.9
	80 wt %	0.87	0.85	< 2.9
D-glucoses	20 wt %	0.69	0.62	< 2.9
	40 wt %	0.97	0.96	< 2.9
	80 wt %	1.05	1.05	< 2.9

Diffusion of guest molecules

The diffusion of the guest molecule is another interesting aspect of the hydrogel because of its importance for bio-applications, such as tissue engineering and drug delivery, in which small guest molecules can be transported. From numerous studies [294-302] focusing on the variables affecting solute transport, it is understood that the transport properties are strongly dependent upon many factors, such as mesh size, swelling ratio, ionization, ionic strength, pH condition, and temperature. In our simulations, the numbers of each guest molecule are the same for all P(VP-*co*-HEMA) hydrogels to check the effect of the water content on the transport properties of the guest molecule. The mean square displacement (MSD) of the guest molecules in the hydrogels was obtained from the last 5 ns of our NPT MD simulations and was used to calculate the diffusion coefficients (D), defined by

$$D = \lim_{t\to\infty} \frac{1}{6t} \left\langle \left(r(t) - r(0) \right)^2 \right\rangle \qquad \textbf{(34)}$$

where $r(t)$ and $r(0)$ are the positions of the target molecules at a time t that is greater than 0 and at t = 0, respectively. It is known that from equation (35) that

$$\left\langle (r(t) - r(0))^2 \right\rangle \sim t^{\alpha} \qquad \textbf{(35)}$$

The diffusion is normal if MSD, $\left\langle (r(t) - r(0))^2 \right\rangle$, is proportional to time *t* with α = 1. If the diffusion of molecules is hindered or obstructed by the structure of the system, the value of α is smaller than 1, which is known as an anomalous subdiffusion [303, 304]. This has been observed in various systems, such as membranes [305, 306], hydrogel [307], and porous media [308]. Weiss at al. [304] reported the anomalous subdiffusion of cytoplasmic macromolecules in a living cell, with values of α between 0.59 and 0.84. Ghosh and Webb [309] found anomalous subdiffusion of the low density lipoprotein receptor molecules in human skin fibroblasts, with α = 0.2 to 0.9. Schwille et al. [310, 311] reported that the IgE receptor and fluorescent lipid analogs in rat basophilic leukemia cells showed anomalous subdiffusion, with values of α between 0.7 and 0.8. Gallo and Rovere [312] studied the mobility of water molecules in a silica pore at the low hydration regime. They found α = 0.46 – 0.48 with 38 % and 58 % hydration levels of the pore. Azurmendi and Ramia [307] investigated the anomalous subdiffusion of water molecules in a cross-linked sucroses and diepoxide hydrogel with 18 %, 40 %, and 96 % hydration levels. They reported α values of 0.43 and 0.61 for 18 % and 40 % hydration levels, respectively. Jang et al. [33] reported that the ascorbic acid and D-glucose in the poly(ethylene oxide)–poly(acrylic acid) double network hydrogel with 76 % water content showed values of α between 0.74 and 0.82.

In this study, shown in Figure 5.7, we obtained α values of 0.36 – 0.47 for 20 wt % water content, 0.62 – 0.80 for 40 wt % water content, and 0.79 – 0.89 for 80 wt % water content P(VP-*co*-HEMA) hydrogels, respectively. These results clearly indicate

that the diffusion of the guest molecules corresponds to the anomalous subdiffusion and is seriously depressed in low hydration hydrogel systems (20 wt % water content). The anomalous subdiffusion approaches normal diffusion as the water content increase to a high level of hydration.

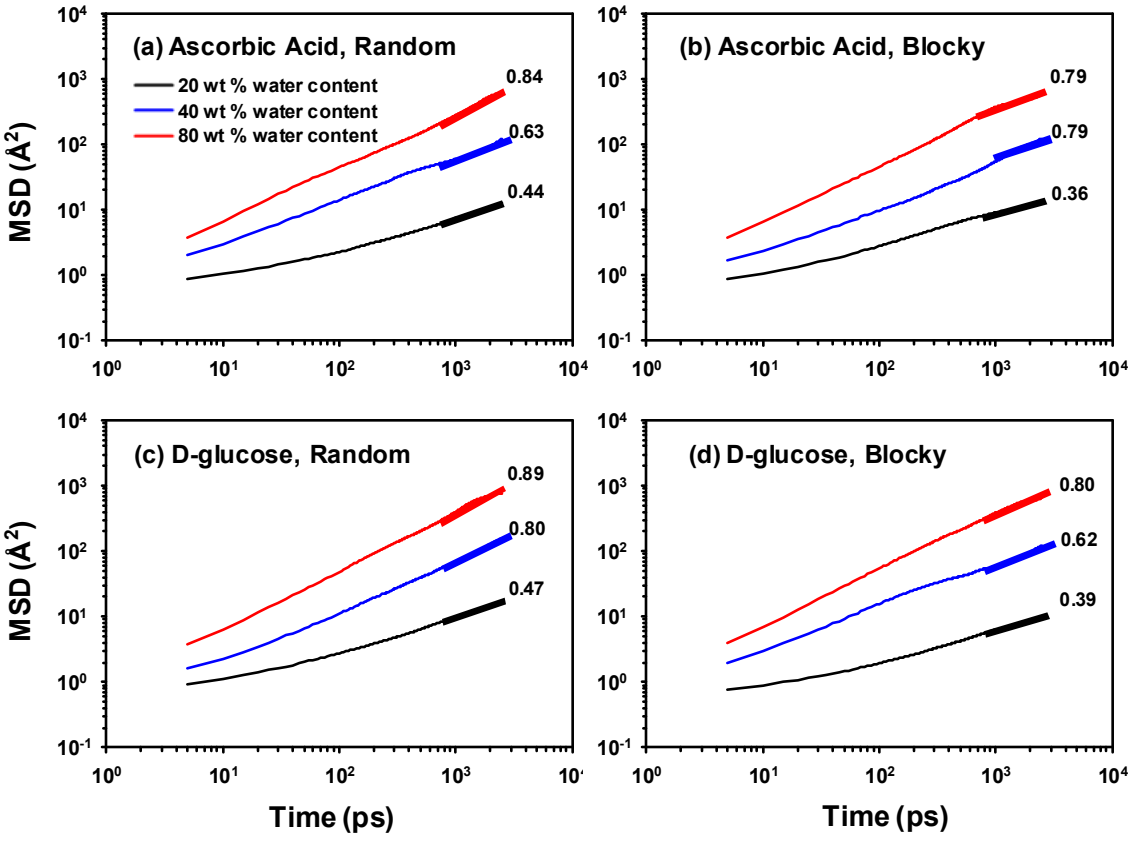

Figure 5.7: Mean square displacement (MSD) of logarithmic plots for the guest molecules in the P(VP-*co*-HEMA) hydrogel, with ascorbic acid in a random sequence (a) and blocky sequence (b) and with D-glucose in a random sequence (c) and blocky sequence (d).

Table 5.5: Chemical formula, molecular weight, and diffusion coefficient of guest molecules at 310 K

		Ascorbic Acid		D-Glucose	
Chemical formula		$C_6H_8O_6$		$C_6H_{12}O_6$	
Molecular weight, MW		176.126		180.157	
Monomeric sequence		Random	Blocky	Random	Blocky
Diffusion coefficient, D ($\times 10^{-6}$ cm^2/s)	**20 wt % water content**	0.02	0.01	0.02	0.01
	40 wt % water content	0.80	0.68	0.79	0.67
	80 wt % water content	2.85	2.83	2.72	2.51

Table 5.5 summarizes the diffusion coefficients for ascorbic acid and D-glucose for each sequence hydrogel. Unfortunately, there is no available experimental diffusion coefficient for our particular systems. However, we found several experimental diffusion coefficient data for the guest molecule in bulk water at room temperature. Thus, we also prepared reference model simulations that contain water molecules with the guest molecules for comparison to the experimental diffusion coefficient results to validate our simulations. Our reference model contains 1200 water molecules with the same number of guest molecules and a similar periodic box size of the models, with 20 wt % water content. The reference models were equilibrated by running 10 ns NPT MD simulations at 298.15 K. Then, an additional 10 ns NPT MD simulation was performed for data collection. The diffusion coefficients are calculated to be 5.76×10^{-6} cm^2/s ($\alpha = 1$) and 6.62×10^{-6} cm^2/s ($\alpha = 1$) for ascorbic acids and D-glucoses, respectively. The experimental values are $5.80 – 5.97 \times 10^{-6}$ cm^2/s and $6.51 – 6.78 \times 10^{-6}$ cm^2/s for ascorbic acids [313] and D-glucoses [314-316], respectively. Thus, the diffusion coefficients from our reference model simulations agree with the experimental values obtained under

similar conditions. We also found the diffusion coefficient of ascorbic acid and D-glucose in the PEO hydrogel system with 76 % and 80 wt % water content, which are comparable with the 80 % water content of P(VP-*co*-HEMA) hydrogel system in this study. Jang et al. [33] reported that the diffusion coefficient of ascorbic acid and D-glucose in the poly(ethylene oxide)–poly(acrylic acid) double network hydrogel with 76 % water content is $1.11 – 2.53 \times 10^{-6}$ cm^2/s and $1.07 – 2.49 \times 10^{-6}$ cm^2/s at 300 K, respectively. Myung et al. observed that the diffusion coefficient of glucose is $0.9 - 1.8 \times 10^{-6}$ cm^2/s in poly(ethylene glycol) hydrogels with 80 wt % water content [317] at room temperature.

Table 5.5 shows that the diffusion coefficients of ascorbic acid and D-glucose in the random sequence hydrogel are twice as high as in the blocky sequence hydrogel for 20 wt % content, while the difference is decreased by ~ 18 % and ~ 8 % when increasing the water content to 40 wt % and 80 wt %, respectively. At the low water content, the guest molecule has more interaction with the *block* of VP units in the blocky sequence hydrogel than in the random sequence hydrogel, leading to the slow diffusion of the hydrophilic guest molecules in the blocky sequence hydrogel. These results agree with the results of the PCFs and CNs. It has been also observed that the dynamics of hydrophilic molecules, such as water, become slow near a hydrophilic substrate in the highly confined environment [318, 319]. Therefore, a hydrophilic domain, such as the VP units in the blocky sequence hydrogel, can slow down the mobility of the hydrophilic molecule at the low water content. However, the monomeric sequence effect on the diffusion coefficients of the guest molecule is significantly decreased with an increasing the water content.

Next, to characterize the diffusion mechanism of the guest molecules, we monitored the total displacement of the center of mass of the guest molecules from the initial position to their position at time t during the last 10 ns of the NPT MD simulation, as shown in Figure 5.8. It is observed that the total displacement of the guest molecules

is significantly suppressed at the low water content (20 wt % water content). The guest molecules at 20 wt % water content seem to be bound at a certain location within the hydrogel or diffused within a confined pocket within the hydrogel. It is observed that the guest molecules in the 40 wt % and the 80 wt % water content hydrogels can diffuse through a water channel in the polymer network.

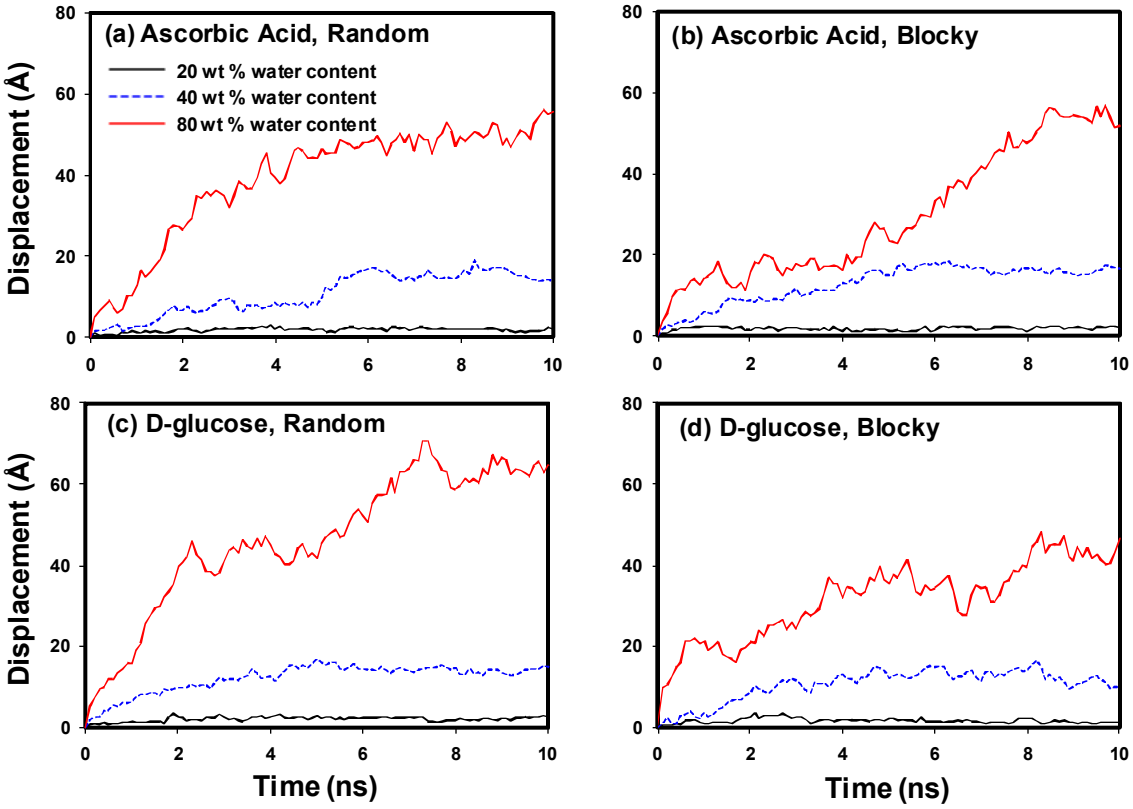

Figure 5.8: Total Displacement of the center of mass of the guest molecules in the P(VP-*co*-HEMA) hydrogel during the last 10 ns of the NPT MD simulation for ascorbic acid in the random sequence (a) and in the blocky sequence (b) and for D-glucose in the random sequence (c) and in the blocky sequence (d).

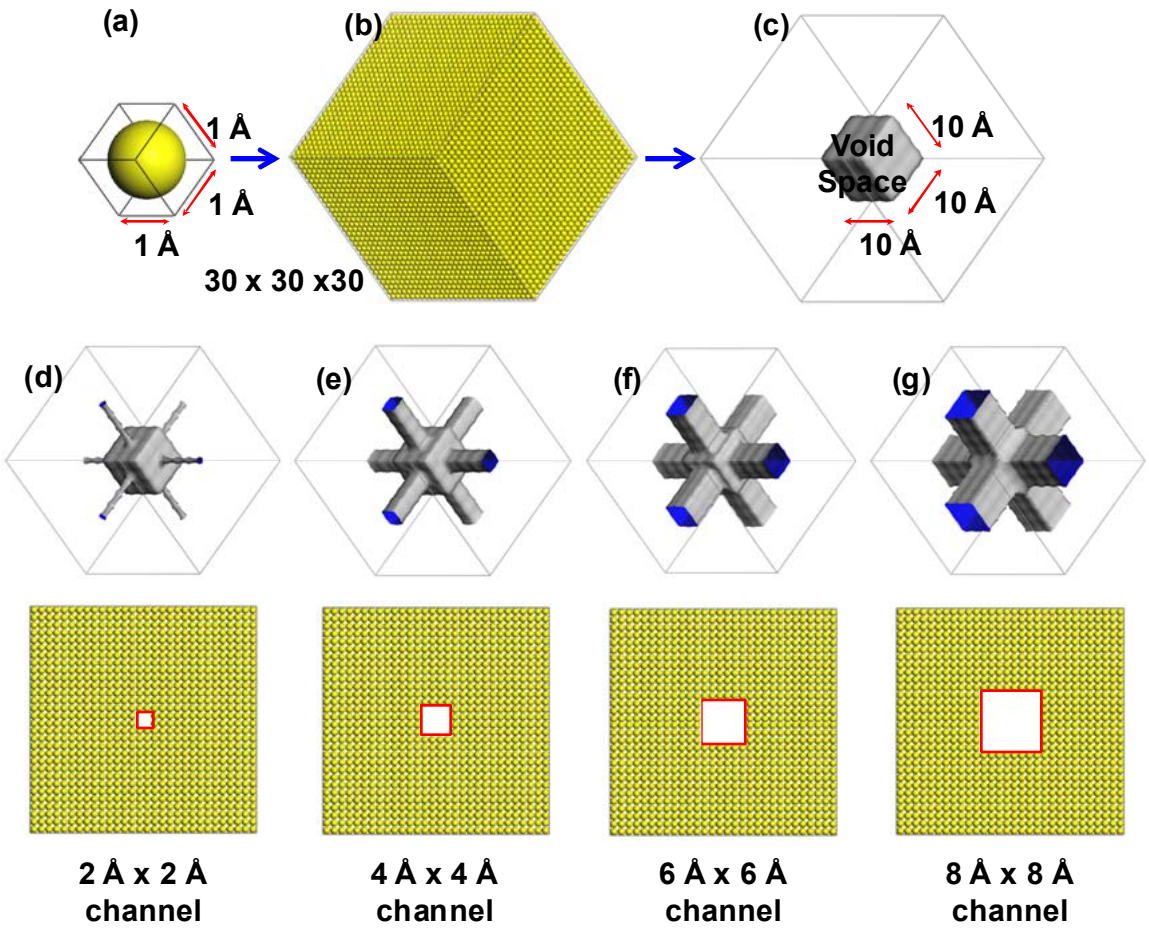

Figure 5.9: Theoretical models to investigate the relationship between the size of the channel in the system and the available surface area; (a) a unit structure with a dummy atom with a van der Waals radius of 0.5 Å; (b) a superstructure made of 30 × 30 × 30 unit structures; and (c) a model with a cubical void of 10 Å × 10 Å × 10 Å at the center. Models with various cross-sectional areas for the channel: (d) 2 Å × 2 Å; (e) 4 Å × 4 Å; (f) 6 Å × 6 Å; and (g) 8 Å × 8 Å. The dummy atoms are invisible in models (c), (d), (e), (f) and (g) to allow for a clear view of the void and the channels.

At this point, it should be noted that the diffusion of small guest molecules in the polymer network also depends on the geometrical conditions such as the size and distribution of the pores as well as the molecular interactions. Thus, we analyzed the porosity of the hydrogels to investigate the effect of geometry on the diffusion of guest molecules by comparing with theoretical models. First, a simple cubic void (10 Å × 10 Å × 10 Å, Figure 5.9 (c)) was built in a periodic box (30 Å × 30 Å × 30 Å, Figure 5.9 (b))

using a dummy atom with a van der Waals radius of 0.5 Å (Figure 5.9 (a)). Then, the simple cubic void was connected via channels of three different cross-sectional areas: 2 Å × 2 Å (Figure 5.9 (d)), 4 Å × 4 Å (Figure 5.9 (e)), 6 Å × 6 Å (Figure 5.9 (f)) and 8 Å × 8 Å (Figure 5.9 (g)). If the spherical molecule has a sufficiently smaller radius, then it can diffuse through the channel. Otherwise, the guest molecule is confined within the simple cubic void. Using such a theoretical model (Figure 5.9) with the solvent accessible surface analysis, we evaluated the inner surface area of the theoretical model, which depends on the probe radius. As shown in Figure 5.10, the inner surface area is decreased with an increasing the probe radius because it is actually the contacting surface area for a given probe radius. Thus, if the probe radius is larger than the radius of the channel size, the inner surface of the channel is not counted in the measurement.

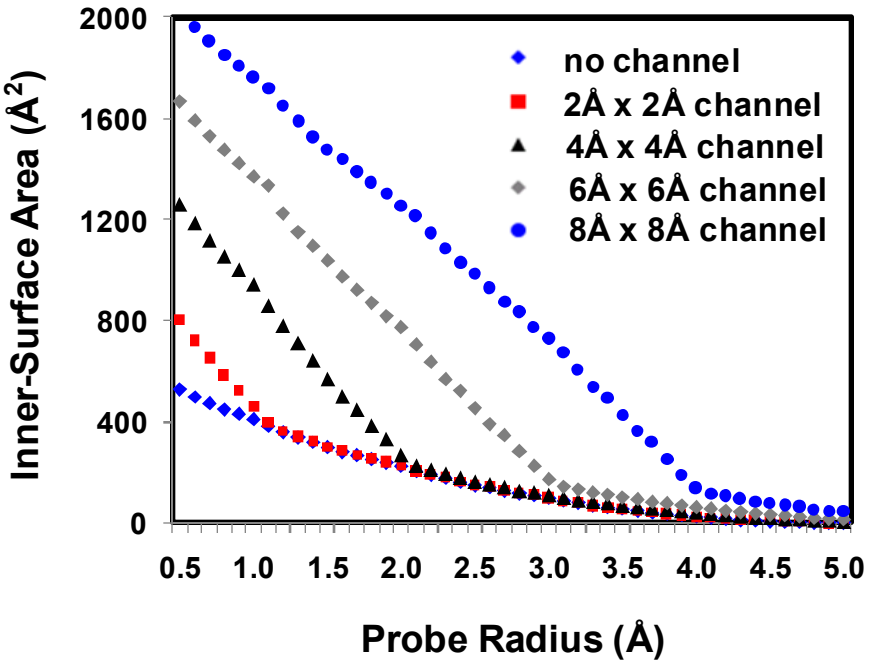

Figure 5.10: Change in the inner surface area from the theoretical models (Figure 5.9) as a function of probe radius.

From Figure 5.10, the threshold value of the probe radius to detect the channel in models d, e, f and g (Figure 5.9) is clearly observed at 1 Å, 2 Å, 3 Å and 4 Å, respectively, which is exactly matched with the size of the radius of the channel. In other words, a solute can diffuse through the channel to move other sites if the solute radius size is smaller than the threshold value for the model. Otherwise, a solute can be confined within the pore. Thus, we believe that this analysis can discriminate the difference in porosity between the hydrogels on nanometer-scale.

The inner surface area of the hydrogels is obtained, as shown in Figure 5.11. We did not see a clear threshold of the probe radius from the hydrogel systems, but rather observed the intermediate zone between two linear regimes (see Figure 5.11 (a)) due to the complicated structures of the hydrogels, with various sizes and shapes of channels and cages. If a solute has a radius within the range of the intermediate zone, then it can diffuse through the proper channel, but it also can be confined simultaneously. Because the hydrodynamic radius of the ascorbic acid and D-glucose is 2.71 Å and 2.78 Å, respectively, it is expected that they are confined within the local voids in the hydrogel for a 20 wt % water content hydrogel. The hydrodynamic radius of the guest molecule is within the range of the intermediate zone at 40 wt % water content, and therefore, diffusion is restricted within the hydrogel. At 80 wt % water content, the threshold of the probe radius is not observed if the range of the probe radius is less than 5 Å, indicating that the guest molecule can diffuse through the channel. This result is consistent with their diffusion behavior, discussed in Figure 5.7, Figure 5.8 and Table 5.5.

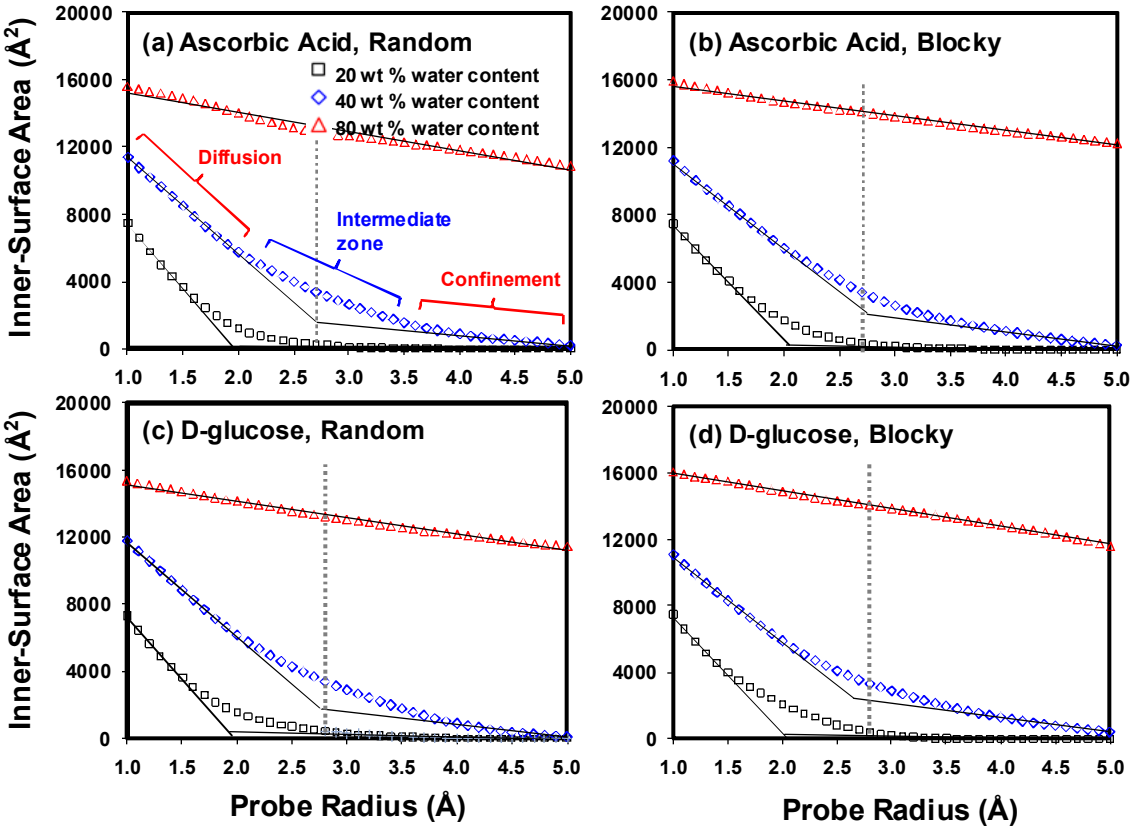

Figure 5.11: Change in the inner surface area from the simulated hydrogels as a function of the probe radius; ascorbic acid in the random sequence (a) and in the blocky sequence (b) and D-glucose in the random sequence (c) and in the blocky sequence (d). The dot-line indicates the radius of either ascorbic acid or D-glucose. The gray dot-line indicates the hydrodynamic radius of the guest molecule.

Conclusion

Using a full-atomistic MD simulation approach, we investigated P(VP-*co*-HEMA) hydrogels containing 20, 40 and 80 wt % water at 310.15K with both random and blocky sequences. Ascorbic acid and D-glucose were used to study the effect of the monomeric sequence on the diffusion of small guest molecules within the hydrogels. By analyzing the pair correlation functions, it was found that the guest molecule has greater accessibility to the VP units than to the HEMA units with both monomeric sequences due

to its higher hydrophilicity compared to the HEMA units. The monomeric sequence effect on the P(VP-*co*-HEMA) hydrogel is clearly observed with 20 wt % water content, but the monomeric sequence effect is significantly reduced with 40 wt % water content and disappears with 80 wt % water content. This is because the hydrophilic guest molecules are more likely to be associated with water molecules than with the polymer network at the high water content. By analyzing the mean square displacement, the displacement of the guest molecules and the inner surface area, it is also found that the guest molecule is confined in the system at 20 wt % water content, resulting in highly anomalous subdiffusion. Therefore, the diffusion of the guest molecules is directly affected by their interaction with the monomer units, the monomeric sequence and the geometrical confinement in the hydrogel at a low water content, but the monomeric sequence effect and the restriction on the diffusion of the guest molecule are significantly decreased with increasing the water content.

CHAPTER 6: DE-SWELLING MECHANISMS OF A SURFACE-GRAFTED P(NIPAAm) BRUSH

Introduction

Among the various types of stimuli-responsive polymer materials, we are particularly interested in a chemically surface-grafted poly(N-isopropylacrylamide) (P(NIPAAm)) brush system with sufficiently high grafting densities, which was inspired by V. V. Tsukruk group [179, 320]. The polymer chains stretched in a direction that was perpendicular to the surface by excluded volume repulsions at a high grafting density condition, and therefore, the behavior of brushes is controlled by the strong entropic repulsion between the polymer chains and the constraints from the chemically cross-linked surface [321]. This surface-grafted P(NIPAAm) brush showed a rapid de-swelling response to temperature changes above the lower critical solution temperature (LCST) due to the immediate dehydration of the water from the free mobile chains, followed by the hydrophobic attraction between the isopropyl groups, which dominate and collapse the brush sequentially [322-324]. These features were suggested for many applications, including aqueous chromatography systems [175, 323, 325-327], permeation-controlled porous membranes [328, 329], chemical sensors [330-332], controlled attachment-detachment surfaces for cultured cells [170-172, 174, 333-338], drug release [339, 340], protein detection [341, 342], and functional composite surfaces [343-345]. The behavior of the surface-grafted P(NIPAAm) chains have been extensively investigated using various characterization techniques, such as dynamic light scattering (DLS) [346-348], surface plasmon spectroscopy (SPR) [349], neutron reflectivity (NR) [350-354], quartz crystal microbalance measurement (QCM) [355-359], atomic force microscopy (AFM)

[179, 360-363], surface force measurement [364-366], nuclear magnetic resonance (NMR) [212], and dynamic contact angle measurement [367, 368].

With many factors at play in the phase transition of the brushes, the grafting density of the P(NIPAAm) brushes plays an important role for the conformational transition. Using neutron reflectivity, Yim et al. investigated the conformational changes of PNIPAAm chains that were tethered to silicon oxide using a low/high surface grafting density [350, 351]. They observed no coil-to-globule transition with a low grafting density, ranging from 0.01 to 0.02 chains/nm^2 using a 33 to 220 kg/mol molecular weight of P(NIPAAm). To check the effect of the molecular weight on the conformational changes of the brushes for high grafting density (0.54 chains/nm^2) of P(NIPAAm) chains with three different molecular weights, 13, 44, and 71 kg/mol, they found a significant conformational transition for all three samples as the temperature passed through the LCST. It is indicated that the high grafting density of the P(NIPAAm) chain is critical for the coil-to-globule transition of the brushes. Plunkett et al. investigated the effect of the grafting density, with 0.05, 0.21, and 0.33 chains/nm^2, and the molecular weight of P(NIPAAm), which ranged from 51 to 263 kg/mol, using surface force measurements [364]. They found that the chain collapse above the LCST decreases with a decreasing grafting density and molecular weight. Malham and Bureau reported that the grafting density greatly affects the collapse of P(NIPAAm) when using surface force measurements [366]. They used grafting densities that ranged from 0.02 to 0.42 chains/nm^2 with the given molecular weight (~ 475 kg/mol), and the thermal response of the brushes increased with the increasing the grafting density of the brushes. Zhu et al. found that the P(NIPAAm) does not collapse above the LCST with very low grafting densities, ranging from 0.12×10^{-7} to 2.56×10^{-7} chains/nm^2 [365]. Using AFM and QCM, Ishida and Biggs investigated the effect of the grafting density, with 0.02, 0.07 and 0.36 chains/nm^2, on the phase transition behavior of P(NIPAAm) brushes [360]. They reported that the phase transition of P(NIPAAm) brushes clearly depends on the grafting

density; the change in the brush layer was more gradual over a broader temperature range with an increasing the grafting density. LeMieux et al. also showed the clear phase transition of P(NIPAAm) brushes above the LCST with a very high grafting density (initiator density on the surface of 2.6 molecules/nm^2) [179]. Because the responsive behavior of the surface-grafted P(NIPAAm) chains is significantly dependant on their grafting densities, we took much caution in deciding the grafting density of the P(NIPAAm) chains in this study.

This well-defined structure with a fast de-swelling feature helps to simplify the model structure for the simulation study, and we may observe the de-swelling phenomena in the MD time scale (usually in nanoseconds). Thus, in our study, we simulated the surface-grafted P(NIPAAm) brushes at the atomic level to pursue the fundamental understanding of the detailed de-swelling mechanisms and the molecular interactions between P(NIPAAm) and water molecules at above/below the LCST using MD simulations.

Models and Simulations Details

Model Constructions

To comply with the rapidly increasing interest in stimulus-response polymer brush systems, a large variety of polymer brush structures have been made and tested on the basis of recent progresses in the synthesis techniques such as atom transfer radical polymerization (ATRP) and reversible addition-fragmentation chain transfer (RAFT), which can control the growth of the brushes and the grafting density on the surface with appropriate initiators and cross-linkers. However, we did not include the initiators and the cross-linkers in this study to simplify the model, as our purposes are to elucidate the interactions between the water-P(NIPAAm) chains and the de-swelling mechanisms of

water molecules above the LCST. A P(NIPAAm) chain with a degree of polymerization of 30 (Figure 6.1 (a)) is attached to the silicon substrate (Figure 6.1 (b)). The thickness of the silicon substrate is ~23 Å, with seven layers. In this calculation, the Si (111) surface was modeled by a slab with a (3.84Å × 3.84Å) surface unit cell. The surface effect from the silicon substrate was not considered; however, the silicon substrate was used to constrain the P(NIPAAm) brushes and to control the grafting density of the P(NIPAAm) brushes. To determine the surface grafting density, we calculated the packing energies of 2×2, 3×3, 4×4, and 5×5 unit structures of the silicon slab (Figure 6.1 (c)) with a single surface-grafted P(NIPAAm) chain using the energy minimization technique. The packing energy was defined by

$$\Delta E_{packing} = E_{silicon\ slab+P(NIPAAm)\ chain} - \left(E_{silicon\ slab} + E_{P(NIPAAm)\ chain}\right) \qquad \textbf{(36)}$$

where $E_{silicon\ slab+P(NIPAAm)\ chain}$, $E_{silicon\ slab}$ and $E_{P(NIPAAm)\ chain}$ denote the energy of the silicon slab with the surface-grafted P(NIPAAm) chain, the energy of the silicon slab and the energy of the P(NIPAAm) chain, respectively. From Figure 6.2, we found that the 3×3 silicon slab showed the lowest packing energy (~-17 kcal/mol) in the models. To simulate the surface-grafted P(NIPAAm) brushes computationally, we first used the 3x3 silicon slab with the single P(NIPAAm) chain and cleave the surface for an orthorhombic simulation box with periodic boundary conditions applied for all three spatial directions, as shown in Figure 6.3 (a). The initial configuration of the surface-grafted P(NIPAAm) brushes consists of twelve P(NIPAAm) chains with lattice parameters of a = 39.91 Å, b = 34.56 Å, and c = 200 Å, as shown in Figure 6.3 (b). The grafting density is the equivalent of 1.15 chains/nm^2 which is sufficiently high to observe phase transition behavior in comparison with other experimental conditions [351, 360, 364, 366]. To hydrate the P(NIPAAm) brushes, we added 1300 water molecules (~ 40 wt % water content) into the brush system (Figure 6.3 (c)), and the density of the hydrated brushes

was ~1.1 g/cm^3 which is similar to the density for bulk P(NIPAAm) at room temperature [369].

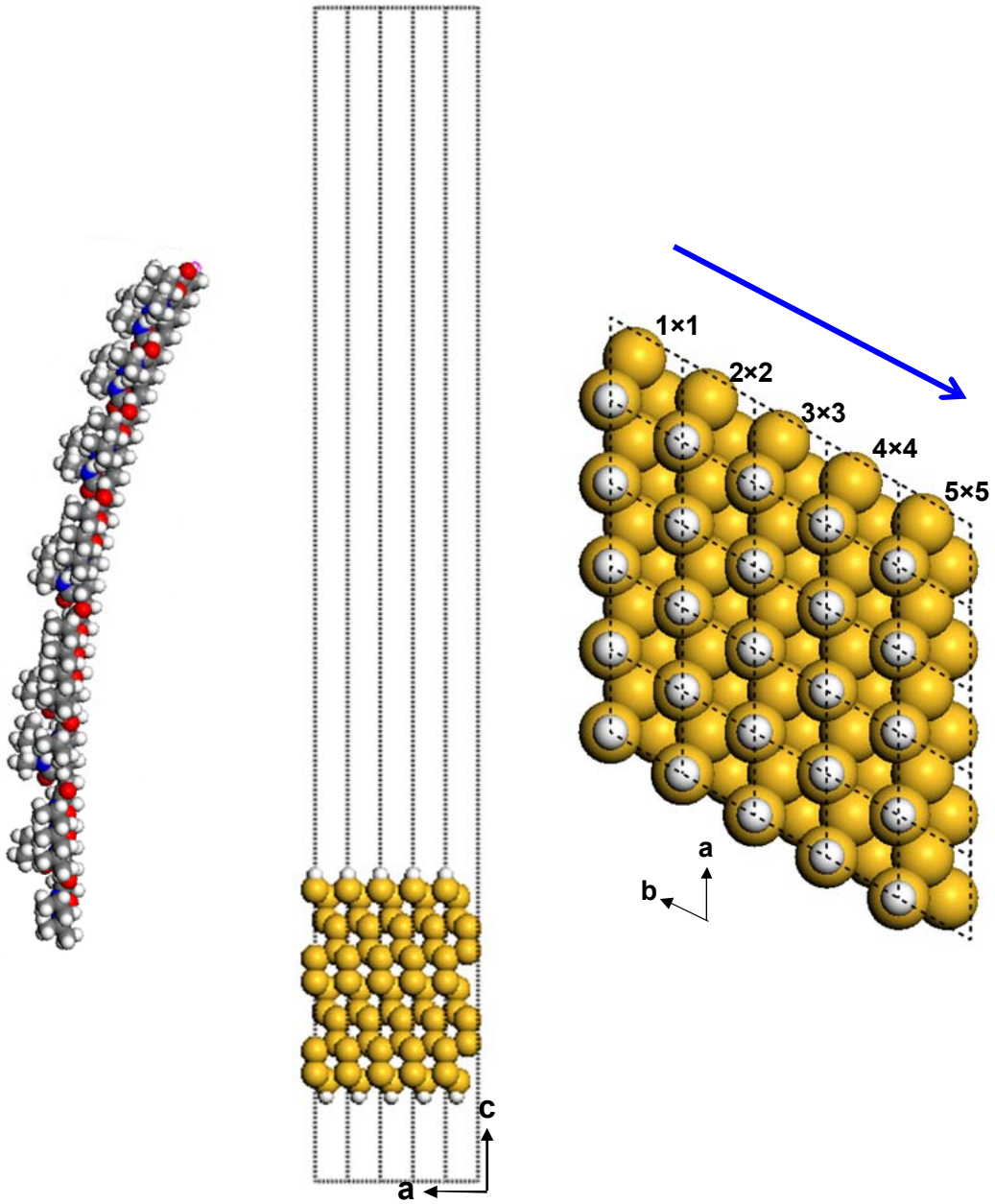

Figure 6.1: Preparation scheme of the surface-grafted P(NIPAAm) chain on silicon substrate; (a) a single chain of P(NIPAAm) with DP=30; (b) side view of the silicon substrate; and (c) top view of silicon substrate.

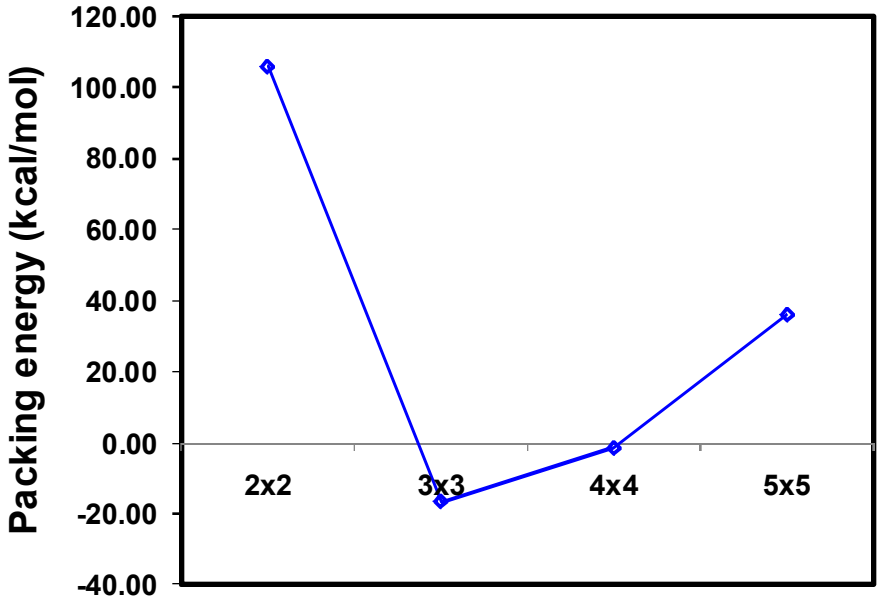

Figure 6.2: Packing energies of the surface-grafted P(NIPAAm) brush.

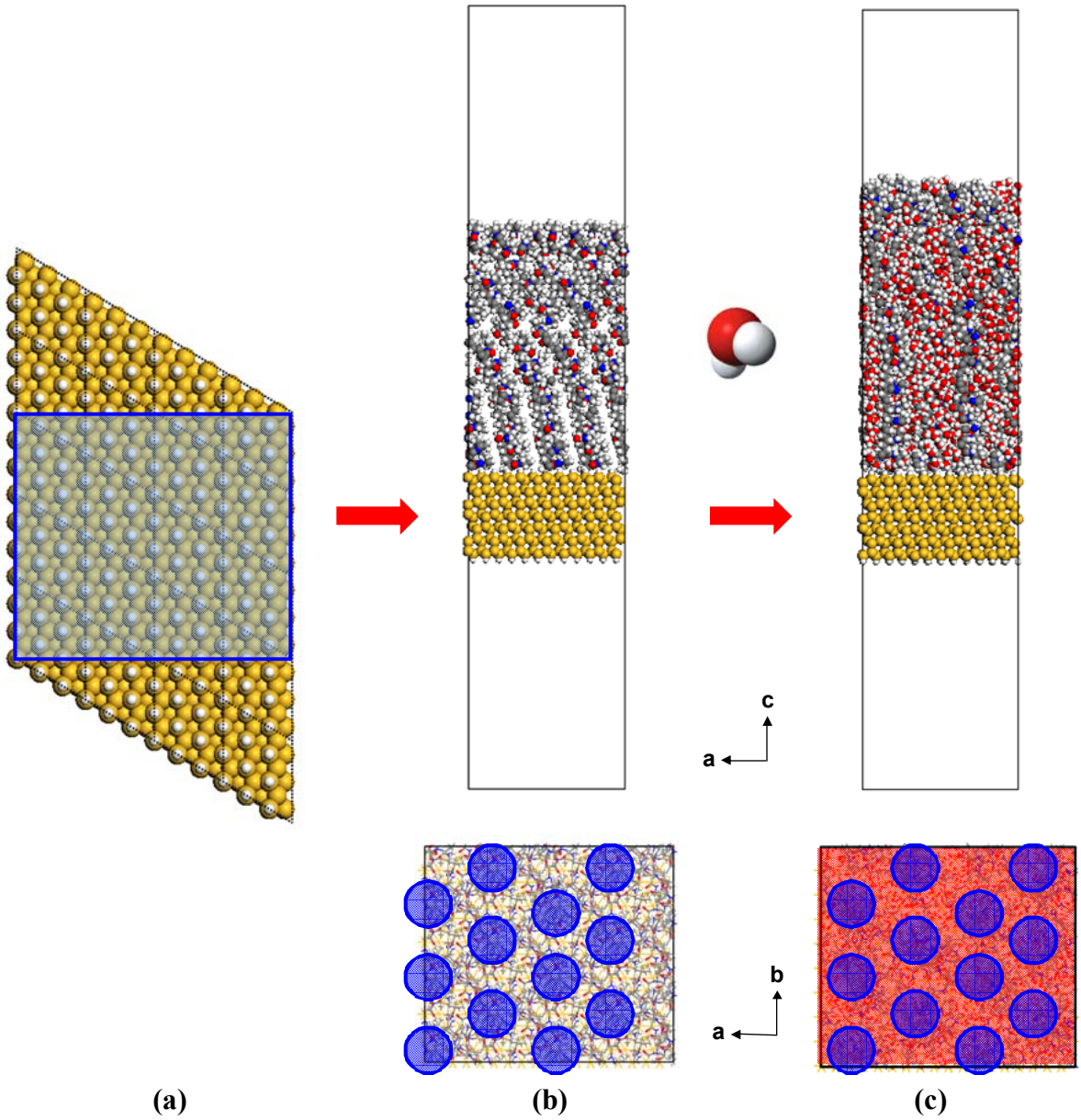

Figure 6.3: Preparation of the initial configurations of the surface-grafted P(NIPAAm) brushes on the silicon slab; (a) a hexagonal closed packing mode is retained in an orthorhombic simulation box (blue box) with the lattice parameters of a = 39.91 Å, b = 34.56 Å, and c = 200 Å; (b) the initial configuration of the surface-grafted P(NIPAAm) brushes, consisting of 12 P(NIPAAm) chains, with blue circles indicating the location of each brush in the system; and (c) hydrated P(NIPAAm) brushes with 1300 water molecules, with blue circles and red color indicating the location of each brush and water molecules in the system, respectively.

Model Equilibration

After this initial configuration was prepared, we equilibrated the system by carrying out NVT MD simulations at 290 K for 20 ns. After this equilibration, we independently simulated the model system under five different temperature conditions, at 275 K, 290 K, 320 K, 345 K and 370 K. Because the aqueous solutions of P(NIPAAm) exhibit LCST at approximately 305 K (32 C°) [152-155], 2 temperature conditions (275 K and 290 K) are below the LCST and 3 temperature conditions (320 K, 345 K, and 370 K) are above the LCST. We completed another 10 – 15 ns of MD simulation for each temperature condition to check the temperature-dependent volumetric change of the P(NIPAAm) brushes until the system was equilibrated.

Force Field and MD Parameters

In this investigation, we employed same conditions for force field and MD parameters from Chapter 3.

Results and Discussion

Density Profiles

The snapshots of the surface-grafted P(NIPAAm) brushes during MD simulation (Figure 6.4) clearly show that the water molecules in the brushes are de-swelled above the LCST (~305 K) of P(NIPAAm), as shown in Figure 6.4 (a) through (c). We observed faster de-swelling of the water molecules from the brushes at higher temperatures. The surface-grafted P(NIPAAm) brushes are completely wetted at 2 ns, 5 ns and 15 ns for

temperatures of 370 K, 345 K and 320 K, respectively. However, we did not observe the de-swelling of water molecules below the LCST, as shown in Figure 6.4 (d) and (e).

We analyzed the snapshots to provide the distributions of each component throughout the hydrated brushes using density profiles. Figure 6.5 through Figure 6.9 show the density profiles of the brushes along the c-axis direction of the simulation box at each temperature. These results were obtained by partitioning the system into 1.0-Å-thick slabs parallel to the ab-plane. The density profile is decomposed into the contributions from the main components: water molecules (blue line), polymer brushes (red line) and silicon substrate (orange color). The density profiles from 370 K (Figure 6.5), 345 K (Figure 6.6) and 320 K (Figure 6.7) clearly show the development of a water slab beyond a 90 Å distance by the de-swelling of water molecules during the simulation above the LCST. Again, we did not observe any water slab out of the brushes below the LCST, as shown in Figure 6.8 (290 K) and Figure 6.9 (275 K).

To quantify the change in the thickness of the brushes, we define the "90 thickness" of the polymer brushes as a function of the distance from the silicon substrate where the density of the brushes is 90 % of its maximum value. In the same manner, we also define the "90 thickness" of the water slab at the water-vacuum interface where the density of the water slab is 90 % of its maximum value. Therefore, the thickness of the water slab is defined by the distance between two points, the "90 thickness" of the polymer brushes and the "90 thickness" of the water slab (Figure 6.10). The thickness of the water slab out of the brushes (Figure 6.11 (a)) increases with increasing numbers of water molecules (Figure 6.11 (b)) above the LCST. A total of 52 %, 46 % and 30 % of the water molecules were squeezed out of the brushes at 370 K, 345 K and 320 K during 15 ns MD simulations, respectively. The density of the water slab out of the brushes (Figure 6.11 (c)) is increased, while the density of the water in the brushes (Figure 6.11 (d)) is decreased above the LCST. The density of the water slab out of the brushes approaches the density of bulk water at 2 ns (370 K), 5 ns (345 K) and 15 ns (320 K), and

it agrees with the required time to wet the surface completely (Figure 6.4 (a) through (c)). Below the LCST, we did not observe any significant changes in the density profiles during the simulations. The thickness of the brushes (Figure 6.11 (e)) decreases with the increasing density of the brushes (Figure 6.11 (f)), indicating the collapse of the brushes above the LCST.

We also prepared a reference system to compare/validate the results of the simulations in this study. The reference system consists of surface-grafted poly(acrylamide) (P(AAm)) brushes instead of P(NIPAAm). The other conditions for the MD simulations are same as the P(NIPAAm) brush systems. P(AAm) has a similar chemical structure to P(NIPAAm), but P(AAm) does not contain the hydrophobic isopropyl group. P(AAm) shows an upper critical solution temperature (UCST) with water at 235 K [370], and therefore, P(AAm) does not show phase separation behavior with liquid water. We expect that the P(AAm) brushes will not go through the de-swelling of the water molecules in the range of the simulated temperatures for the P(NIPAAm) brushes. To check this expectation, we simulated the surface-grafted P(AAm) brushes with 1300 water molecules (~ 50 wt % water content) at 275 K, 290 K, 320 K, 345 K and 370 K. Because we observed the rapid de-swelling of the water molecules within 5 ns for the P(NIPAAm) brushes (Figure 6.11 (b)), we performed MD simulations of the P(AAm) brushes for 5 ns. From the snapshots (Figure 6.12) and the density profiles (Figure 6.13 to Figure 6.17), the P(AAm) brushes did not show any significant de-swelling of the water molecules or the development of a water slab, even with a higher water content (~ 50 wt %) than that of the P(NIPAAm) brushes (~ 40 wt %). The thickness of the P(AAm) brushes (Figure 6.18) increases with increasing temperature due to thermal expansion. The change in thickness of the P(AAm) brushes as a function of temperature occurs in the opposite direction from that of the P(NIPAAm) brushes above the LCST, as shown in Figure 6.11 (e).

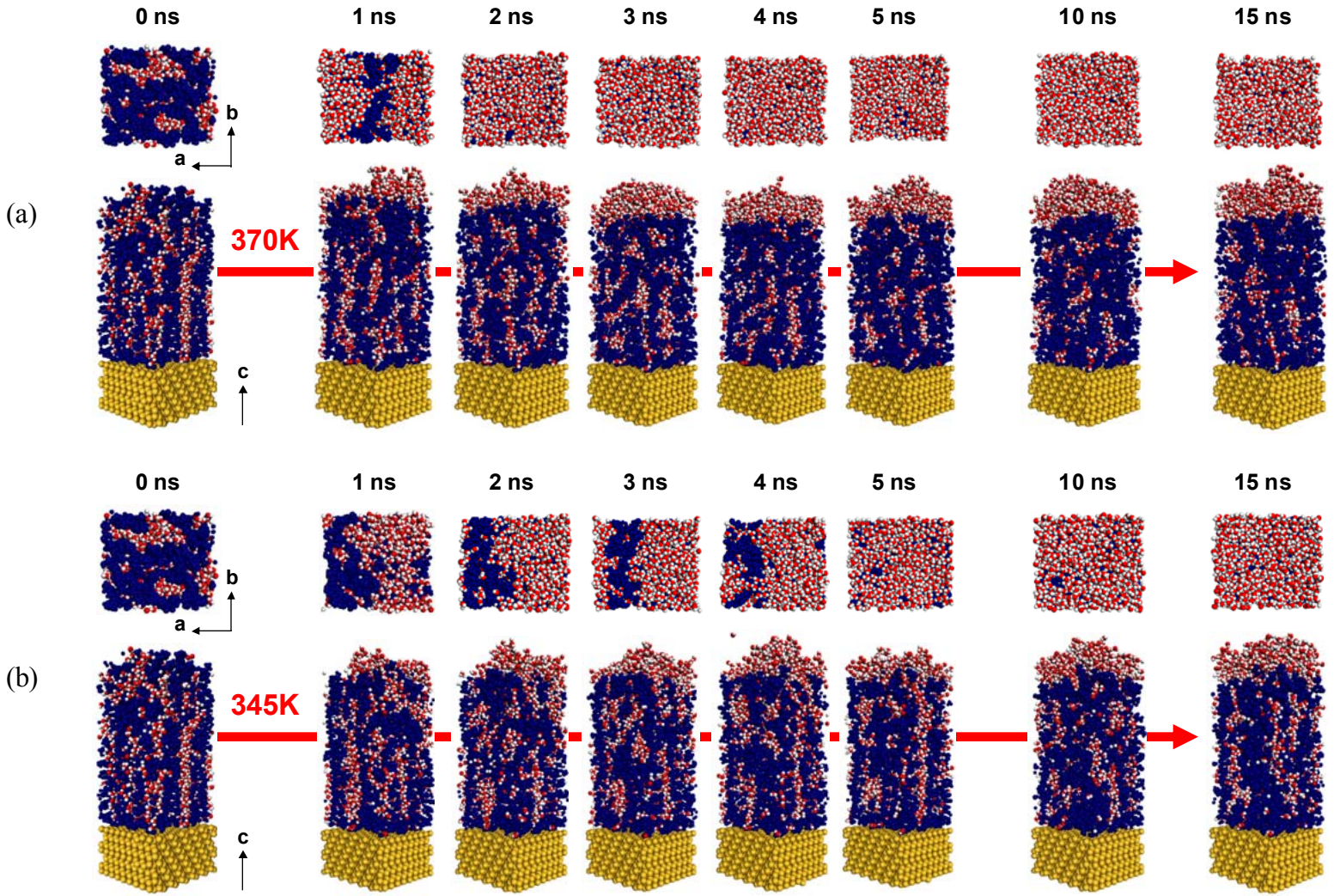

Figure 6.4: (Continued on next page.)

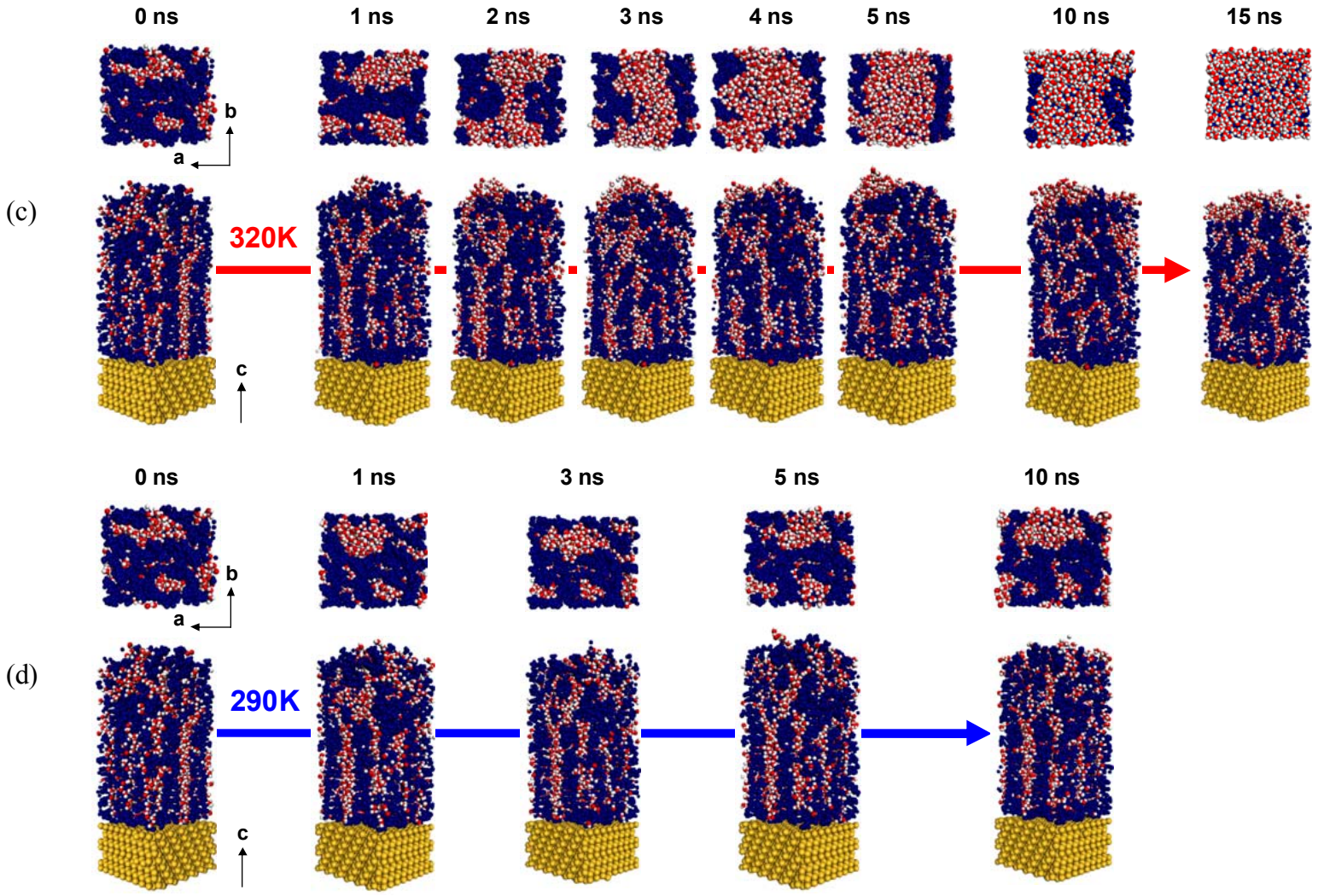

Figure 6.4: (Continued on next page.)

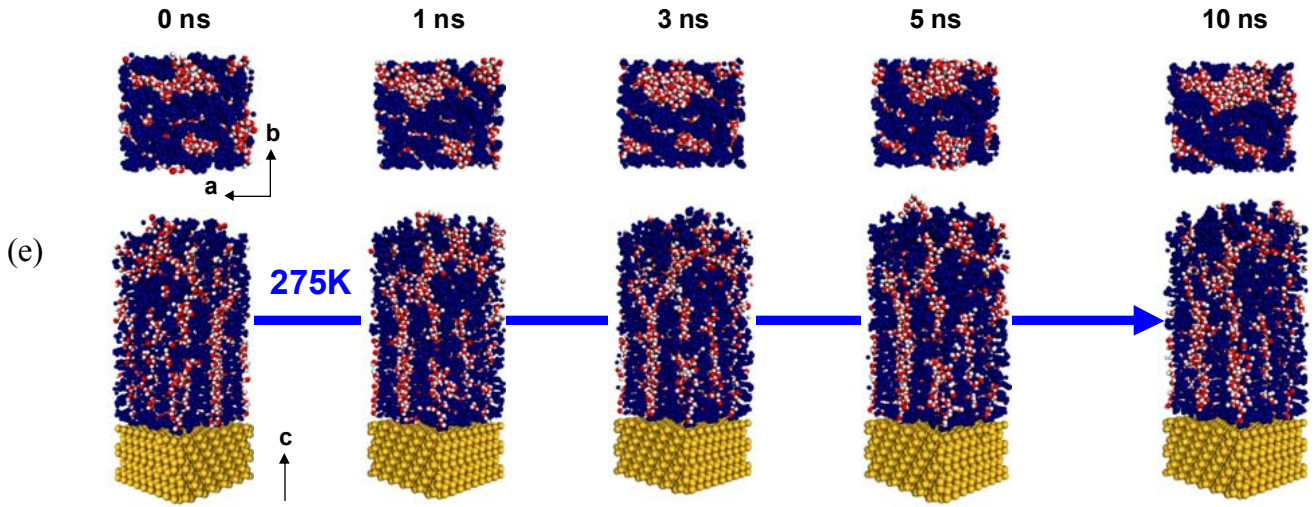

Figure 6.4: Snapshots of the hydrated surface-grafted P(NIPAAm) brushes during the MD simulation at (a) 370 K; (b) 345 K; (c) 320 K; (d) 290 K; and (e) 275 K. Blue, yellow, red, and white color denote polymer brushes, silicon substrate, oxygen of water, and hydrogen of water, respectively.

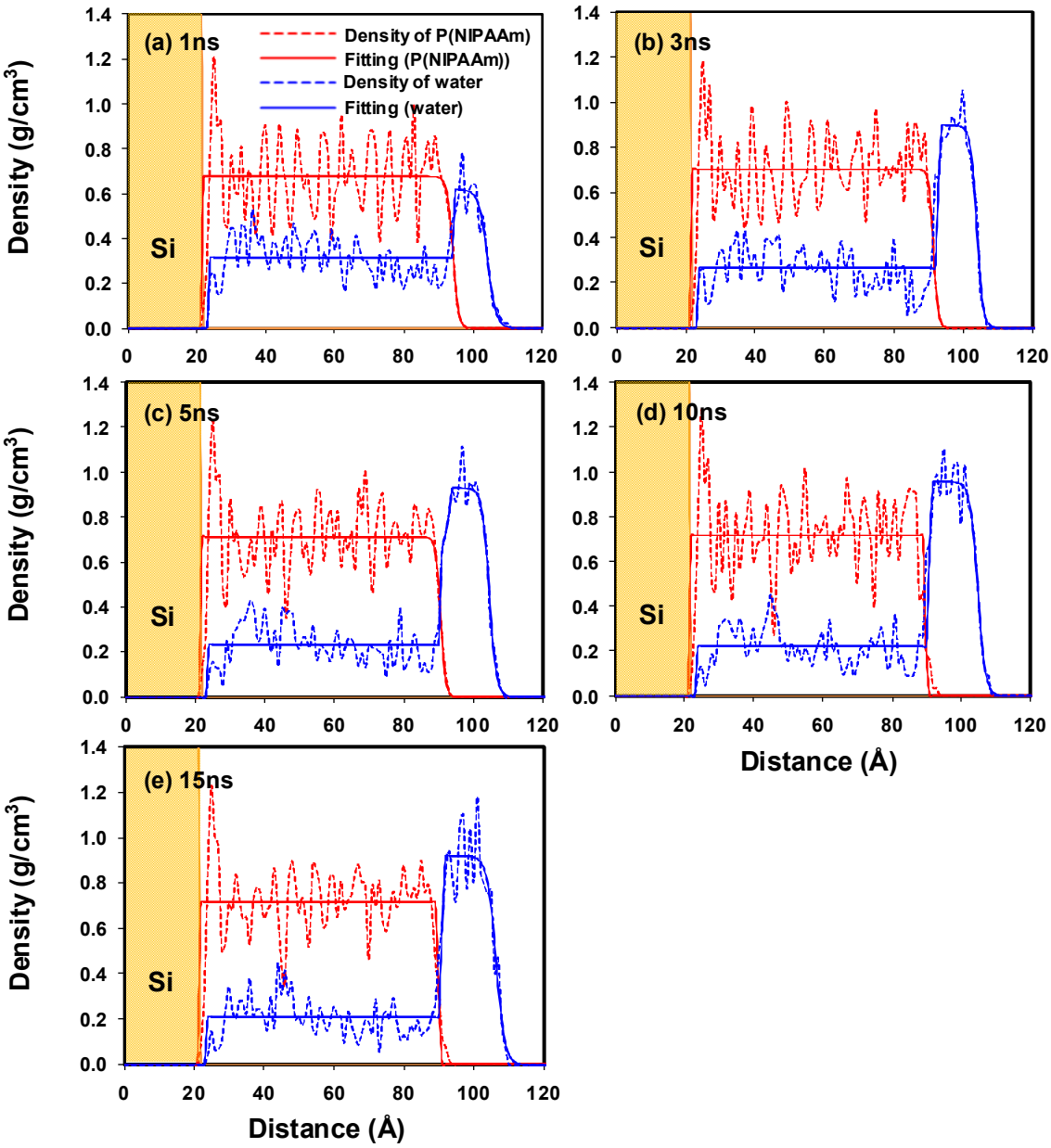

Figure 6.5: Density profiles of the surface-grafted P(NIPAAm) brushes at 370 K: (a) 1 ns; (b) 3 ns; (c) 5 ns; (d) 10 ns; and (e) 15 ns.

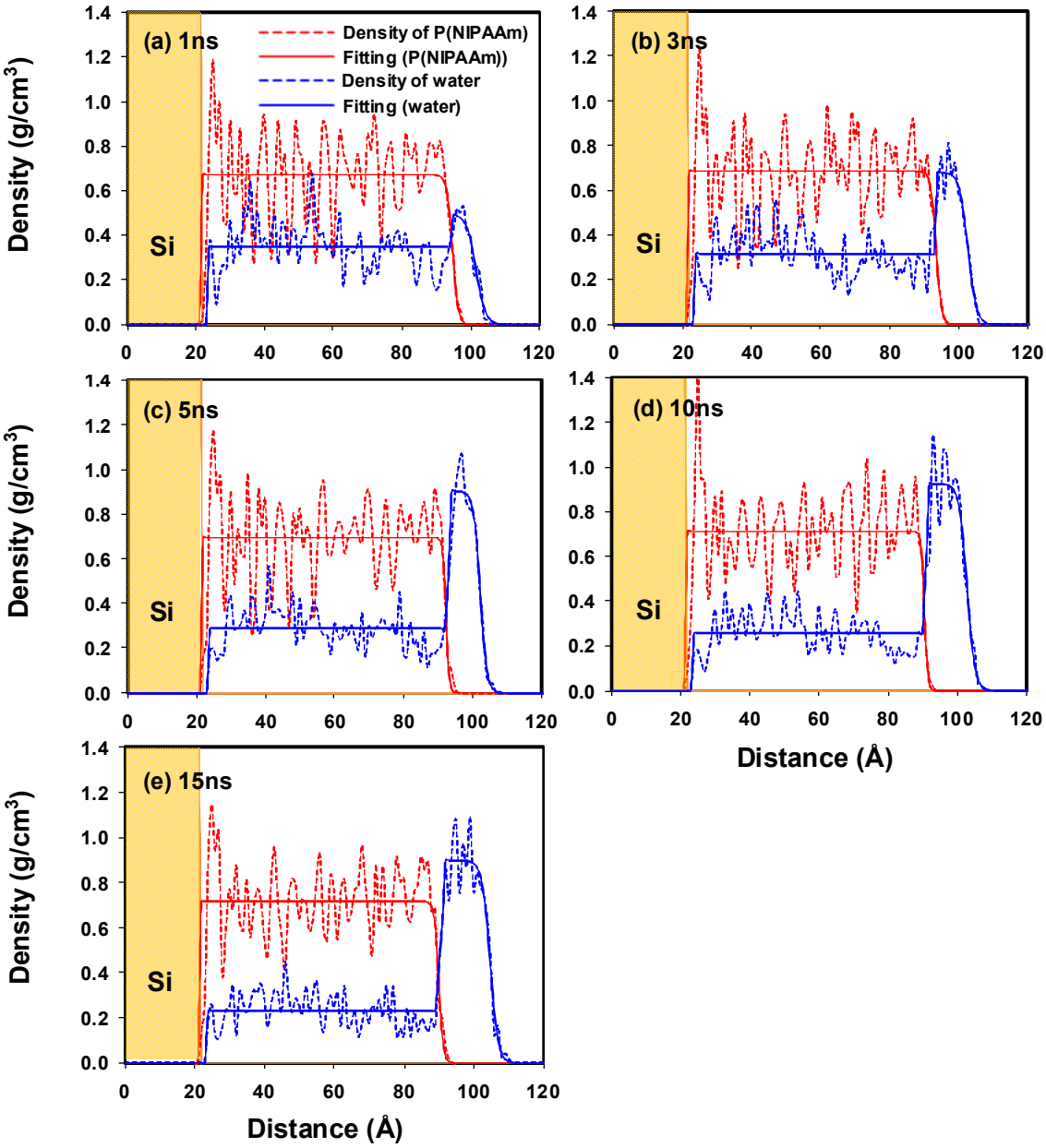

Figure 6.6: Density profiles of the surface-grafted P(NIPAAm) brushes at 345 K: (a) 1 ns; (b) 3 ns; (c) 5 ns; (d) 10 ns; and (e) 15 ns.

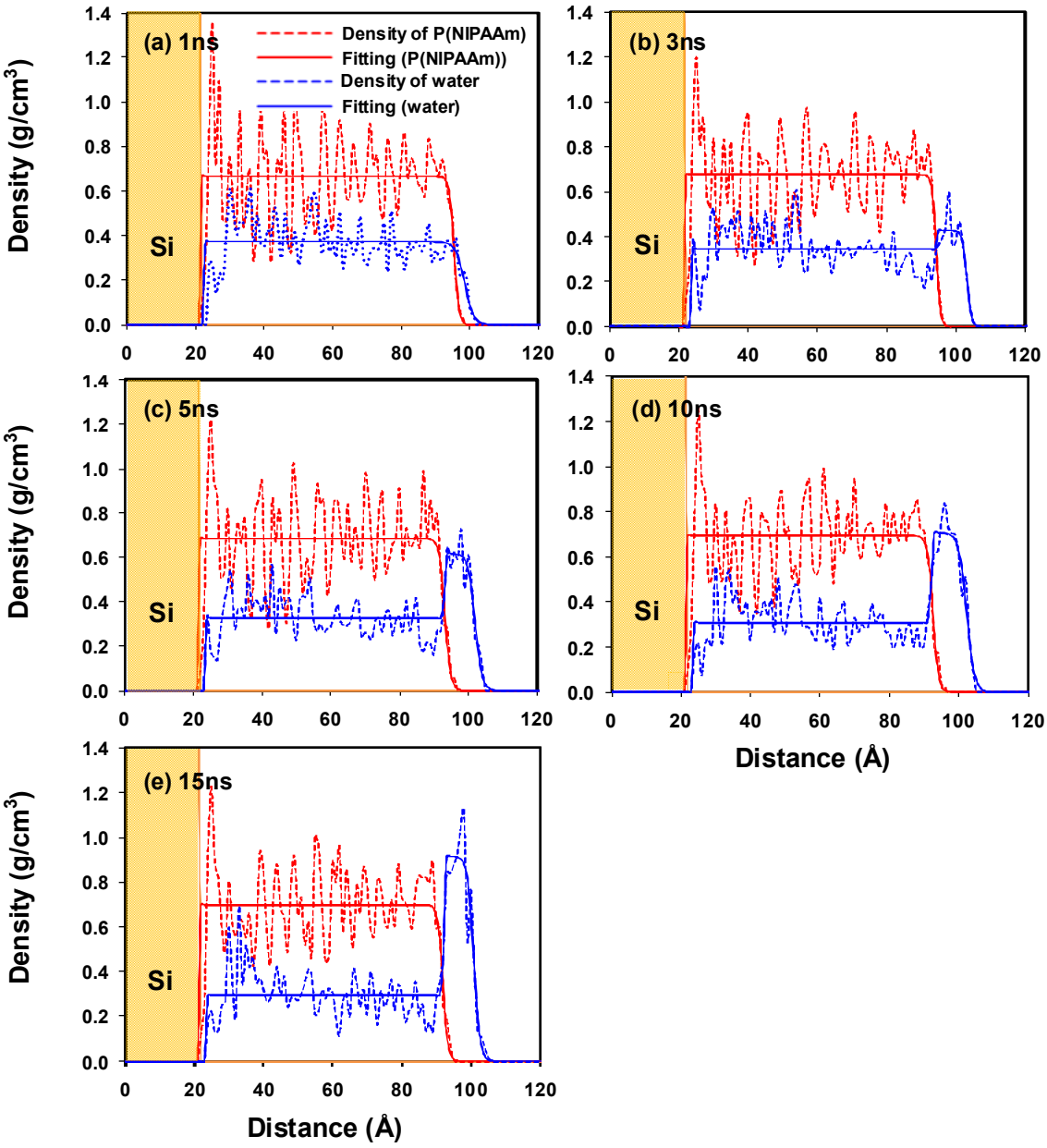

Figure 6.7: Density profiles of the surface-grafted P(NIPAAm) brushes at 320 K: (a) 1 ns; (b) 3 ns; (c) 5 ns; (d) 10 ns; and (e) 15 ns.

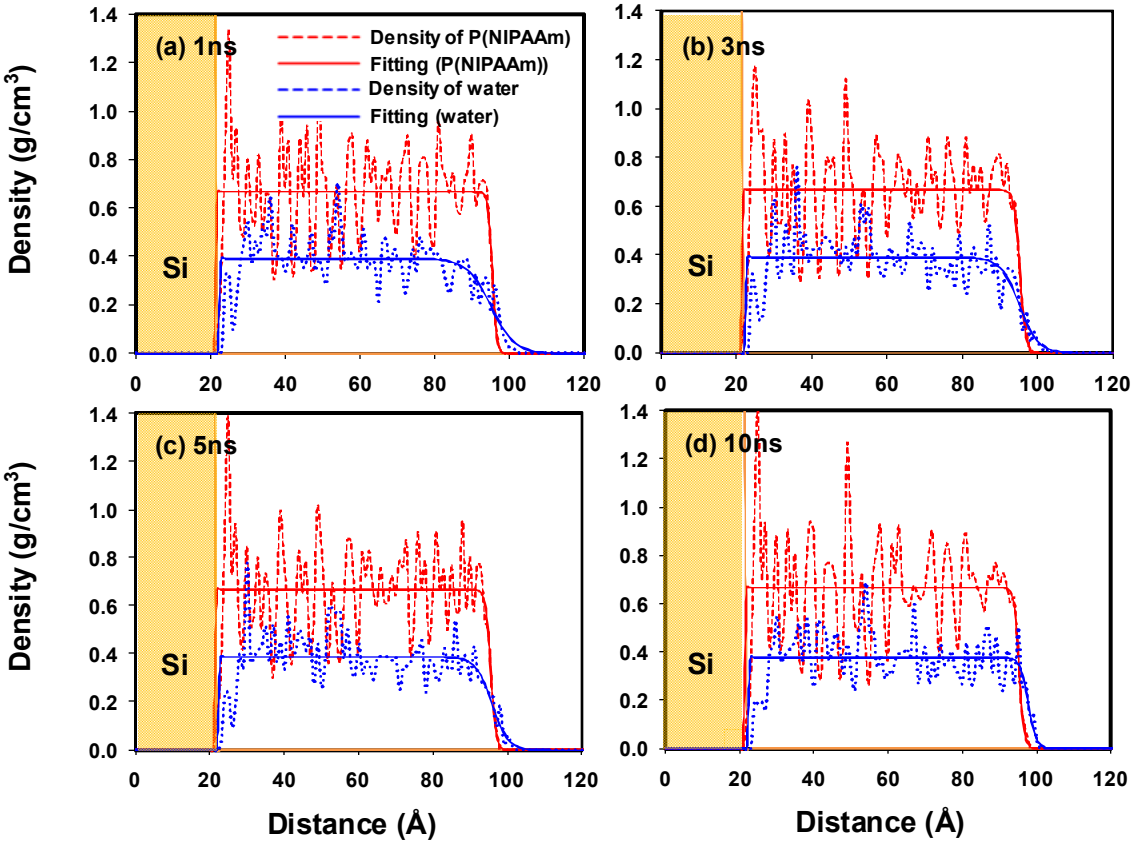

Figure 6.8: Density profiles of the surface-grafted P(NIPAAm) brushes at 290 K: (a) 1 ns; (b) 3 ns; (c) 5 ns; and (d) 10 ns.

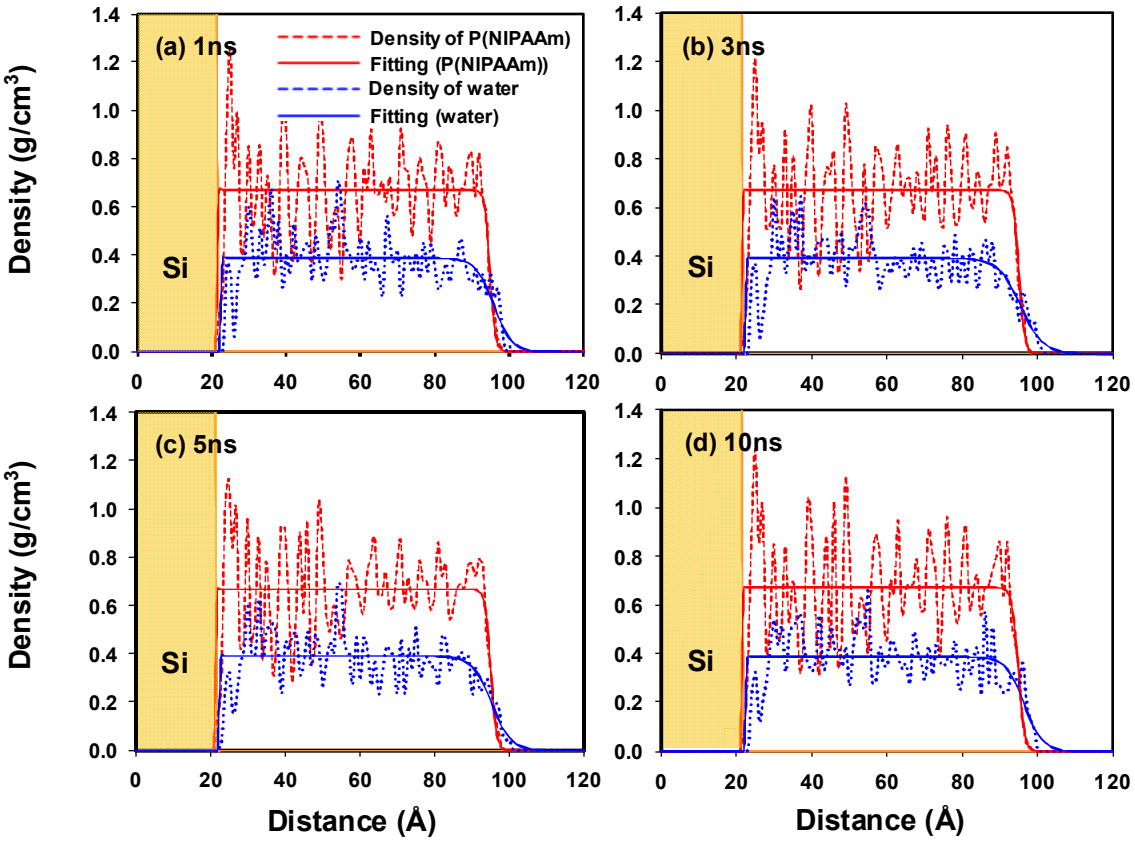

Figure 6.9: Density profiles of the surface-grafted P(NIPAAm) brushes at 275 K: (a) 1 ns; (b) 3 ns; (c) 5 ns; and (d) 10 ns.

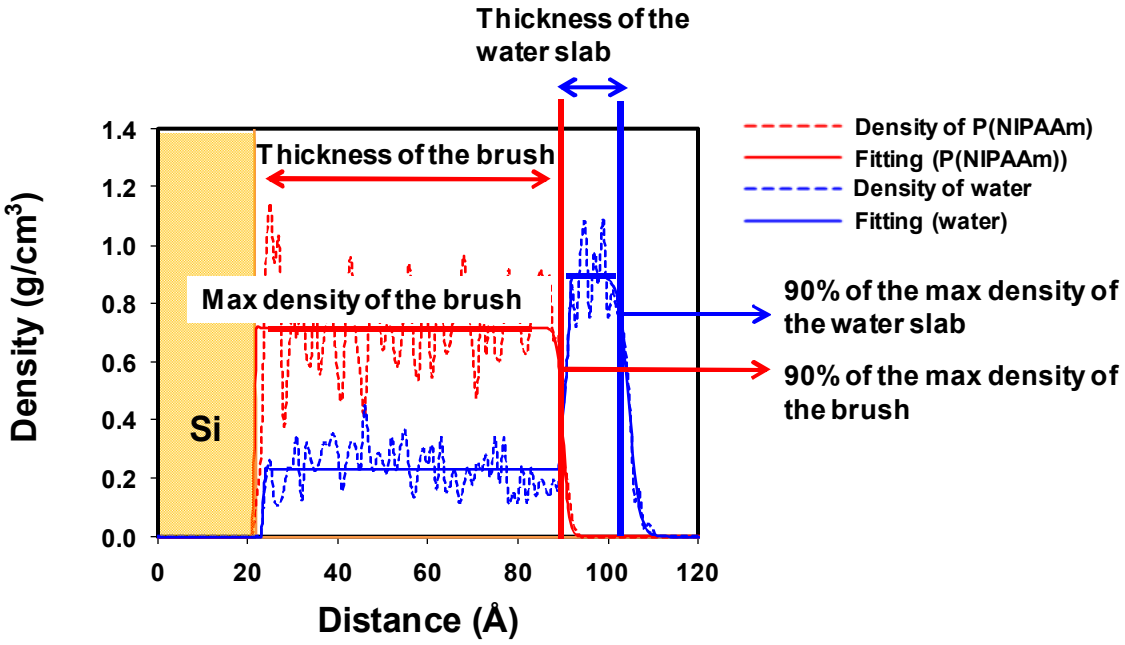

Figure 6.10: Scheme to determine the thickness of the brushes and the water slab

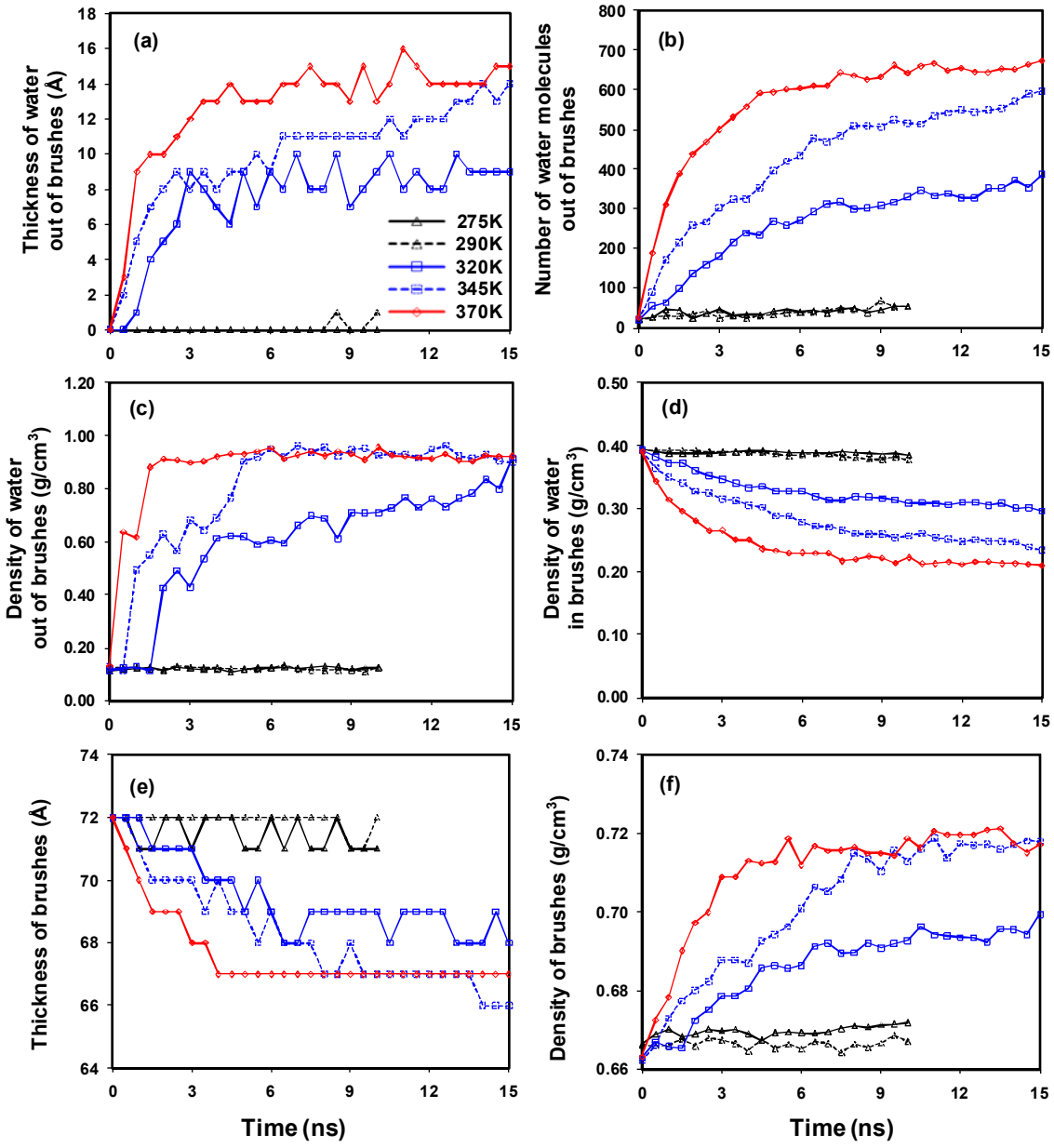

Figure 6.11: (a) Thickness of the water out of the P(NIPAAm) brushes; (b) number of water molecules out of the P(NIPAAm) brushes; (c) density of the water out of the P(NIPAAm) brushes; (d) density of the water in the P(NIPAAm) brushes; (e) thickness of the P(NIPAAm) brushes; and (f) density of the P(NIPAAm) brushes.

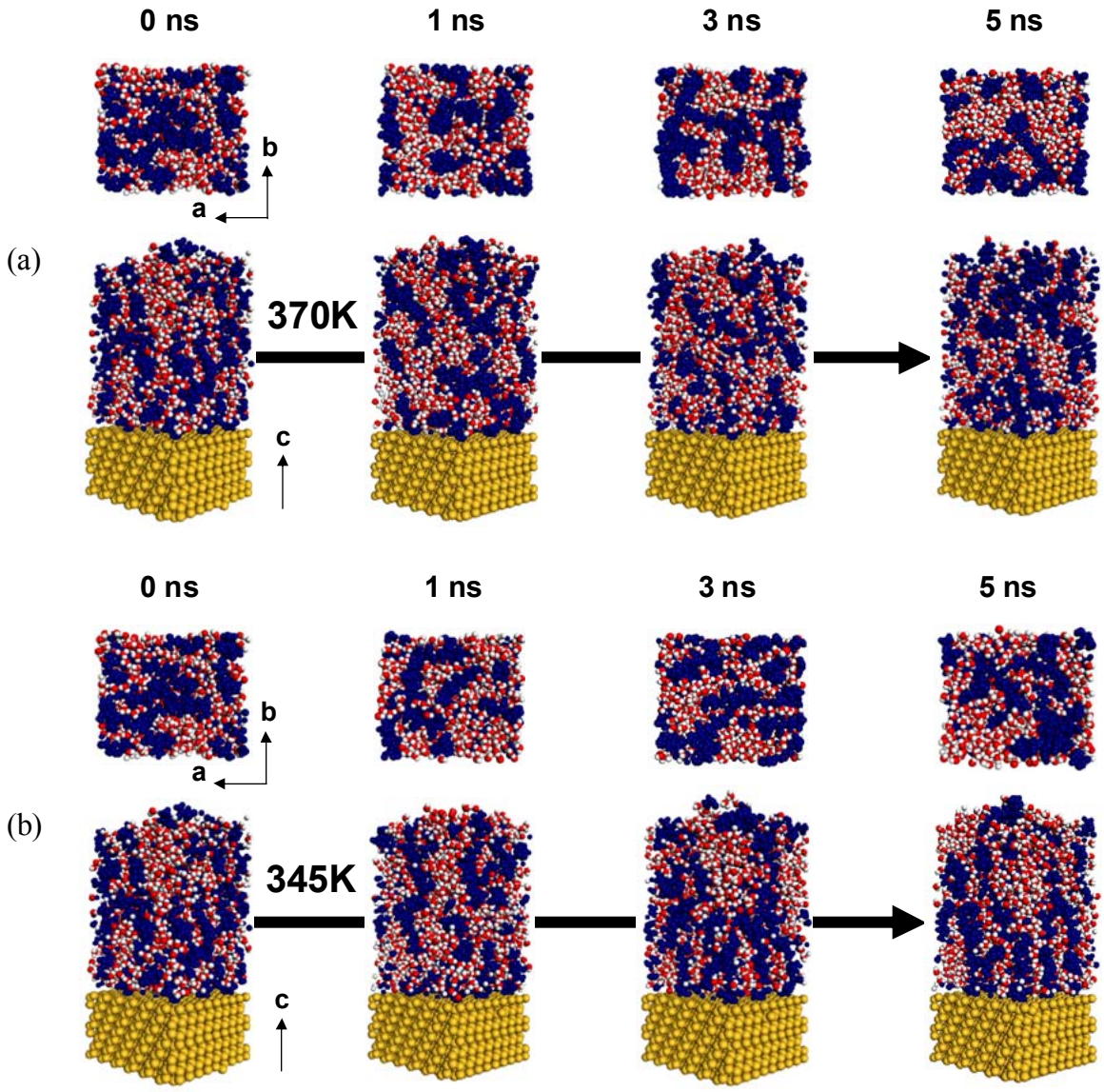

Figure 6.12: (Continued on next page.)

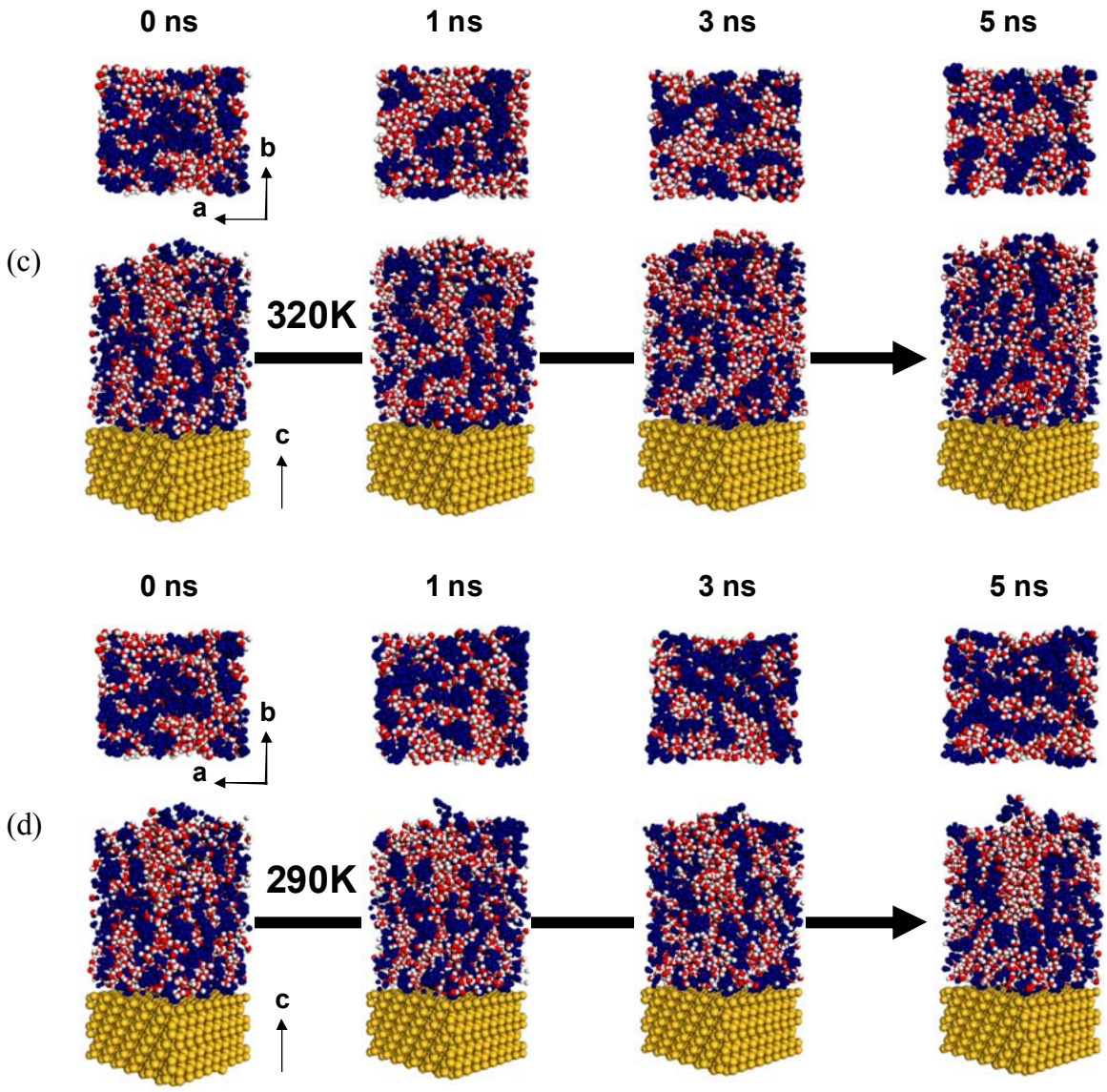

Figure 6.12: (Continued on next page.)

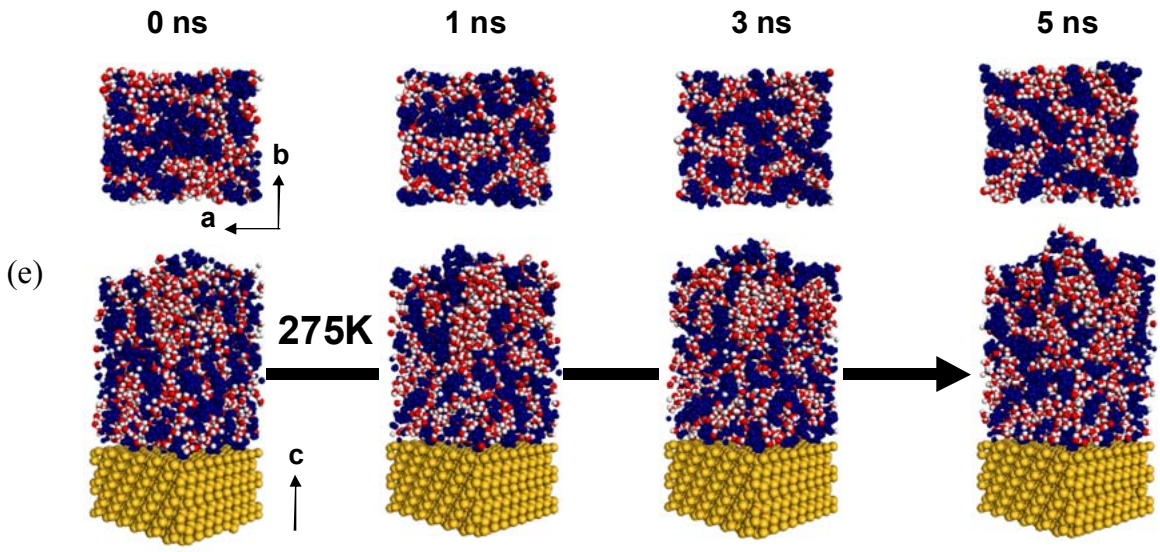

Figure 6.12: Snapshots of the hydrated surface-grafted P(AAm) brushes during simulation at (a) 370 K; (b) 345 K; (c) 320 K; (d) 290 K; and (e) 275 K. Blue, yellow, red, and white color denote polymer brushes, silicon substrate, oxygen of water, and hydrogen of water, respectively.

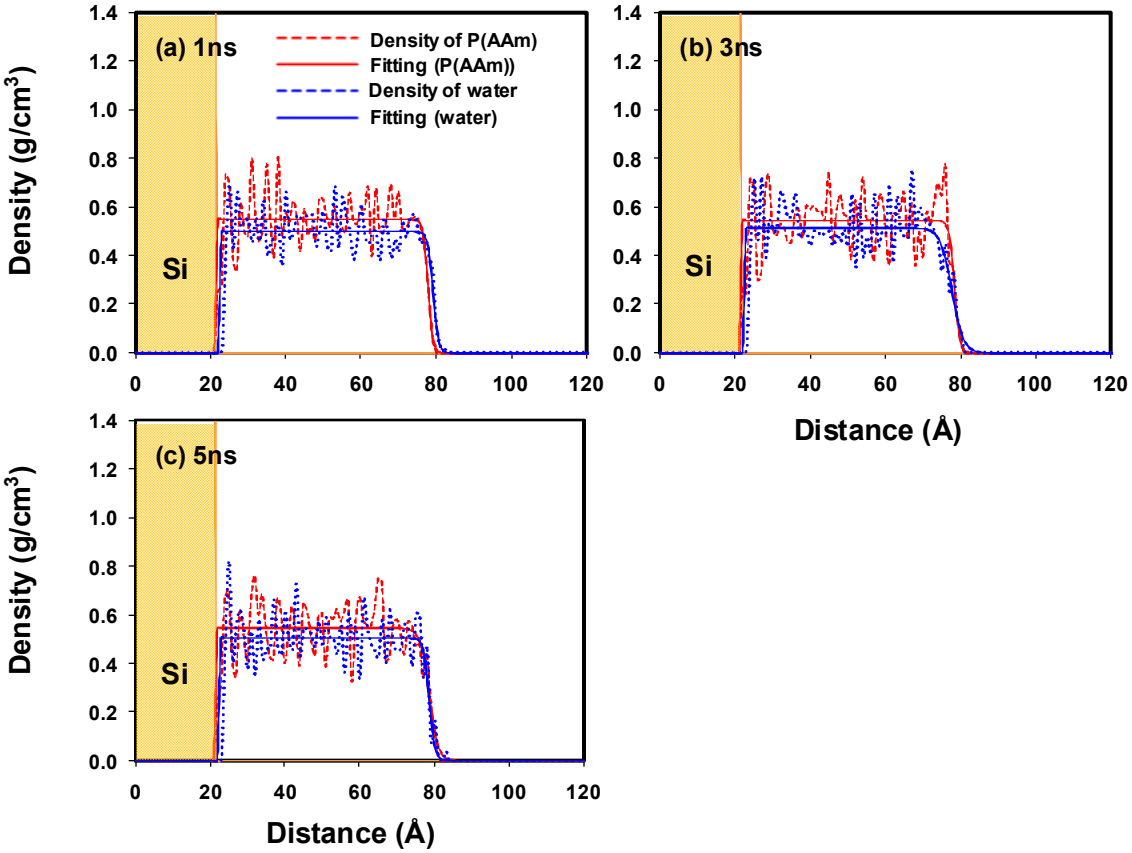

Figure 6.13: Density profiles of the surface-grafted P(AAm) brushes at 370 K: (a) 1 ns; (b) 3 ns; and (c) 5 ns.

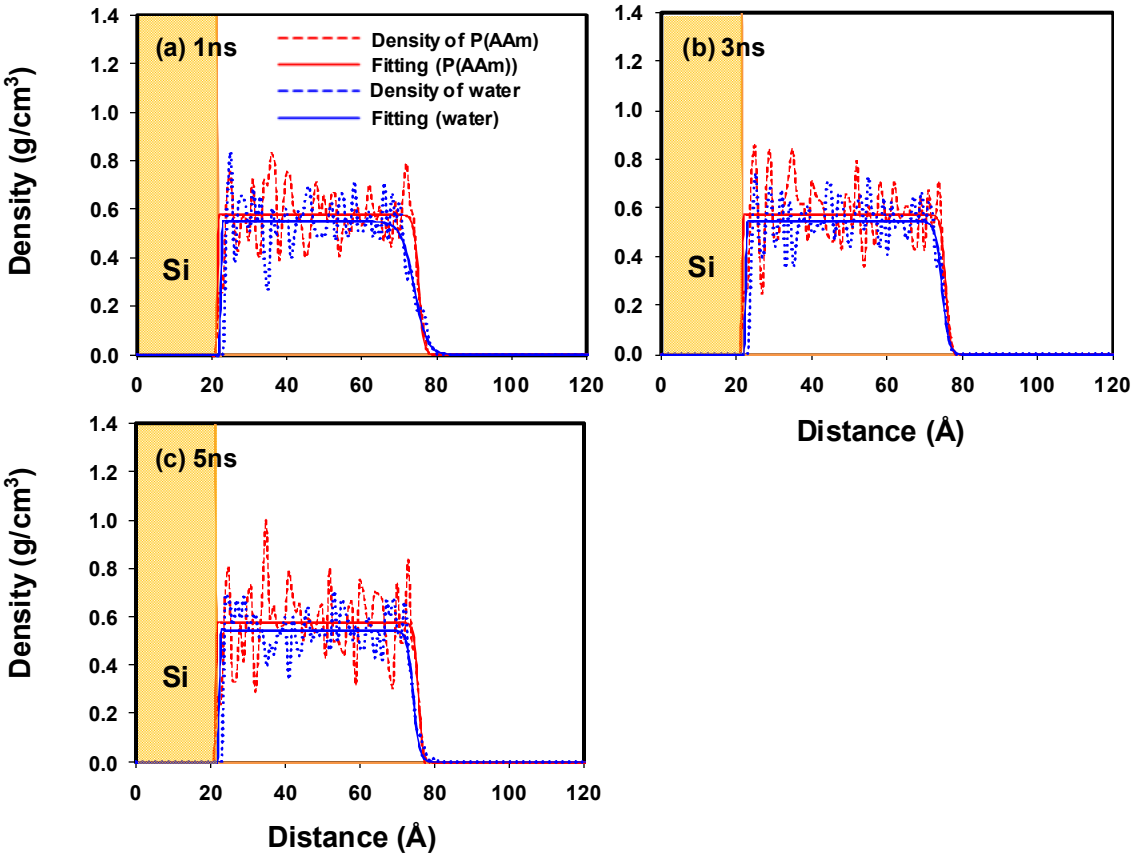

Figure 6.14: Density profiles of the surface-grafted P(AAm) brushes at 345 K: (a) 1 ns; (b) 3 ns; and (c) 5 ns.

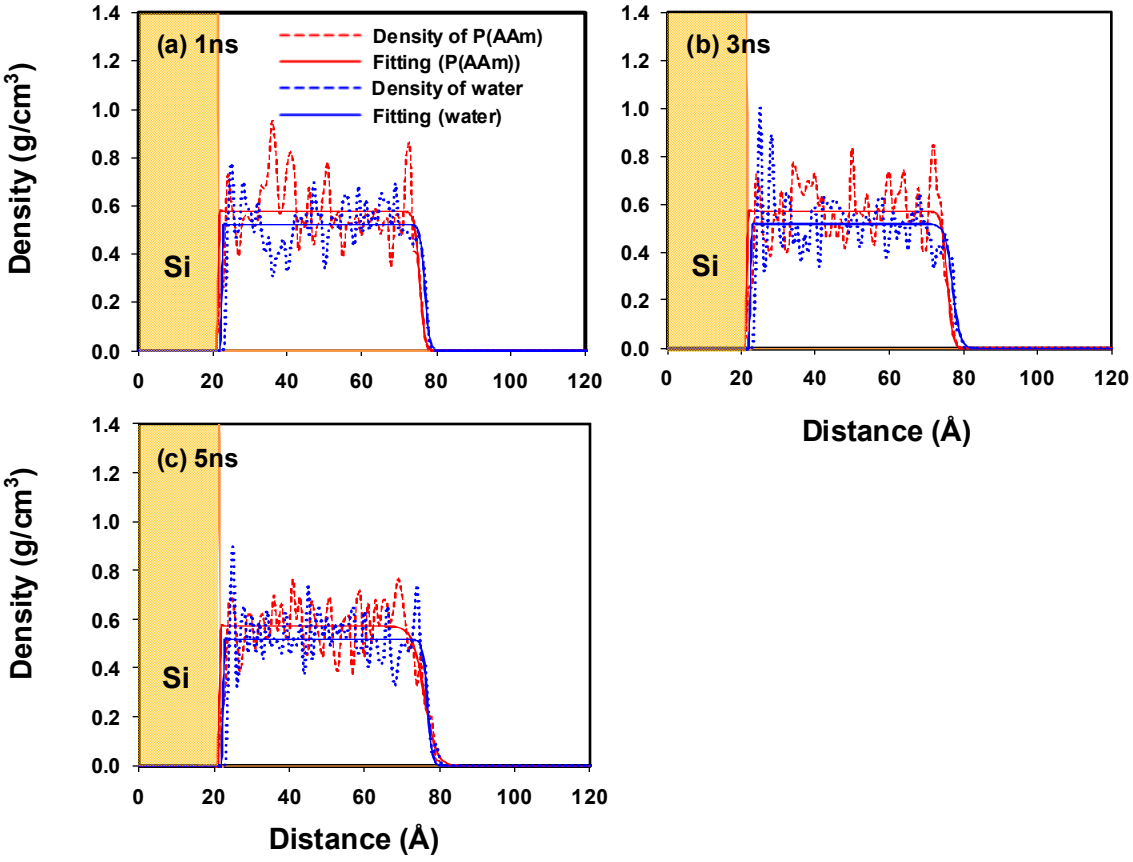

Figure 6.15: Density profiles of the surface-grafted P(AAm) brushes at 320 K: (a) 1 ns; (b) 3 ns; and (c) 5 ns.

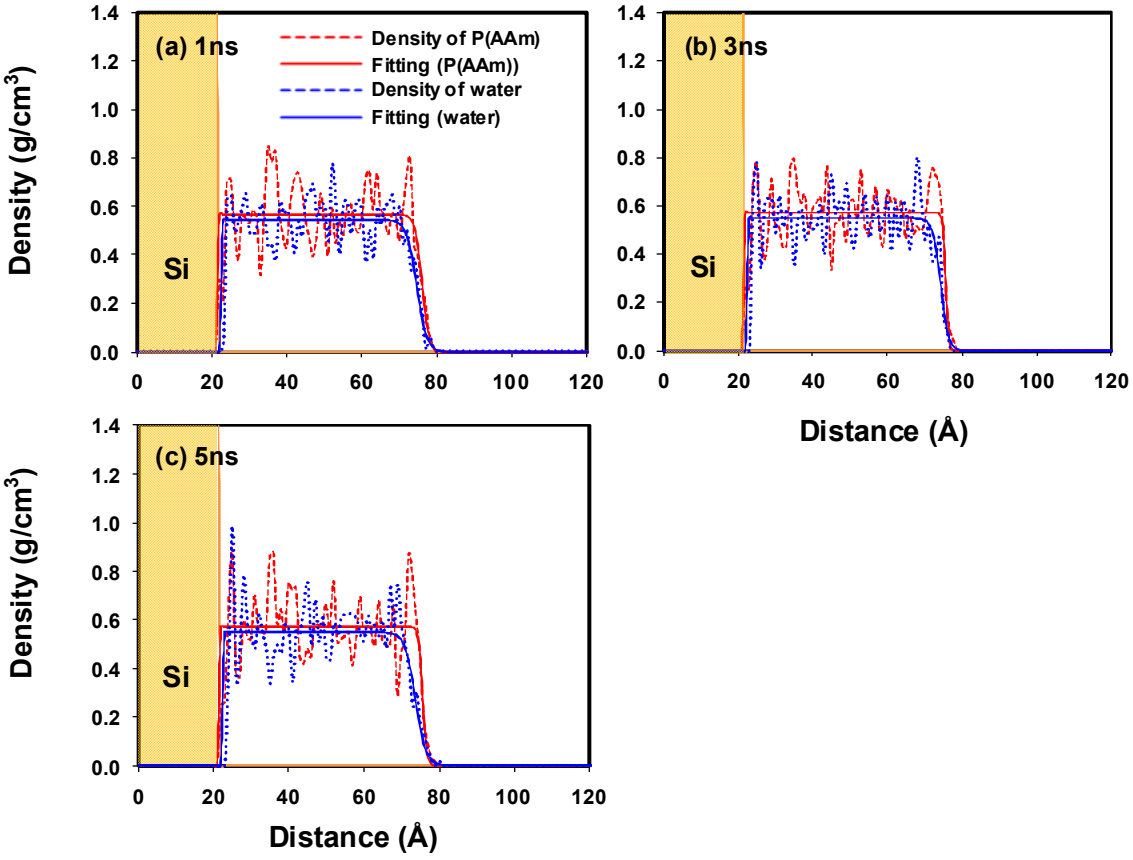

Figure 6.16: Density profiles of the surface-grafted P(AAm) brushes at 290 K: (a) 1 ns; (b) 3 ns; and (c) 5 ns.

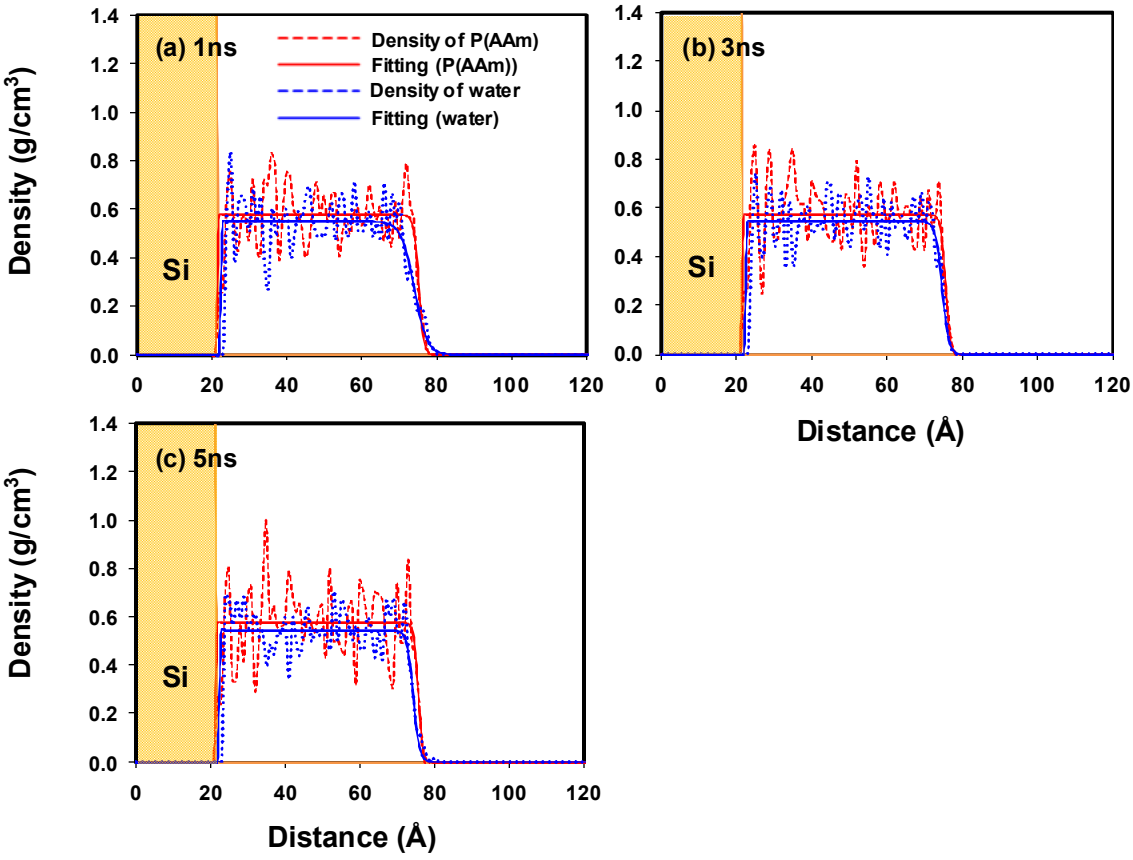

Figure 6.17: Density profiles of the surface-grafted P(AAm) brushes at 275 K: (a) 1 ns; (b) 3 ns; and (c) 5 ns.

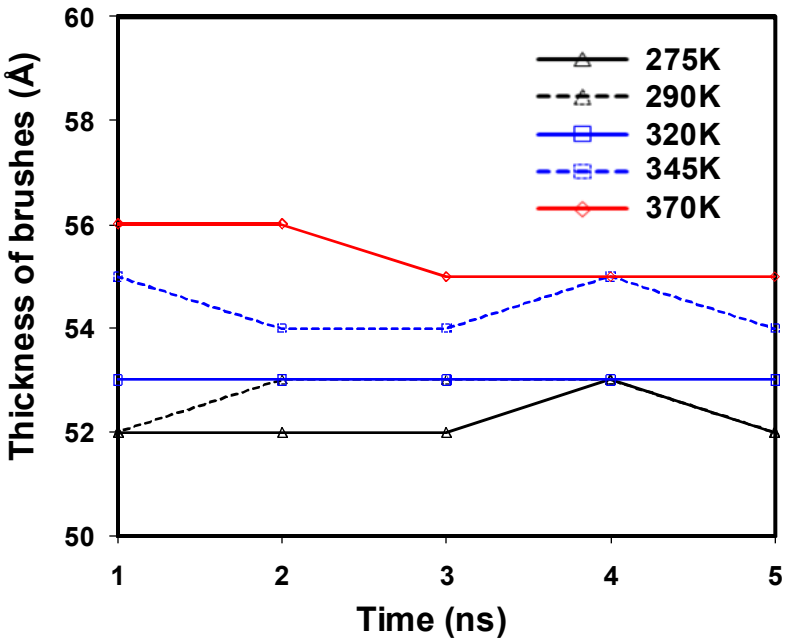

Figure 6.18: Thickness of the P(AAm) brushes.

Pair Correlation Functions of the Surface-grafted Brushes and Water Molecules

To investigate the inner structures of the surface-grafted brushes with the water molecules, we analyzed the pair correlation function (PCF, see Equation 25) of the following (Figure 6.19):

i) The oxygen (NIPAAm)–oxygen (water) pair ($\rho g_{O(NIPAAm)-O(water)}$); the oxygen (AAm)–oxygen (water) pair ($\rho g_{O(AAm)-O(water)}$);

ii) The nitrogen (NIPAAm)–oxygen (water) pair ($\rho g_{N(NIPAAm)-O(water)}$); the nitrogen (AAm)–oxygen (water) pair ($\rho g_{N(AAm)-O(water)}$);

iii) The carbon (NIPAAm)–oxygen (water) pair ($\rho g_{C(NIPAAm)-O(water)}$).

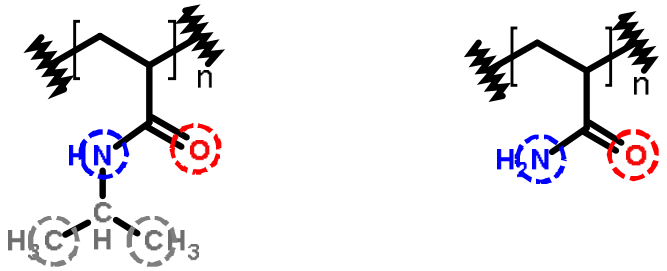

P(NIPAAm) **P(AAm)**

Figure 6.19: Atoms used to calculate the pair correlation function.

Figure 6.20 (a) to (c) shows the PCFs of $\rho g_{O(NIPAAm)-O(water)}$, indicating that the heights of the peaks decrease due to de-swelling of the water molecules above the LCST. The heights of the peaks are not changed during the simulation below the LCST, as shown in Figure 6.20 (d) and (e). The PCFs of $\rho g_{O(AAm)-O(water)}$ (Figure 6.21) also show that the distributions of the pair are not changed during the simulation at a given range of temperatures. Figure 6.22 shows that the PCFs of $\rho g_{N(NIPAAm)-O(water)}$ are decreased above the LCST, but the intensities of the PCFs are not changed below the LCST. It should be noted that the intensities of the PCFs in the short distance range (< 4 Å) are much suppressed in comparison with those of $\rho g_{N(AAm)-O(water)}$ (Figure 6.23), clearly showing the first peaks at the short distance. This is due to the steric hindrances of the isopropyl group, which constrain the hydration of $N_{(NIPAAm)}$. Figure 6.24 shows the PCFs for water around the hydrophobic group of the brush ($\rho g_{C(NIPAAm)-O(water)}$). Again, the heights of the peaks are decreased above the LCST, but the heights of the peaks are not changed below the LCST. Above the LCST, we clearly observe that the intensities of the PCFs for the P(NIPAAm) brush are decreased due to de-swelling of the water molecules, while the

intensities of the PCFs for P(NIPAAm) below the LCST and for P(AAm) at a given range of temperatures are not changed during the simulations. These observations agree with the results of the density profiles.

To quantify the change in the PCFs, we calculated the coordination number (CN) by integrating the first solvation shell. Figure 6.25 shows that the CNs of $C_{(NIPAAm)}$-$O_{(water)}$ and $O_{(NIPAAm)}$-$O_{(water)}$ pairs decreased rapidly above the LCST. The change of the CNs is more significant for the $C_{(NIPAAm)}$-$O_{(water)}$ pairs than for the $O_{(NIPAAm)}$-$O_{(water)}$ pairs. The differences in the CNs from the initial time frame to the final time frame are 0.88 - 1.36 for the $C_{(NIPAAm)}$-$O_{(water)}$ pairs and 0.21 - 0.38 for the $O_{(NIPAAm)}$-$O_{(water)}$ pairs, as shown in Table 6.1. Because $C_{(NIPAAm)}$ does not offer sufficient interaction with water molecules via the hydrogen bonding type of secondary interaction, the de-swelling of the water molecules occurs distinctly around the isopropyl group of the P(NIPAAm) brushes above the LCST. The contribution of $N_{(NIPAAm)}$-$O_{(water)}$ pairs is quite small because of the steric hindrance of the isopropyl group for P(NIPAAm). In contrast, the CNs of the $N_{(AAm)}$-$O_{(water)}$ pairs are ~13 times larger than are those of the $N_{(NIPAAm)}$-$O_{(water)}$ pairs (Table 6.1 and Figure 6.26) in the same distance range (< 3.6 Å), indicating that $N_{(AAm)}$ is well hydrated by the water molecules (no steric hindrance). The change in the CNs for P(NIPAAm)-water pairs below the LCST (Figure 6.25) and P(AAm)-water pairs at a given range of temperatures (Figure 6.26) is not significant, as shown in Table 6.1.

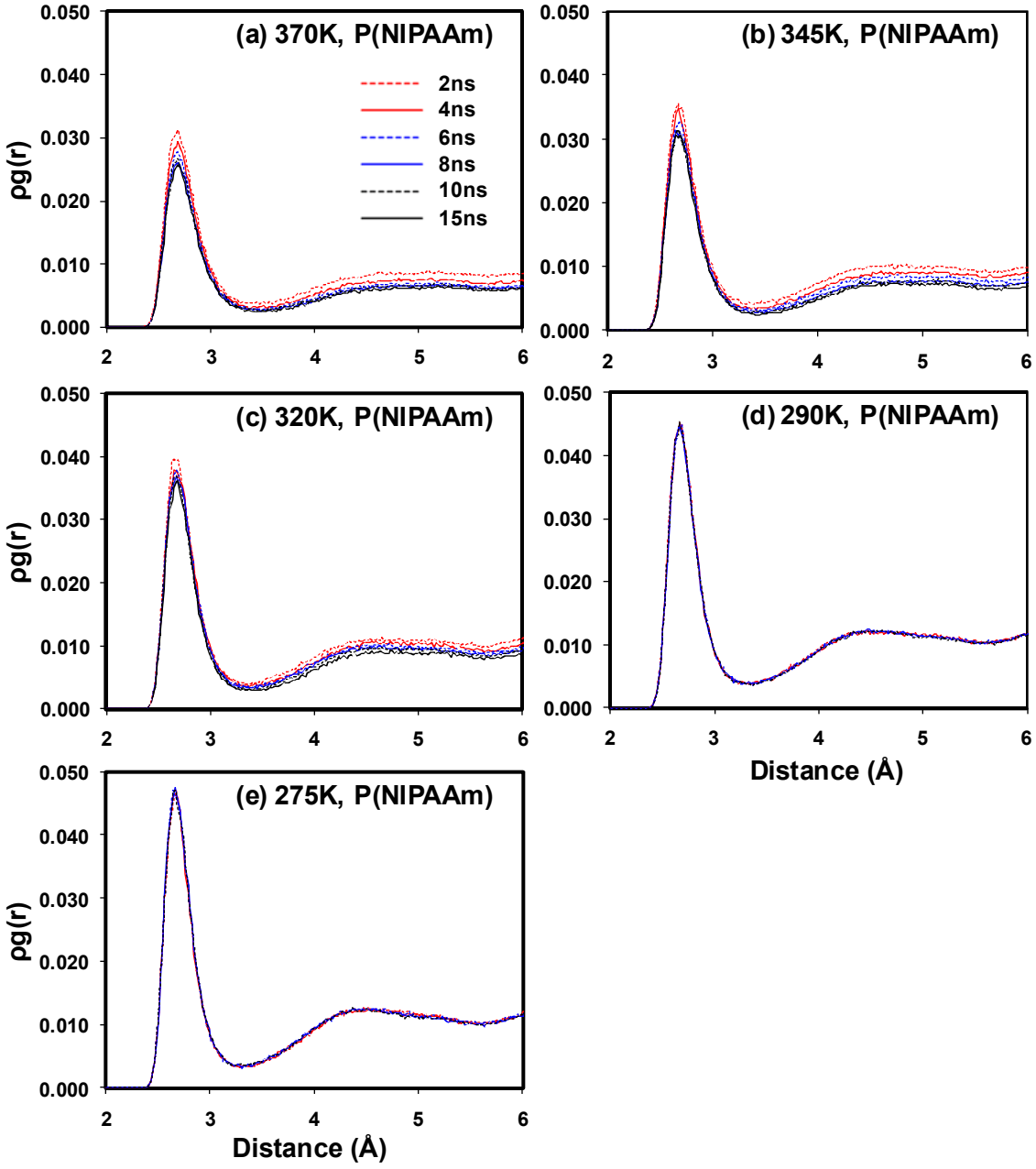

Figure 6.20: Pair correlation functions of O(NIPAAm)-O(water) pairs at 370 K (a); 345 K (b); 320 K (c); 290 K (d); and 275 K (e).

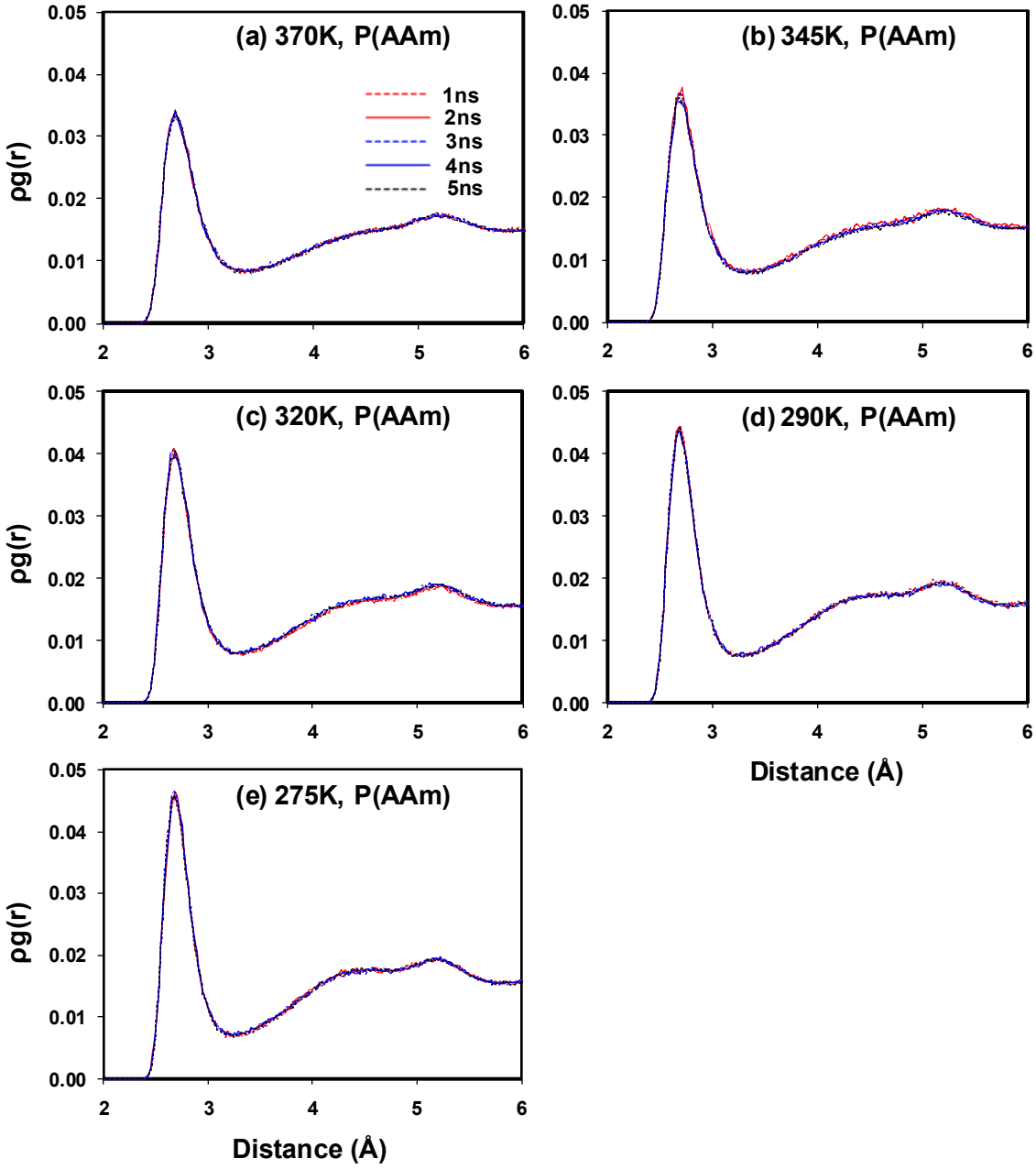

Figure 6.21: Pair correlation functions of O(AAm)-O(water) pairs at 370 K (a); 345 K (b); 320 K (c); 290 K (d); and 275 K (e).

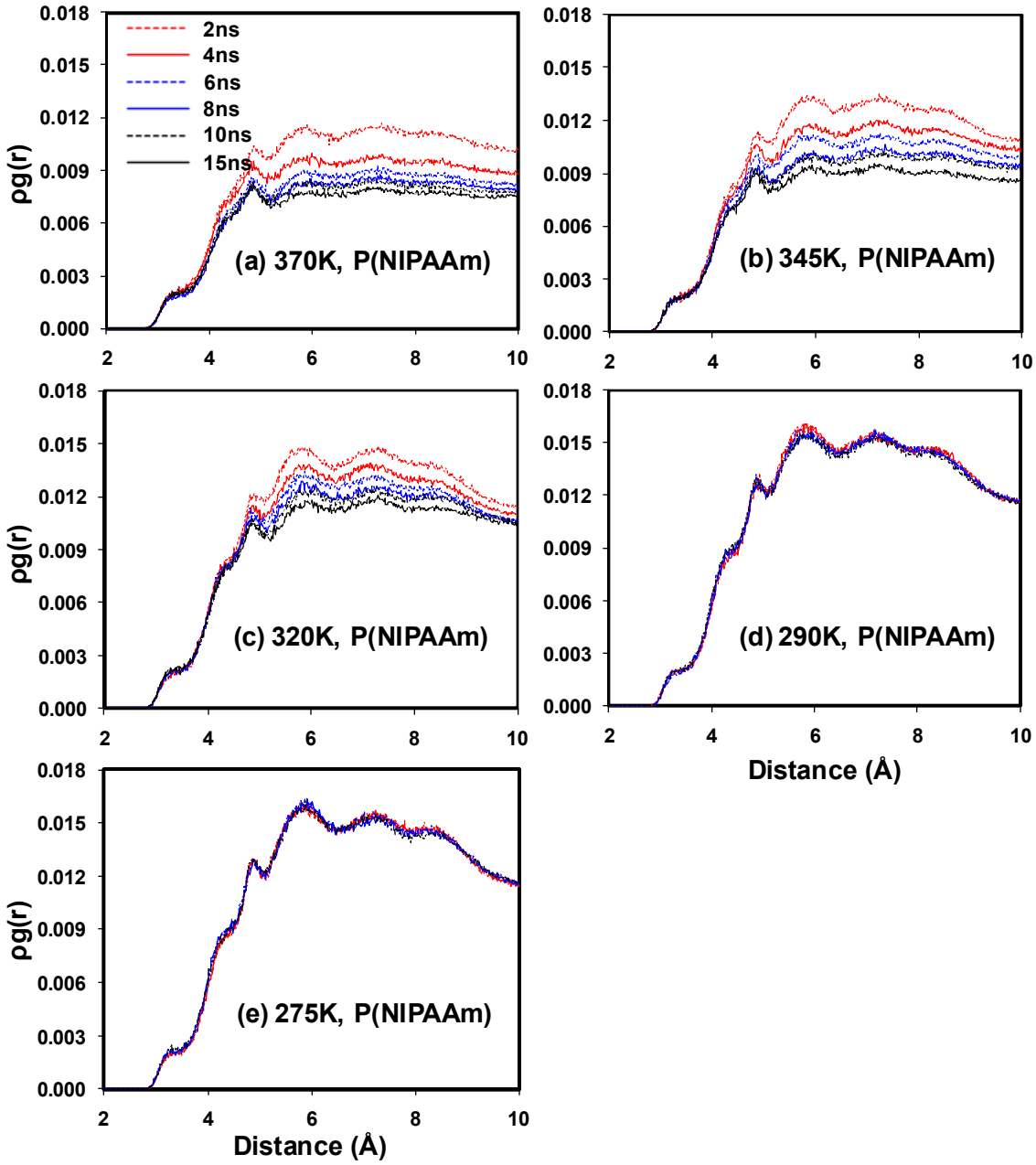

Figure 6.22: Pair correlation functions of N(NIPAAm)-O(water) pairs at 370 K (a); 345 K (b); 320 K (c); 290 K (d); and 275 K (e).

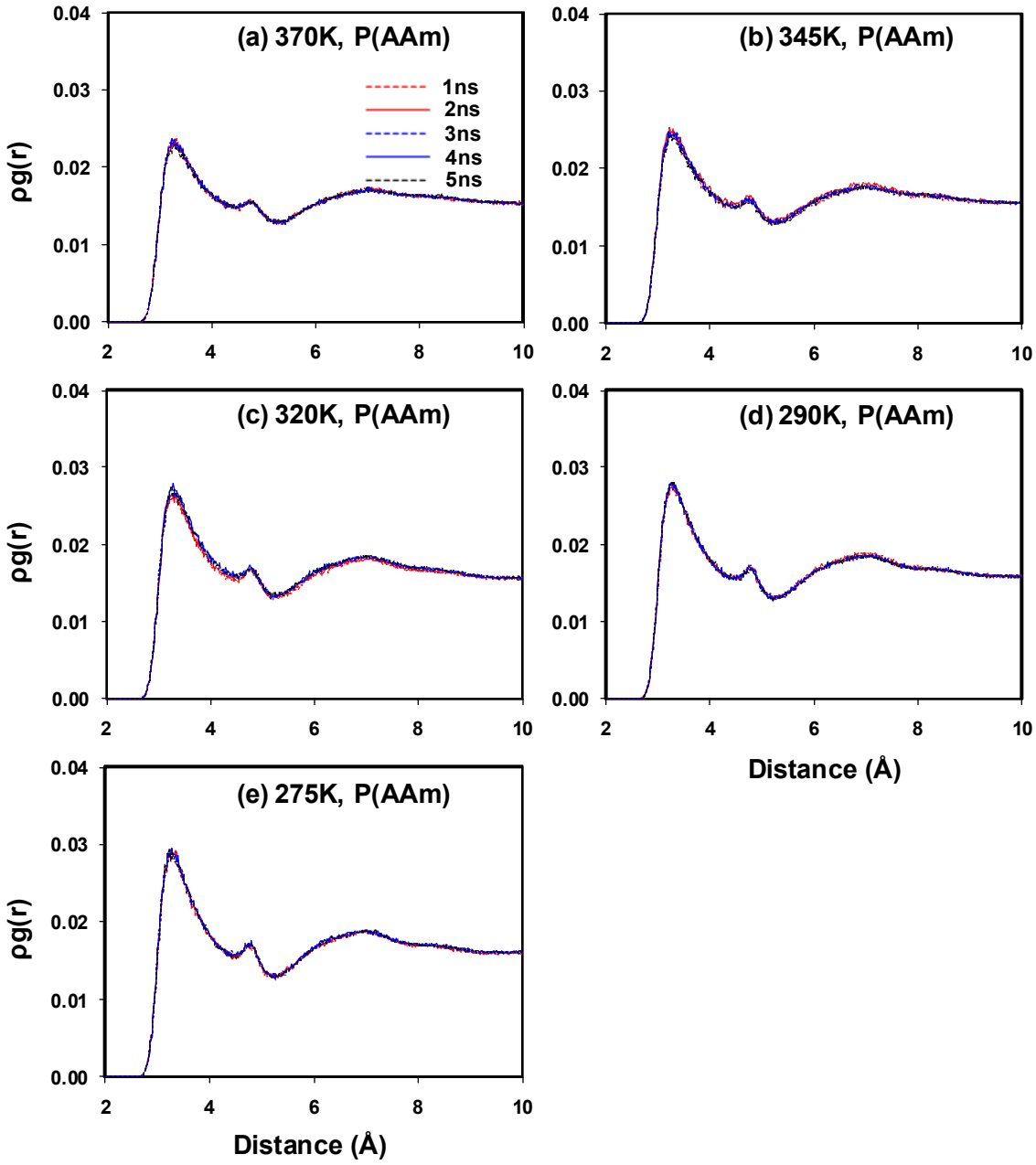

Figure 6.23: Pair correlation functions of N(AAm)-O(water) pairs at 370 K (a); 345 K (b); 320 K (c); 290 K (d); and 275 K (e).

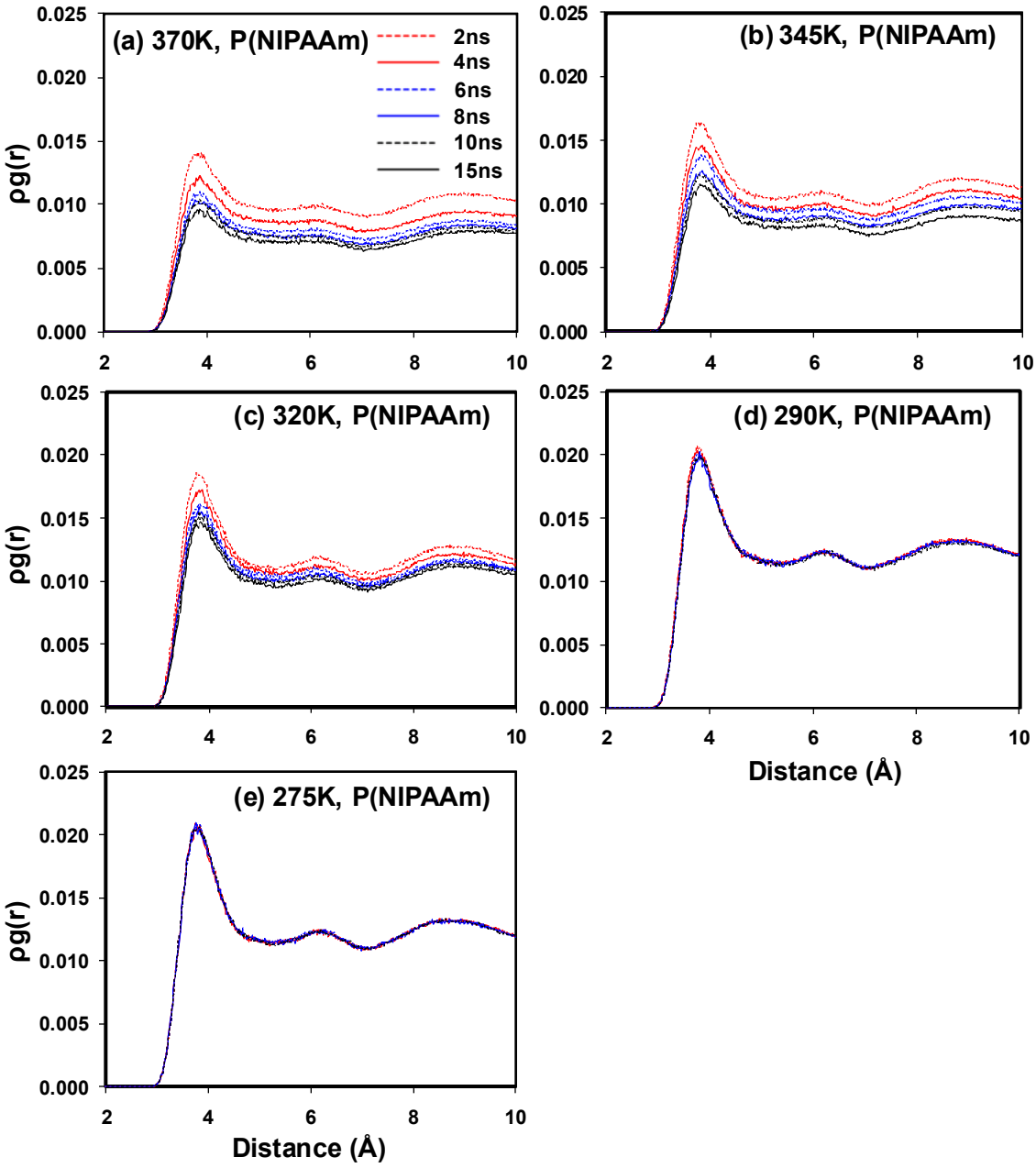

Figure 6.24: Pair correlation functions of C(NIPAAm)-O(water) pairs at 370 K (a); 345 K (b); 320 K (c); 290 K (d); and 275 K (e).

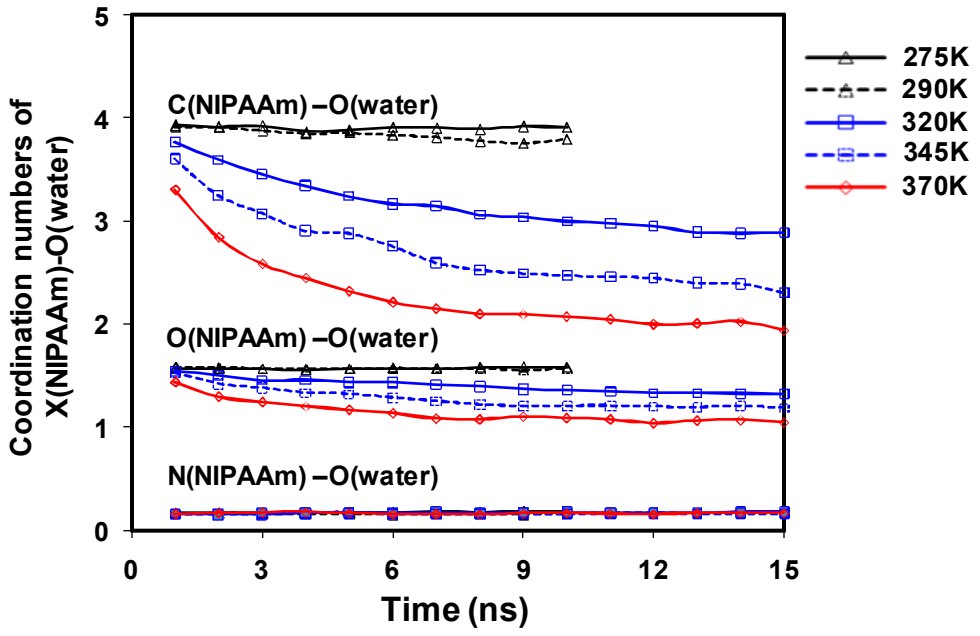

Figure 6.25: Change in the coordination numbers of X(NIPAAm)-O(water) pairs: X = C, O or N.

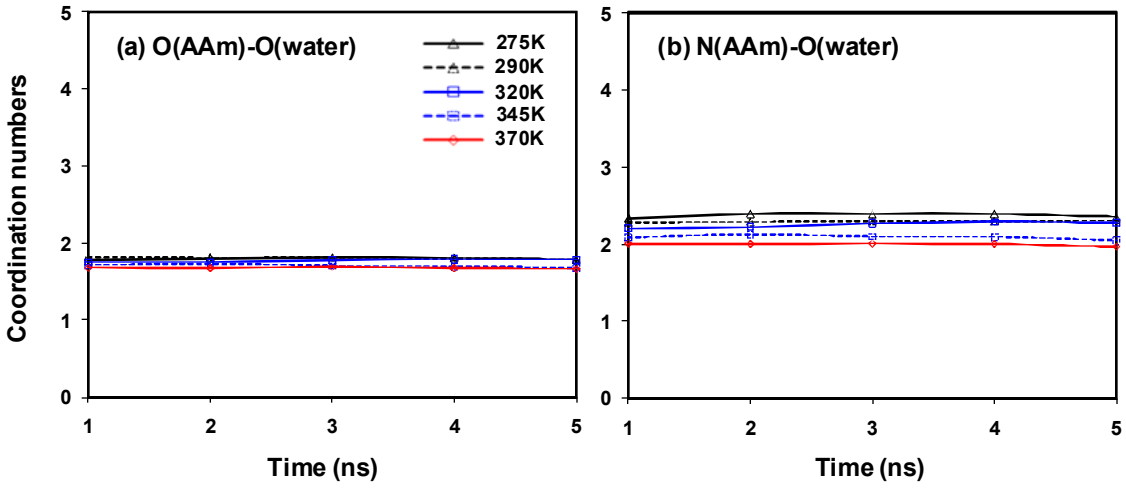

Figure 6.26: Change in the coordination numbers of (a) O(AAm)-O(water) pairs and (b) N(AAm)-O(water) pairs.

Table 6.1: Coordination numbers from the PCFs of P(NIPAAm)-water pairs and P(AAm)-water pairs

pairs	Temperature (K)	CN		Difference in CNs	Range of distance, r(Å)
		From initial time frame	From final time frame		
O_{NIPAAm}-O_{water}	370	1.43	1.05	0.38	< 3.4
	345	1.52	1.18	0.34	
	320	1.54	1.33	0.21	
	290	1.59	1.56	0.03	
	275	1.58	1.58	0.00	
N_{NIPAAm}-O_{water}	370	0.16	0.16	0.00	< 3.6
	345	0.16	0.16	0.00	
	320	0.16	0.18	0.02	
	290	0.16	0.17	0.01	
	275	0.16	0.18	0.02	
C_{NIPAAm}-O_{water}	370	3.30	1.94	1.36	< 4.5
	345	3.60	2.31	1.29	
	320	3.77	2.89	0.88	
	290	3.92	3.79	0.13	
	275	3.93	3.91	0.02	
O_{AAm}-O_{water}	370	1.68	1.67	0.01	< 3.4
	345	1.71	1.67	0.04	
	320	1.76	1.78	0.02	
	290	1.82	1.78	0.04	
	275	1.77	1.78	0.01	
N_{AAm}-O_{water}	370	2.00	1.97	0.03	< 3.6
	345	2.08	2.05	0.03	
	320	2.20	2.27	0.07	
	290	2.28	2.31	0.03	
	275	2.33	2.35	0.02	

Hydrogen Bonding Analysis

Because hydrogen bonding plays an important role in describing the LCST [197, 199, 324], we monitored the change in the hydrogen bonds between polar groups and water molecules. In this investigation, the hydrogen bond is defined by the geometry definition, as described by D. Chandler [371]. A hydrogen bond can exist between a pair of molecules if the distances and angle satisfy the following conditions:

$$\begin{aligned} R_{OO} &\leq 3.60 \text{ Å} \\ R_{OH} &\leq 2.45 \text{ Å} \\ \Phi &\leq 30° \end{aligned} \qquad \textbf{(37)}$$

where R_{OO} and R_{OH} are the distances between the water molecules of $O_1 \cdots O_2$ and $O_1 \cdots H_2$ and Φ is an angle of $O_1 \cdots O_2$ -H_2.

Figure 6.27 shows the change in the total number of hydrogen bonds between the polar groups, =O and –NH for P(NIPAAm) and =O and –NH_2 for P(AAm), and the water molecules. The total number of hydrogen bonds for the O(NIPAAm)-water pairs is changed from 419 (at the initial time frame) to 330 (at the final time frame) for 370 K, from 469 to 388 for 345 K, from 496 to 421 for 320 K, from 501 to 505 for 290 K, and from 503 to 504 for 275 K. Above the LCST, the hydrogen bonds between the polar groups and the water molecules weaken with increasing temperatures, which leads to the de-swelling of water molecules out of the brush. Below the LCST, the change in the hydrogen bonds is not significant. The contribution of the NH(NIPAAm)-water pairs is also insignificant; the total number of hydrogen bonds is ~20, indicating that the interaction between the NH group and the water molecules is not significant due to steric hindrances. These results agree with the results of the PCFs and CNs. The total number

of hydrogen bonds for P(AAm)-water pairs is insignificant at a given range of temperatures but decreases with increasing temperature.

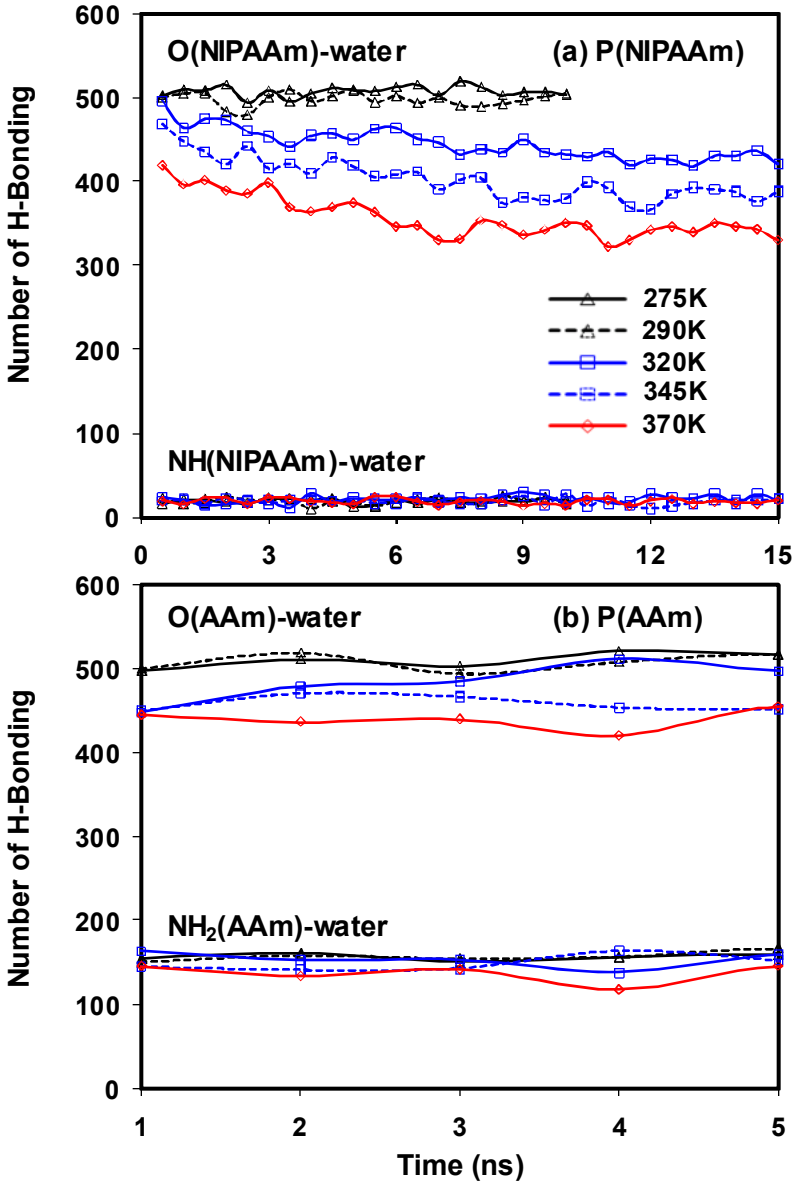

Figure 6.27: Total number of hydrogen bonds: (a) P(NIPAAm) brushes and (b) P(AAm) brushes.

Total Surface Area of the Surface-grafted Brush

Above the LCST, we expect that the total surface area of the P(NIPAAm) brushes will be decreased by collapsing of the brushes followed by de-swelling of the water molecules, and therefore, the collapsed brushes will not provide accessible sites to the water molecules. To check this, we monitored the change in the total surface area of the P(NIPAAm) and P(AAm) brushes that is accessible to the water molecules (solvent), as shown in Figure 6.28. This solvent accessible surface area (SASA) is generated by the center of a solvent rolling over the van der Waals surface of the solute, which is equivalent to constructing the SASA as the surface of the solute atomic spheres have radii equal to the atomic van der Waals radius plus the solvent radius. A solvent radius of 1.4 Å is used to detect the accessible surface area of the brushes for the water molecules. Figure 6.28 (a) clearly shows that the total surface area of the P(NIPAAm) brushes is decreased above the LCST. The change in the total surface area is more significant at high temperatures. However, we did not observe a significant change in the total surface area for the P(NIPAAm) brushes below the LCST or for the P(AAm) brushes at a given range of temperatures.

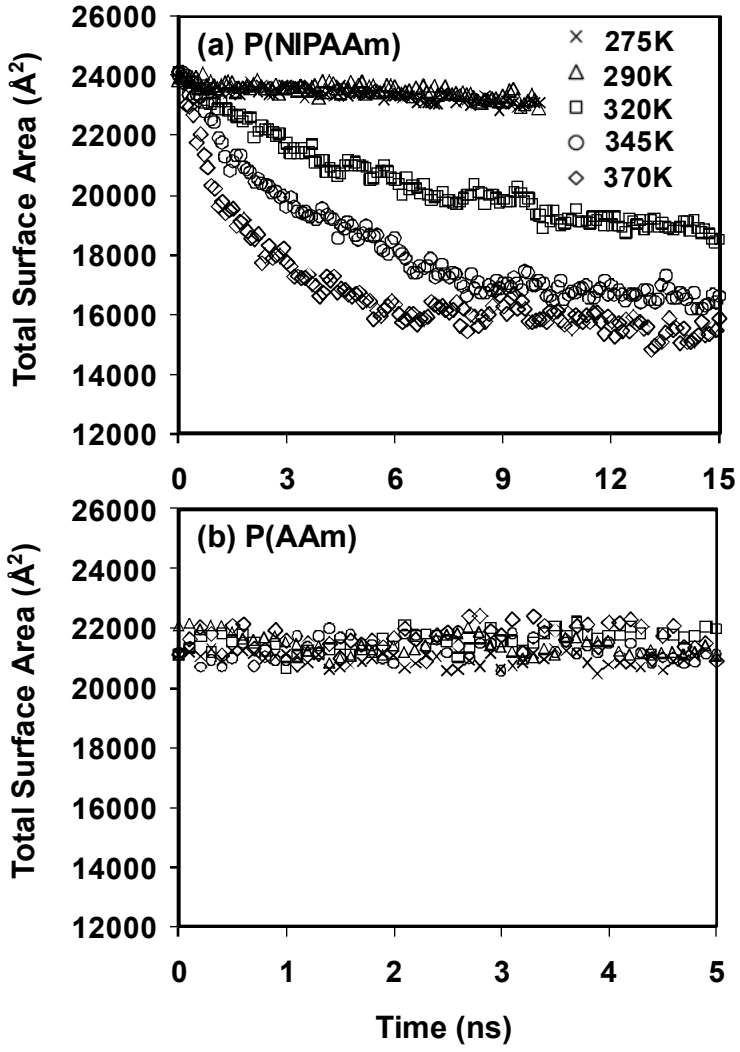

Figure 6.28: Total surface area : (a) P(NIPAAm) brushes and (b) P(AAm) brushes.

Conclusion

Using a full-atomistic MD simulation approach, we investigated the de-swelling mechanisms of the surface-grafted P(NIPAAm) brushes containing 1300 water molecules at 275 K, 290 K, 320 K, 345 K, and 370 K. In this study, we observed a partially collapsed state of the P(NIPAAm) brush above the LCST. The partially collapsed state of the P(NIPAAm) brushes can be formed by the rapid de-swelling of the water from the

free mobile chains [322-324], leading to some of the water molecules being trapped in the dense brushes and gradually diffusing out of the brushes above the LCST [356]. In this study, the detailed de-swelling mechanisms are described by fully atomistic MD simulations. First of all, we clearly observed the de-swelling of the water molecules for P(NIPAAm) above the LCST, whereas we did not observe the de-swelling of the water molecules below the LCST. Using UCST systems (P(AAm) brush) for comparison purposes, we did not observe the de-swelling of water molecules at a given range of temperatures. By analyzing the pair correlation functions and the coordination numbers, the de-swelling of the water molecules occurred distinctly around the isopropyl group of the P(NIPAAm) brush above the LCST because $C_{(NIPAAm)}$ does not offer sufficient interaction with the water molecules via the hydrogen bonding type of secondary interaction. We also found that the contribution of the $N_{(NIPAAm)}$-$O_{(water)}$ pair is quite small because of the steric hindrance of the isopropyl group. By analyzing the change in the hydrogen bonds, the hydrogen bonds between polar groups and water molecules in the P(NIPAAm) brushes weaken with increasing temperature, which leads to the de-swelling of the water molecules out of the brushes above the LCST. Below the LCST, the change in the hydrogen bonds is not significant. Again, the contribution of the NH(NIPAAm)-water pairs is insignificant; the total number of hydrogen bonds is ~20, indicating that the interaction between the NH group and the water molecules is not significant due to steric hindrances. Lastly, we observed that the total surface area of the P(NIPAAm) brushes that is accessible to water molecules is decreased by collapsing the brushes followed by the de-swelling of water molecules above the LCST.

CHAPTER 7: CONCLUSIONS

In this dissertation, we have utilized molecular dynamics simulations to investigate (i) the monomeric sequence effects of P(VP-*co*-HEMA) hydrogels on equilibrated structures, deformation mechanisms, and the diffusion behavior of guest molecules at various water contents (0, 20, 40, and 80 wt%); and (ii) the detailed de-swelling mechanisms and molecular interactions between surface-grafted P(NIPAAm) brushes and water molecules above/below LCST. In summary:

(i) At low water content (~20 wt%), we observed that the monomeric units in the random sequence hydrogel are solvated more than those in the blocky sequence hydrogel. This is because the buried monomers in the blocky sequence hydrogel do not provide accessible sites to the water molecules. It also reveals that the distribution of water in the early stages of swelling (at low hydration) is nonuniform due to the different hydrophilicity of the monomeric units as well as the distribution of the monomer units in the polymer chain. For the deformation mechanism, it was found that the structural relaxation takes place mainly through the VP monomers, especially in the blocky sequence, so that the blocky sequence hydrogel has lower levels of mechanical stress as compared to the random sequence hydrogel. The diffusion coefficients of the guest molecules in the random sequence were higher than those in the blocky sequence, because the hydrophilic domain consists of VP units, especially in the blocky sequence, and interacts with the hydrophilic guest molecules, which reduces the diffusivity of the guest molecules. The abovementioned dependence on the monomeric sequence, however, disappears with increasing water content, because water

dominates the properties of the hydrogel by fully solvating the monomeric units and guest molecules.

This dissertation provides a clear example that the monomeric sequence differences in the polymer chain can influence the equilibrated structure, mechanical, and transport properties of the P(VP-*co*-HEMA) hydrogel. Therefore, it is concluded that the structures and physical properties of the P(VP-*co*-HEMA) hydrogel can be controlled by designing molecular variables such as a monomeric sequence in the polymer chain, especially at low water content.

(ii) We clearly observed the de-swelling of the water molecules in the P(NIPAAm) brushes above the LCST, whereas we did not observe the de-swelling of the water molecules below the LCST. First, the de-swelling of the water molecules occurred distinctly around the isopropyl group of the P(NIPAAm) brush above the LCST, because the isopropyl group does not offer sufficient interaction with the water molecules via the hydrogen bond type of the secondary interaction. In contrast, we found that the contribution of the nitrogen of P(NIPAAm) for the de-swelling of the water is quite small because of the steric hindrance of the isopropyl group. We also observed that the hydrogen bonds between the polar groups and water molecules in the P(NIPAAm) brushes weaken with increasing temperature, which leads to the de-swelling of the water molecules out of the brushes above the LCST. Lastly, the total surface area of the P(NIPAAm) brushes that is accessible to water molecules is decreased by collapsing the brushes and was followed by de-swelling of the water molecules above the LCST. Because the detailed mechanisms of the de-swelling of the water molecules in the P(NIPAAm) hydrogel at the molecular level are not well understood, we were able to provide the first thorough investigation of the detailed de-swelling mechanism of the water molecules using the molecular dynamics simulation

approach. To control the smart responses, it will be important to provide a fundamental understanding of the temperature-sensitive hydrogels at the atomistic level by alternating the nature of the components and the molecular structure of the hydrogel. Therefore, the use of molecular dynamics techniques to investigate molecular mechanisms on smart responsive hydrogels could provide an initial step.

The results presented in this dissertation have raised several questions, which should be pursued:

(i) We assumed that our models for P(VP-*co*-HEMA) have a defect-free ideal network structure. However, experimental samples potentially have structural variations such as free dangling chain ends and self-looping. We expect that the stress relaxation mainly occurs in the vicinity of the defects because the defects provide a greater degree of freedom for structural deformation. Therefore, by developing fine defect models, we will be able to provide more realistic stress responses of deformations in hydrogels.

(ii) Recently, Malham and Bureau [366] reported that the grafting density greatly affects the collapse of P(NIPAAm) hydrogel and the thermal response of the brushes increased with the grafting density of the brushes. Because the detailed mechanisms of the grafting density dependence of the P(NIPAAm) brushes at the atomic level are not well understood, it would be beneficial to be able to evaluate the detailed molecular mechanisms under various grafting densities of the P(NIPAAm) brushes.

(iii) It has been known that the hydrogels respond to a variety of external stimuli such as pH, solution ionic strength, and applied electrode potential [320]. However, the detailed molecular mechanisms of the multi-stimuli systems are not well understood. We expect that the computational molecular simulation can be a useful tool to study the responsive properties of hydrogel to external stimuli by investigating the molecular interactions among the components in the presence of specific stimuli as well as thermodynamic conditions, which will enhance our understanding of hydrogel systems.

REFERENCES

[1] LOWMAN, A. M. and PEPPAS, N. A., Hydrogels. in: MATHIOWITZ, E. (Ed.), Encyclopedia of Controlled Drug Delivery, Vol. 2, John Wiley & Sons, 1999, pp. 397-406.

[2] WICHTERLE, O. and LIM, D. "Hydrophilic gels for biological use," Nature, vol. 185, pp. 117-118, 1960.

[3] PEPPAS, N. A. "Hydrogels and drug delivery," Current Opinion in Colloid & Interface Science, vol. 2, pp. 531-537, 1997.

[4] PEPPAS, N. A., HUANG, Y., TORRES-LUGO, M., WARD, J. H. and ZHANG, J. "Physicochemical, foundations and structural design of hydrogels in medicine and biology," Annual Review of Biomedical Engineering, vol. 2, pp. 9-29, 2000.

[5] LEE, K. Y. and MOONEY, D. J. "Hydrogels for tissue engineering," Chemical Reviews, vol. 101, pp. 1869-1879, 2001.

[6] BYRNE, M. E., PARK, K. and PEPPAS, N. A. "Molecular imprinting within hydrogels," Advanced Drug Delivery Reviews, vol. 54, pp. 149-161, 2002.

[7] LANGER, R. and PEPPAS, N. A. "Advances in biomaterials, drug delivery, and bionanotechnology," AIChE Journal, vol. 49, pp. 2990-3006, 2003.

[8] LANGER, R. and TIRRELL, D. A. "Designing materials for biology and medicine," Nature, vol. 428, pp. 487-492, 2004.

[9] PARK, K., CHEN, J. and PARK, H., in: OTTENBRITE, R. M. and KIM, S. W. (Eds.), Polymeric Drugs & Drug Delivery Systems, CRC Press, Boca Raton, 2001.

[10] JEONG, S. H., HUH, K. M. and PARK, K., in: KWON, G. S. (Ed.), Polymeric Drug Delivery Systems, Taylor & Francis, Boca Raton, 2006.

[11] TANAKA, Y., GONG, J. P. and OSADA, Y. "Novel hydrogels with excellent mechanical performance," Progress in Polymer Science, vol. 30, pp. 1-9, 2005.

[12] FRIENDS, G. D., KUNZLER, J. F. and OZARK, R. M. "Recent Advances in the Design of Polymers for Contact-Lenses," Macromolecular Symposia, vol. 98, pp. 619-631, 1995.

[13] CHANDRASEKARAN, S. K., BOWMAN, L. and HARVEY, T. "Polymers for Contact-Lens Applications," Abstr Pap Am Chem S, vol. 189, pp. 105-INDE, 1985.

[14] YANG, W. H., SMOLEN, V. F. and PEPPAS, N. A. "Oxygen Permeability Coefficients of Polymers for Hard and Soft Contact-Lens Applications," Journal of Membrane Science, vol. 9, pp. 53-67, 1981.

[15] NG, C. O. and TIGHE, B. J. "Polymers in Contact-Lens Applications .6. Dissolved-Oxygen Permeability of Hydrogels and Design of Materials for Use in Continuous-Wear Lenses," British Polymer Journal, vol. 8, pp. 118-123, 1976.

[16] NG, C. O., PEDLEY, D. G. and TIGHE, B. J. "Polymers in Contact-Lens Applications .7. Oxygen Permeability and Surface Hydrophilicity of Poly(4-Methylpent-1-Ene) and Related Polymers," British Polymer Journal, vol. 8, pp. 124-130, 1976.

[17] PEPPAS, N. A. "Hydrogels in medicine and pharmacy," CRC Press, Boca Raton, 1987.

[18] "Biomaterials science, An introduction to materials in medicine," RATNER, B. D., HOFFMAN, A. S., SCHOEN, F. J. and LEMONS, J. E., Elsevier Academic Press, San Diego, CA, 2004.

[19] HARTMANN, S. "The world as a process. Simulations in the natural and social sciences," HEGSELMANN, R., MUELLER, U. and TROITZSCH, K. G., Modelling and simulation in the social sciences from the philosophy of science point of view, Kluwer, Dordrecht, 1996.

[20] FRENKEL, D. and SMIT, B. "Understanding molecular simulation ", Academic Press, San Diego, 2001.

[21] ALLEN, M. P. and TILDESLEY, D. J. "Computer simulation of liquids," Oxford University Press, New York, 1987.

[22] RAPPE, A. K. and CASEWIT, C. J. "Molecular mechanics across chemistry," University Science Books, Sausalito, 1997.

[23] BULTINCK, P., WINTER, H. D., LANGENAEKER, W. and TOLLENAERE, J. P., Computational medicinal chemistry for drug discovery, Marcel Dekker, New York, 2004.

[24] BECKER, O. M., ALEXANDER D. MACKERELL, J., ROUX, B. and WATANABE, M., Computational biochemistry and biophysics, Marcel Dekker, New York, 2001.

[25] TSAI, C. S. "An introduction to computational biochemistry," Wiley-Liss, New York, 2002.

[26] TAMAI, Y., TANAKA, H. and NAKANISHI, K. "Molecular dynamics study of polymer-water interaction in hydrogels .1. Hydrogen-bond structure," Macromolecules, vol. 29, pp. 6750-6760, 1996.

[27] TAMAI, Y., TANAKA, H. and NAKANISHI, K. "Molecular dynamics study of polymer-water interaction in hydrogels .2. Hydrogen-bond dynamics," Macromolecules, vol. 29, pp. 6761-6769, 1996.

[28] TAMAI, Y. and TANAKA, H. "Effects of polymer chains on structure and dynamics of supercooled water in poly(vinyl alcohol)," Physical Review E, vol. 59, pp. 5647-5654, 1999.

[29] TAMAI, Y. and TANAKA, H. "Structure and dynamics of poly(vinyl alcohol) hydrogel," Molecular Simulation, vol. 21, pp. 283-301, 1999.

[30] OLDIGES, C. and TONSING, T. "Molecular dynamic simulation of structural, mobility effects between dilute aqueous CH3CN solution and crosslinked PAA - Part 1. Structure," Physical Chemistry Chemical Physics, vol. 4, pp. 1628-1636, 2002.

[31] OLDIGES, C., TONSING, T. and WITTLER, K. "Molecular dynamics simulation of structural, mobility effects between dilute aqueous CH3CN solution and crosslinked PAA - Part 2. Dynamics," Physical Chemistry Chemical Physics, vol. 4, pp. 5135-5141, 2002.

[32] OLDIGES, C., WITTLER, K., TONSING, T. and ALIJAH, A. "MD calculated structural properties of clusters in liquid acetonitrile/water mixtures with various contents of acetonitrile," Journal of Physical Chemistry A, vol. 106, pp. 7147-7154, 2002.

[33] JANG, S. S., GODDARD, W. A. and KALANI, M. Y. S. "Mechanical and transport properties of the poly(ethylene oxide)-poly(acrylic acid) double network hydrogel from molecular dynamic simulations," Journal of Physical Chemistry B, vol. 111, pp. 1729-1737, 2007.

[34] JANG, S. S., GODDARD, W. A., KALANI, M. Y. S., MYUNG, D. and FRANK, C. W. "Mechanical and transport properties of the poly(ethylene oxide)-poly(acrylic acid) double network hydrogel from molecular dynamic Simulations (vol 111B, pg 1729, 2007)," Journal of Physical Chemistry B, vol. 111, pp. 14440, 2007.

[35] RATNER, B. D., HOFFMAN, A. S., SCHOEN, F. J. and LEMONS, J. E. "Biomaterials science: An introduction to materials in medicine," Elsevier Academic Press, San Diego, CA, 2004.

[36] K LAL, J. "The use of methacrylic polymers in medicine," Die Makromolekulare Chemie, vol. 7, pp. 31-39, 1984.

[37] RATNER, B. D. and HOFFMAN, A. S. "Synthetic Hydrogels for Biomedical Applications," Acs Symposium Series, pp. 1-36, 1976.

[38] DENIZLI, A., KIREMITCI, M. and PISKIN, E. "Subcutaneous Polymeric Matrix System Poly(Hema-Bga) for Controlled Release of an Anticancer Drug (5-Fluorouracil) .1. Synthesis and Structure," Biomaterials, vol. 9, pp. 257-262, 1988.

[39] MONTHEARD, J. P., CHATZOPOULOS, M. and CHAPPARD, D. "2-Hydroxyethyl Methacrylate (Hema) - Chemical-Properties and Applications in Biomedical Fields," Journal of Macromolecular Science-Reviews in Macromolecular Chemistry and Physics, vol. C32, pp. 1-34, 1992.

[40] NETTI, P. A., SHELTON, J. C., REVELL, P. A., PIRIE, C., SMITH, S., AMBROSIO, L., NICOLAIS, L. and BONFIELD, W. "Hydrogels as an Interface between Bone and an Implant," Biomaterials, vol. 14, pp. 1098-1104, 1993.

[41] ARICA, M. Y., SENEL, S., ALAEDDINOGLU, N. G., PATIR, S. and DENIZLI, A. "Invertase immobilized on spacer-arm attached poly(hydroxyethyl methacrylate) membrane: Preparation and properties," Journal of Applied Polymer Science, vol. 75, pp. 1685-1692, 2000.

[42] BARAN, T., ARICA, M. Y., DENIZLI, A. and HASIRCI, V. "Comparison of beta-galactosidase immobilization by entrapment in and adsorption on poly(2-hydroxyethylmethacrylate) membranes," Polymer International, vol. 44, pp. 530-536, 1997.

[43] ARICA, M. Y., ALAEDDINOGLU, N. G. and HASIRCI, V. "Immobilization of glucoamylase onto activated pHEMA/EGDMA microspheres: properties and application to a packed-bed reactor," Enzyme and Microbial Technology, vol. 22, pp. 152-157, 1998.

[44] YOSHIDA, M., ASANO, M., KAETSU, I., IMAI, K., MASHIMO, T., YUASA, H., YAMANAKA, H., KAWAHARADA, U. and SUZUKI, K. "Studies of the Slow Releasing of Testosterone from Radiation-Polymerized Testicular Prostheses Implanted Subcutaneously in the Back of Castrated Rabbits," Biomaterials, vol. 8, pp. 124-128, 1987.

[45] FERREIRA, L., VIDAL, M. M. and GIL, M. H. "Evaluation of poly(2-hydroxyethyl methacrylate) gels as drug delivery systems at different pH values," International Journal of Pharmaceutics, vol. 194, pp. 169-180, 2000.

[46] HONG, Y., CHIRILA, T. V., CUYPERS, M. J. H. and CONSTABLE, I. J. "Polymers of 1-vinyl-2-pyrrolidinone as potential vitreous substitutes: Physical selection," Journal of Biomaterials Applications, vol. 11, pp. 135-181, 1996.

[47] HOFFMAN, A. S. "Hydrogels for biomedical applications," Advanced Drug Delivery Reviews, vol. 54, pp. 3-12, 2002.

[48] PEPPAS, N. A., MOYNIHAN, H. J. and LUCHT, L. M. "The Structure of Highly Crosslinked Poly(2-Hydroxyethyl Methacrylate) Hydrogels," Journal of Biomedical Materials Research, vol. 19, pp. 397-411, 1985.

[49] TRIGO, R. M., BLANCO, M. D., HUERTA, P., OLMO, R. and TEIJON, J. M. "L-Ascorbic-Acid release from PHEMA hydrogels," Polymer Bulletin, vol. 31, pp. 577-584, 1993.

[50] SONG, S. Z., CARDINAL, J. R., KIM, S. H. and KIM, S. W. "Progestin Permeation through Polymer Membranes .5. Progesterone Release from Monolithic Hydrogel Devices," Journal of Pharmaceutical Sciences, vol. 70, pp. 216-219, 1981.

[51] NATHAN, P., ROBB, E. C., LAW, E. J. and MACMILLAN, B. G. "A clinical study of antimicrobial agents delivered to burn wounds from a drug-loaded synthetic dressing," J Trauma, vol. 22, pp. 1015-1018, 1982.

[52] GOKCE, M., AKATA, R. F. and KIREMITCIGUMUSDERELIOGLU, M. "5-FU loaded pHEMA drainage implants for glaucoma-filtering surgery: Device design and in vitro release kinetics," Biomaterials, vol. 17, pp. 941-949, 1996.

[53] GARCIA, O., TRIGO, R. M., BLANCO, M. D. and TEIJON, J. M. "Influence of degree of crosslinking on 5-fluorouracil release from poly(2-hydroxyethyl methacrylate) hydrogels," Biomaterials, vol. 15, pp. 689-694, 1994.

[54] SOMMADOSSI, J. P., GEWIRTZ, D. A., DIASIO, R. B., AUBERT, C., CANO, J. P. and GOLDMAN, I. D. "Rapid Catabolism of 5-Fluorouracil in Freshly Isolated Rat Hepatocytes as Analyzed by High-Performance Liquid-Chromatography," Journal of Biological Chemistry, vol. 257, pp. 8171-8176, 1982.

[55] KIREMITCIGUMUSDERELIOGLU, M., GOKCE, M. and AKATA, R. F. "A novel MMC-loaded pHEMA drainage device for the treatment of glaucoma: In vitro and in vivo studies," Journal of Biomaterials Science-Polymer Edition, vol. 7, pp. 857-869, 1996.

[56] PYWELL, E. J., YALKOWSKY, S. H. and COLLETT, J. H. "The Effect of a Rate Controlling Membrane on Release from Polyhema Hydrogels," Drug Development and Industrial Pharmacy, vol. 12, pp. 1767-1775, 1986.

[57] LU, S. X. and ANSETH, K. S. "Photopolymerization of multilaminated poly(HEMA) hydrogels for controlled release," Journal of Controlled Release, vol. 57, pp. 291-300, 1999.

[58] BLANCO, M. D., TRIGO, R. M., TEIJON, C., GOMEZ, C. and TEIJON, J. M. "Slow releasing of ara-C from poly(2-hydroxyethyl methacrylate) and poly(2-hydroxyethyl methacrylate-co-N-vinyl-2-pyrrolidone) hydrogels implanted subcutaneously in the back of rats," Biomaterials, vol. 19, pp. 861-869, 1998.

[59] TEIJON, J. M., TRIGO, R. M., GARCIA, O. and BLANCO, M. D. "Cytarabine trapping in poly(2-hydroxyethyl methacrylate) hydrogels: Drug delivery studies," Biomaterials, vol. 18, pp. 383-388, 1997.

[60] TRIGO, R. M., BLANCO, M. D., TEIJON, J. M. and SASTRE, R. "Anticancer Drug, Ara-C, Release from Phema Hydrogels," Biomaterials, vol. 15, pp. 1181-1186, 1994.

[61] HUGLIN, M. B. and SLOAN, D. J. "Release of Ergotamine from Poly (2-Hydroxyethyl Methacrylate)," British Polymer Journal, vol. 15, pp. 165-171, 1983.

[62] HUGLIN, M. B. and SLOAN, D. J. "Incorporation of Ergotamine into Un-Crosslinked Poly(2-Hydroxyethyl Methacrylate)," Angewandte Makromolekulare Chemie, vol. 118, pp. 197-202, 1983.

[63] WOOD, J. M., ATTWOOD, D. and COLLETT, J. H. "The Influence of Gel Formulation on the Diffusion of Salicylic-Acid in Polyhema Hydrogels," Journal of Pharmacy and Pharmacology, vol. 34, pp. 1-4, 1982.

[64] LEE, P. I. "Dimensional Changes during Drug Release from a Glassy Hydrogel Matrix," Polymer Communications, vol. 24, pp. 45-47, 1983.

[65] MESLARD, J. C., YEAN, L., SUBIRA, F. and VAIRON, J. P. "Reversible Immobilization of Drugs on a Hydrogel Matrix .1. Synthesis of Unsaturated Chloramphenicol Derivatives and Copolymerization with 2-Hydroxyethyl Methacrylate," Makromolekulare Chemie-Macromolecular Chemistry and Physics, vol. 187, pp. 787-794, 1986.

[66] YEAN, L., BUNEL, C. and VAIRON, J. P. "Reversible Immobilization of Drugs on a Hydrogel Matrix .2. Diffusion of Free Chloramphenicol from Poly(2-

Hydroxyethyl Methacrylate) Hydrogels," Makromolekulare Chemie-Macromolecular Chemistry and Physics, vol. 191, pp. 1119-1129, 1990.

[67] YEAN, L., MESLARD, J. C., SUBIRA, F., BUNEL, C. and VAIRON, J. P. "Reversible Immobilization of Drugs on a Hydrogel Matrix .3. Hydrolysis of Chloramphenicol Precursors," Makromolekulare Chemie-Macromolecular Chemistry and Physics, vol. 191, pp. 1131-1142, 1990.

[68] HSIUE, G. H., GUU, J. A. and CHENG, C. C. "Poly(2-hydroxyethyl methacrylate) film as a drug delivery system for pilocarpine," Biomaterials, vol. 22, pp. 1763-1769, 2001.

[69] SEFTON, M. V. and NISHIMURA, E. "Insulin Permeability of Hydrophilic Polyacrylate Membranes," Journal of Pharmaceutical Sciences, vol. 69, pp. 208-209, 1980.

[70] KLIMENT, K., STOL, M., FAHOUN, K. and STOCKAR, B. "Use of spongy hydron in plastic surgery," J Biomed Mater Res, vol. 2, pp. 237-243, 1968.

[71] VOLDRICH, Z., TOMANEK, Z. and KOPECEK, J. "Long-Term Experience with Poly(Glycol Monomethacrylate) Gel in Plastic Operations of Nose," Journal of Biomedical Materials Research, vol. 9, pp. 675-685, 1975.

[72] YOUNG, C. D., WU, J. R. and TSOU, T. L. "Fabrication and characteristics of polyHEMA artificial skin with improved tensile properties," Journal of Membrane Science, vol. 146, pp. 83-93, 1998.

[73] YOUNG, C. D., WU, J. R. and TSOU, T. L. "High-strength, ultra-thin and fiber-reinforced pHEMA artificial skin," Biomaterials, vol. 19, pp. 1745-1752, 1998.

[74] NATHAN, P., MACMILLA.BG and HOLDER, I. A. "Effect of a Synthetic Dressing Formed on a Burn Wound in Rats - Comparison of Allografts, Collagen Sheets, and Polyhydroxyethylmethacrylate in Control of Wound-Infection," Applied Microbiology, vol. 28, pp. 465-468, 1974.

[75] HUSAIN, M. T., AKHTAR, M. and AKHTAR, N. "Report on evaluation of hydron film as burn wound dressing," Burns Incl Therm Inj, vol. 9, pp. 330-334, 1983.

[76] MIGLIARESI, C., CARFAGNA, C. and NICOLAIS, L. "Laminates of Poly(2-Hydroxyethyl Methacrylate) and Polybutadiene as Potential Burn Covering," Biomaterials, vol. 1, pp. 205-208, 1980.

[77] WARREN, R. J. and SNELLING, C. F. T. "Clinical-Evaluation of the Hydron Burn Dressing," Plastic and Reconstructive Surgery, vol. 66, pp. 361-368, 1980.

[78] LEE, S. D., HSIUE, G. H., KAO, C. Y. and CHANG, P. C. T. "Artificial cornea: Surface modification of silicone rubber membrane by graft polymerization of pHEMA via glow discharge," Biomaterials, vol. 17, pp. 587-595, 1996.

[79] SMETANA, K., SULC, J., KRCOVA, Z. and PITROVA, S. "Intraocular Biocompatibility of Hydroxyethyl Methacrylate and Methacrylic-Acid Copolymer Partially Hydrolyzed Poly(2-Hydroxyethyl Methacrylate)," Journal of Biomedical Materials Research, vol. 21, pp. 1247-1253, 1987.

[80] CHIRILA, T. V. "Melanized poly(HEMA) hydrogels: basic research and potential use," Journal of biomaterials applications, vol. 8, pp. 106-145, 1993.

[81] KIDANE, A., SZABOCSIK, J. M. and PARK, K. "Accelerated study on lysozyme deposition on poly(HEMA) contact lenses," Biomaterials, vol. 19, pp. 2051-2055, 1998.

[82] DOWNES, R., LAVIN, M. and COLLIN, R. "Hydrophilic expanders for the congenital anophthalmic socket," Adv Ophthalmic Plast Reconstr Surg, vol. 9, pp. 57-61, 1992.

[83] ARICA, M. Y., DENIZLI, A., BARAN, T. and HASIRCI, V. "Dye derived and metal incorporated affinity poly(2-hydroxyethyl methacrylate) membranes for use in enzyme immobilization," Polymer International, vol. 46, pp. 345-352, 1998.

[84] MABILLEAU, G., MOREAU, M. F., FILMON, R., BASLE, M. F. and CHAPPARD, D. "Biodegradability of poly (2-hydroxyethyl methacrylate) in the presence of the J774.2 macrophage cell line," Biomaterials, vol. 25, pp. 5155-5162, 2004.

[85] PELUSO, G., PETILLO, O., ANDERSON, J. M., AMBROSIO, L., NICOLAIS, L., MELONE, M. A. B., ESCHBACH, F. O. and HUANG, S. J. "The differential effects of poly(2-hydroxyethyl methacrylate) and poly(2-hydroxyethyl methacrylate)/poly(caprolactone) polymers on cell proliferation and collagen synthesis by human lung fibroblasts," Journal of Biomedical Materials Research, vol. 34, pp. 327-336, 1997.

[86] HARKES, G., FEIJEN, J. and DANKERT, J. "Adhesion of Escherichia-Coli on to a Series of Poly(Methacrylates) Differing in Charge and Hydrophobicity," Biomaterials, vol. 12, pp. 853-860, 1991.

[87] LOPEZ, G. P., RATNER, B. D., RAPOZA, R. J. and HORBETT, T. A. "Plasma Deposition of Ultrathin Films of Poly(2-Hydroxyethyl Methacrylate) - Surface-Analysis and Protein Adsorption Measurements," Macromolecules, vol. 26, pp. 3247-3253, 1993.

[88] MORRA, M. and CASSINELLI, C. "Surface Field of Forces and Protein Adsorption Behavior of Poly(Hydroxyethylmethacrylate) Films Deposited from Plasma," Journal of Biomedical Materials Research, vol. 29, pp. 39-45, 1995.

[89] BOSE, R. K. and LAU, K. K. S. "Mechanical Properties of Ultrahigh Molecular Weight PHEMA Hydrogels Synthesized Using Initiated Chemical Vapor Deposition," Biomacromolecules, vol. 11, pp. 2116-2122, 2010.

[90] HWANG, J. R. and SEFTON, M. V. "The effects of polymer concentration and a pore-forming agent (PVP) on HEMA-MMA microcapsule structure and permeability," Journal of Membrane Science, vol. 108, pp. 257-268, 1995.

[91] AKASHI, M. and TAKEMOTO, K. "New Aspects of Polymer Drugs," Advances in Polymer Science, vol. 97, pp. 107-146, 1990.

[92] BELL, C. L. and PEPPAS, N. A. "Biomedical membranes from hydrogels and interpolymer complexes," Advances in Polymer Science, vol. 122, pp. 125-175, 1995.

[93] LAPORTE, R. J. "Hydrophilic polymer coatings for medical devices ", CRC Press, Lancaster, PA, 1997.

[94] CAMERON, A. M. "Blood plasma expander-PVP," Delaware medical journal, vol. 26, pp. 149-151, 1954.

[95] HAAF, F., SANNER, A. and STRAUB, F. "Polymers of N-Vinylpyrrolidone - Synthesis, Characterization and Uses," Polymer Journal, vol. 17, pp. 143-152, 1985.

[96] KING, J. H., JR. and MCTIGUE, J. W. "The Reformation of the Anterior Chamber with Polyvinylpyrrolidone," South Med J, vol. 57, pp. 1369-1372, 1964.

[97] SCUDERI, G. "Ricerche sperimentali sul trapianto del vitreo (Tentativi di sostituzione parziale con vitreo omologo, con liquor eterologo, con soluzioni di polivinilpirrolidone)," Ann. Ottalrnol. Clin. Ocul., vol. 80, pp. 213-220, 1954.

[98] HAYANO, S. and YOSHINO, T. "Local application of polyvinylpyrrolidone (PVP) for some ocular diseases," Rinsho ganka, Japanese journal of clinical ophthalmology, vol. 13, pp. 449-453, 1959.

[99] CHIRILA, T. V. and HONG, Y. "Poly(1-vinyl-2-pyrrolidinone) hydrogels as vitreous substitutes: a rheological study," Polymer International, vol. 46, pp. 183-195, 1998.

[100] SARDA, R. P., MAKHIJA, J. M. and SHARMA, R. G. "Polyvinyl Pyrrolidone (Pvp) in Cataract Surgery," British Journal of Ophthalmology, vol. 53, pp. 477-&, 1969.

[101] KIM, C. S., LEE, C. H., SHIN, J. S., CHUNG, Y. S. and HYUNG, N. I. "A simple and rapid method for isolation of high quality genomic DNA from fruit trees and conifers using PVP," Nucleic Acids Research, vol. 25, pp. 1085-1086, 1997.

[102] ROBINSON, B. V., SULLIVAN, F. M., BORZELLECA, J. F. and SCHWARTZ, S. L. "PVP: A critical review of the kinetics and toxicology of polyvinylpyrrolidone (povidone)," Lewis Publishers, Chelsea, MI, 1990.

[103] BLANCO, M. D., TRIGO, R. M., GARCIA, O. and TEIJON, J. M. "Controlled release of cytarabine from poly(2-hydroxyethyl methacrylate-co-N-vinyl-2-pyrrolidone) hydrogels," Journal of Biomaterials Science-Polymer Edition, vol. 8, pp. 709-719, 1997.

[104] GALLARDO, A., FERNANDEZ, F., BERMEJO, P., REBUELTA, M., CIFUENTES, A., DIEZ-MASA, J. C. and SAN ROMAN, J. "Controlled release of cyclosporine from VP-HEMA copolymer systems of adjustable resorption monitorized by MEKC," Biomaterials, vol. 21, pp. 915-921, 2000.

[105] DAVIS, T. P. and HUGLIN, M. B. "Studies on copolymeric hydrogels of N-Vinyl-2-Pyrrolidone with 2-Hydroxyethyl Methacrylate," Macromolecules, vol. 22, pp. 2824-2829, 1989.

[106] ATTA, A. M. and ARNDT, K. F. "Swelling behaviour of pH- and temperature-sensitive copolymers containing 2-hydroxy-ethyl methacrylate and N-vinyl-2-pyrrolidone crosslinked with new crosslinkers," Polymer International, vol. 53, pp. 1870-1881, 2004.

[107] ZALDIVAR, D., PENICHE, C., GALLARDO, A. and SANROMAN, J. "Biocompatible Hydrogels of Controlled Hydrophobicity from Copolymers of N-Vinyl-2-Pyrrolidone and Furfuryl Methacrylate," Biomaterials, vol. 14, pp. 1073-1079, 1993.

[108] LANGER, R., CIMA, L. G., TAMADA, J. A. and WINTERMANTEL, E. "Future-Directions in Biomaterials," Biomaterials, vol. 11, pp. 738-745, 1990.

[109] Title 21 CFR (Code of Federal Regulations) 175.105. in: FDA (Ed.), 2010.

[110] MABILLEAU, G., AGUADO, E., STANCU, I. C., CINCU, C., BASLE, M. E. and CHAPPARD, D. "Effects of FGF-2 release from a hydrogel polymer on bone mass and microarchitecture," Biomaterials, vol. 29, pp. 1593-1600, 2008.

[111] CIFUENTES, A., DIEZ-MASA, J. C., MONTENEGRO, C., REBUELTA, M., GALLARDO, A., ELVIRA, C. and SAN ROMAN, J. "Recombinant growth hormone delivery systems based on vinylpyrrolidone-hydroxyethyl methacrylate copolymer matrices: Monitoring optimization by capillary zone electrophoresis," Journal of Biomaterials Science-Polymer Edition, vol. 11, pp. 993-1005, 2000.

[112] CAPIZZI, R. L., WHITE, J. C., POWELL, B. L. and PERRINO, F. "Effect of Dose on the Pharmacokinetic and Pharmacodynamic Effects of Cytarabine," Seminars in Hematology, vol. 28, pp. 54-69, 1991.

[113] WYSOCKI, M., KURYLAK, A., PILECKI, O. and BALCAR-BORON, A. "Preliminary evaluation of adverse effects after administration of arabinoside cytosine (Ara-C) in high doses to children with acute myelogenous leukemia," Acta Haematol Pol, vol. 25, pp. 37-42, 1994.

[114] FRUTOS, P., DIEZ-PENA, E., FRUTOS, G. and BARRALES-RIENDA, J. M. "Release of gentamicin sulphate from a modified commercial bone cement. Effect of (2-hydroxyethyl methacrylate) comonomer and poly(N-vinyl-2-pyrrolidone) additive on release mechanism and kinetics," Biomaterials, vol. 23, pp. 3787-3797, 2002.

[115] GALLARDO, A., FERNANDEZ, F., CIFUENTES, A., DIEZ-MASA, J. C., BERMEJO, P., REBUELTA, M., LOPEZ-BRAVO, A. and ROMAN, J. S. "Modulated release of cyclosporine from soluble vinyl pyrrolidone-hydroxyethyl methacrylate copolymer hydrogels - A correlation of 'in vitro' and 'in vivo' experiments," Journal of Controlled Release, vol. 72, pp. 1-11, 2001.

[116] AHMAD, B., BASHIR, S., NISA, S. U. and HUGLIN, M. B. "Chemically crosslinked N-vinyl-2-pyrrolidone/2-hydroxyethyl methacrylate (VP/HEMA) copolymer for the controlled release of cyclic oligopeptide," Turkish Journal of Chemistry, vol. 28, pp. 279-285, 2004.

[117] KORSMEYER, R. W. and PEPPAS, N. A. "Solute and penetrant diffusion in swellable polymers. III. Drug release from glassy poly(HEMA-co-NVP) copolymers " Journal of Controlled Release, vol. 1, pp. 89-98, 1984.

[118] MATSUSHIMA, S., TAKASU, A., INAI, Y., HIRABAYASHI, T., ERA, S., SOGAMI, M., SASAKI, F., OHSAKI, H. and KINOSADA, Y. "Equivalent cross-relaxation rate imaging in the synthetic copolymer gels and invasive ductal carcinomas of the breast," Magnetic Resonance Imaging, vol. 20, pp. 285-293, 2002.

[119] LOU, X., GARRETT, K. L., RAKOCZY, P. E. and CHIRILA, T. V. "Synthetic hydrogels as carriers in antisense therapy: Preliminary evaluation of an oligodeoxynucleotide covalent conjugate with a copolymer of 1-vinyl-2-

pyrrolidinone and 2-hydroxyethyl methacrylate," Journal of Biomaterials Applications, vol. 15, pp. 307-320, 2001.

[120] BASRI, M., SAMSUDIN, S., BIN AHMAD, M., RAZAK, C. N. A. and SALLEH, A. B. "Lipase immobilized on poly(VP-co-HEMA) hydrogel for esterification reaction," Applied Biochemistry and Biotechnology, vol. 81, pp. 205-217, 1999.

[121] BASRI, M., WONG, C. C., AHMAD, M. B., RAZAK, C. N. A. and SALLEH, A. B. "Immobilization of lipase on poly(N-vinyl-2-pyrrolidone-co-2-hydroxyethyl methacrylate) hydrogel for the synthesis of butyl oleate," Journal of the American Oil Chemists Society, vol. 76, pp. 571-577, 1999.

[122] DEMIRCIOGLU, H., BEYENAL, H., TANYOLAC, A. and HASIRCI, N. "Immobilization of Urease and Estimation of Effective Diffusion-Coefficients of Urea in Hema and Vp Copolymer Matrices," Polymer International, vol. 35, pp. 321-327, 1994.

[123] HOSAKA, S., YAMADA, A., TANZAWA, H., MOMOSE, T., MAGATANI, H. and NAKAJIMA, A. "Mechanical-Properties of the Soft Contact-Lens of Poly(Methyl Methacrylate-N-Vinylpyrrolidone)," Journal of Biomedical Materials Research, vol. 14, pp. 557-566, 1980.

[124] COMPAN, V., GARRIDO, J., MANZANARES, J. A., ANDRES, J., ESTEVE, J. S. and LOPEZ, M. L. "True and Apparent Oxygen Permeabilities of Contact-Lenses," Optometry and Vision Science, vol. 69, pp. 685-690, 1992.

[125] SWAN, M. C., BUCKNALL, D. G., GOODACRE, T. E. and CZERNUSZKA, J. T. "Synthesis and properties of a novel anisotropic self-inflating hydrogel tissue expander," Acta Biomater, vol. 7, pp. 1126-1132, 2011.

[126] SWAN, M., Anisotropic self-inflating tissue expanders in reconstructive plastic surgery. Oxford University, 2008.

[127] SWAN, M. C., GOODACRE, T. E. E., CZERNUSZKA, J. T. and BUCKNALL, D. G. "Cleft palate repair with the use of osmotic expanders: a response," Journal of Plastic Reconstructive and Aesthetic Surgery, vol. 61, pp. 220-221, 2008.

[128] WIESE, K. G. "Osmotically induced tissue expansion with hydrogels: a new dimension in tissue expansion? A preliminary report," J Craniomaxillofac Surg, vol. 21, pp. 309-313, 1993.

[129] WIESE, K. G., HEINEMANN, D. E. H., OSTERMEIER, D. and PETERS, J. H. "Biomaterial properties and biocompatibility in cell culture of a novel self-inflating hydrogel tissue expander," Journal of Biomedical Materials Research, vol. 54, pp. 179-188, 2001.

[130] WIESE, K. G., VOGEL, M., GUTHOFF, R. and GUNDLACH, K. K. H. "Treatment of congenital anophthalmos with self-inflating polymer expanders: a new method," Journal of Cranio-Maxillofacial Surgery, vol. 27, pp. 72-76, 1999.

[131] CHUMMUN, S., ADDISON, P. and STEWART, K. J. "The osmotic tissue expander: A 5-year experience," Journal of Plastic Reconstructive and Aesthetic Surgery, vol. 63, pp. 2128-2132, 2010.

[132] OBDEIJN, M. C., NICOLAI, J. P. A. and WERKER, P. M. N. "The osmotic tissue expander: a three-year clinical experience," Journal of Plastic Reconstructive and Aesthetic Surgery, vol. 62, pp. 1219-1222, 2009.

[133] MISCHKOWSKI, R. A. and KUBLER, A. C. "Correction of congenital nasal hypoplasia associated with Kallmann syndrome using self inflating injectable tissue expander pellets," Plastic and Reconstructive Surgery, vol. 118, pp. 1447-1452, 2006.

[134] RONERT, M. A., HOFHEINZ, H., MANASSA, E., ASGAROULADI, H. and OLBRISCH, R. R. "The beginning of a new era in tissue expansion: Self-filling osmotic tissue expander-four-year clinical experience," Plastic and Reconstructive Surgery, vol. 114, pp. 1025-1031, 2004.

[135] RONERT, M. A., HOFHEINZ, H. and OLBRISCH, R. R. "The beginning of a new era: Self-filling tissue expander for defect coverage in a 3-year-old boy with a retroauricular nevus," Plastic and Reconstructive Surgery, vol. 112, pp. 189-191, 2003.

[136] VON SEE, C., RUCKER, M., BORMANN, K. H. and GELLRICH, N. C. "Using a novel self-inflating hydrogel expander for intraoral gingival tissue expansion prior to bone augmentation," Br J Oral Maxillofac Surg, vol. 48, pp. e5-6, 2010.

[137] KOBUS, K. F. "Cleft palate repair with the use of osmotic expanders: a preliminary report," Journal of Plastic Reconstructive and Aesthetic Surgery, vol. 60, pp. 414-421, 2007.

[138] BERGE, S. J., WIESE, K. G., VON LINDERN, J. J., NIEDERHAGEN, B., APPEL, T. and REICH, R. H. "Tissue expansion using osmotically active hydrogel systems for direct closure of the donor defect of the radial forearm flap," Plastic and Reconstructive Surgery, vol. 108, pp. 1-5, 2001.

[139] "Polymeric Biomaterials," DUMITRIU, S., Marcel Dekker, New York, 2002.

[140] FORNASIERO, F., UNG, M., RADKE, C. J. and PRAUSNITZ, J. M. "Glass-transition temperatures for soft-contact-lens materials. Dependence on water content," Polymer, vol. 46, pp. 4845-4852, 2005.

[141] GALLARDO, A., LEMUS, A. R., ROMAN, J. S., CIFUENTES, A. and DIEZ-MASA, J. C. "Micellar electrokinetic chromatography applied to copolymer systems with heterogeneous distribution," Macromolecules, vol. 32, pp. 610-617, 1999.

[142] ODIAN, G. "Principles of polymerization," John Wiley & Sons, Inc., Hoboken, Nwe Jersey, 2004.

[143] DIONISIO, J. M. and ODRISCOLL, K. F. "High-Conversion Co-Polymerization of Styrene and Methyl-Methacrylate," Journal of Polymer Science Part C-Polymer Letters, vol. 17, pp. 701-707, 1979.

[144] ELIAS, H. G. "An Introduction to Polymer Science," VCH, Weinheim, Germany, 1997.

[145] HAUTUS, F. L. M., LINSSEN, H. N. and GERMAN, A. L. "Dependence of Computed Copolymer Reactivity Ratios on the Calculation Method .2. Effects of Experimental-Design and Error Structure," Journal of Polymer Science Part a-Polymer Chemistry, vol. 22, pp. 3661-3671, 1984.

[146] HAUTUS, F. L. M., LINSSEN, H. N. and GERMAN, A. L. "Dependence of Computed Copolymer Reactivity Ratios on the Calculation Method .1. Effect of Experimental Setup," Journal of Polymer Science Part a-Polymer Chemistry, vol. 22, pp. 3487-3498, 1984.

[147] HAMIELIC, A. E., MACGREGOR, J. F. and PENDILIS, A. "Copolymerization " EASTMOND, G. C., LEDWITH, A., RUSSO, S. and SIGWALT, P., Comprehensive Polymer Science, Pergamon New York, USA, 1989.

[148] JENKINS, A. D. "Reactivity in Radical Copolymerization," AGGARWAL, S. L. and RUSSO, S., Comprehensive Polymer Science Second Supplement, Pergamon Press, New York, USA, 1996.

[149] FARAGALLA, M. M., HILL, D. J. T. and WHITTAKER, A. K. "The copolymerization of N-vinyl-2-pyrrolidone with 2-hydroxyethyl methacrylate," Polymer Bulletin, vol. 47, pp. 421-427, 2002.

[150] ALISSA, M. A., DAVIS, T. P., HUGLIN, M. B. and YIP, D. C. F. "Copolymerizations involving N-Vinyl-2-Pyrrolidone," Polymer, vol. 26, pp. 1869-1874, 1985.

[151] REDDY, B. S. R., ARSHADY, R. and GEORGE, M. H. "Copolymerization of N-Vinyl-2-Pyrrolidone with 2,4,5-Trichlorophenyl Acrylate and with 2-Hydroxyethyl Methacrylate - Reactivity ratios and molecular-weights," European Polymer Journal, vol. 21, pp. 511-515, 1985.

[152] BAE, Y. H., OKANO, T. and KIM, S. W. "Temperature-Dependence of Swelling of Cross-Linked Poly(N,N'-Alkyl Substituted Acrylamides) in Water," Journal of Polymer Science Part B-Polymer Physics, vol. 28, pp. 923-936, 1990.

[153] BAE, Y. H., OKANO, T. and KIM, S. W. "On-Off Thermocontrol of Solute Transport .2. Solute Release from Thermosensitive Hydrogels," Pharmaceutical Research, vol. 8, pp. 624-628, 1991.

[154] BAE, Y. H., OKANO, T. and KIM, S. W. "On Off Thermocontrol of Solute Transport .1. Temperature-Dependence of Swelling of N-Isopropylacrylamide Networks Modified with Hydrophobic Components in Water," Pharmaceutical Research, vol. 8, pp. 531-537, 1991.

[155] MATSUO, E. S. and TANAKA, T. "Kinetics of Discontinuous Volume Phase-Transition of Gels," J Chem Phys, vol. 89, pp. 1695-1703, 1988.

[156] DONG, L. C. and HOFFMAN, A. S. "Synthesis and Application of Thermally Reversible Heterogels for Drug Delivery," Journal of Controlled Release, vol. 13, pp. 21-31, 1990.

[157] LIM, Y. H., KIM, D. and LEE, D. S. "Drug releasing characteristics of thermo- and PH-sensitive interpenetrating polymer networks based on poly(N-isopropylacrylamide)," Journal of Applied Polymer Science, vol. 64, pp. 2647-2655, 1997.

[158] OKANO, T., BAE, Y. H., JACOBS, H. and KIM, S. W. "Thermally on Off Switching Polymers for Drug Permeation and Release," Journal of Controlled Release, vol. 11, pp. 255-265, 1990.

[159] YOSHIDA, R., SAKAI, K., OKANO, T. and SAKURAI, Y. "A New Model for Zero-Order Drug Release .1. Hydrophobic Drug Release from Hydrophilic Polymeric Matrices," Polymer Journal, vol. 23, pp. 1111-1121, 1991.

[160] RAMKISSOON-GANORKAR, C., LIU, F., BAUDYS, M. and KIM, S. W. "Modulating insulin-release profile from pH thermosensitive polymeric beads through polymer molecular weight," Journal of Controlled Release, vol. 59, pp. 287-298, 1999.

[161] VERNON, B., KIM, S. W. and BAE, Y. H. "Insulin release from islets of Langerhans entrapped in a poly(N-isopropylacrylamide-co-acrylic acid) polymer gel," Journal of Biomaterials Science-Polymer Edition, vol. 10, pp. 183-198, 1999.

[162] SHI, J., LIU, L. H., LIU, X. P., SUN, X. M. and CAO, S. K. "Inorganic-organic hybrid alginate beads with LCST near human body temperature for sustained

dual-sensitive drug delivery," Polymers for Advanced Technologies, vol. 19, pp. 1467-1473, 2008.

[163] LI, B. A., JIANG, Y. M., LIU, Y., WU, Y. T., YU, H. and ZHU, M. F. "Novel Poly(N-isopropylacrylamide)/Clay/Poly(acrylamide) IPN Hydrogels with the Response Rate and Drug Release Controlled by Clay Content," Journal of Polymer Science Part B-Polymer Physics, vol. 47, pp. 96-106, 2009.

[164] SERPE, M. J., YARMEY, K. A., NOLAN, C. M. and LYON, L. A. "Doxorubicin uptake and release from microgel thin films," Biomacromolecules, vol. 6, pp. 408-413, 2005.

[165] TA, T., CONVERTINE, A. J., REYES, C. R., STAYTON, P. S. and PORTER, T. M. "Thermosensitive Liposomes Modified with Poly(N-isopropylacrylamide-co-propylacrylic acid) Copolymers for Triggered Release of Doxorubicin," Biomacromolecules, vol. 11, pp. 1915-1920, 2010.

[166] DING, Z. L., FONG, R. B., LONG, C. J., STAYTON, P. S. and HOFFMAN, A. S. "Size-dependent control of the binding of biotinylated proteins to streptavidin using a polymer shield," Nature, vol. 411, pp. 59-62, 2001.

[167] KAWANO, T., NIIDOME, Y., MORI, T., KATAYAMA, Y. and NIIDOME, T. "PNIPAM Gel-Coated Gold Nanorods, for Targeted Delivery Responding to a Near-Infrared Laser," Bioconjugate Chemistry, vol. 20, pp. 209-212, 2009.

[168] BIKRAM, M., GOBIN, A. M., WHITMIRE, R. E. and WEST, J. L. "Temperature-sensitive hydrogels with SiO2-Au nanoshells for controlled drug delivery," Journal of Controlled Release, vol. 123, pp. 219-227, 2007.

[169] SERSHEN, S. R., WESTCOTT, S. L., HALAS, N. J. and WEST, J. L. "Temperature-sensitive polymer-nanoshell composites for photothermally modulated drug delivery," Journal of Biomedical Materials Research, vol. 51, pp. 293-298, 2000.

[170] OKANO, T., YAMADA, N., SAKAI, H. and SAKURAI, Y. "A Novel Recovery-System for Cultured-Cells Using Plasma-Treated Polystyrene Dishes Grafted with Poly(N-Isopropylacrylamide)," Journal of Biomedical Materials Research, vol. 27, pp. 1243-1251, 1993.

[171] YAMADA, N., OKANO, T., SAKAI, H., KARIKUSA, F., SAWASAKI, Y. and SAKURAI, Y. "Thermoresponsive Polymeric Surfaces - Control of Attachment and Detachment of Cultured-Cells," Makromolekulare Chemie-Rapid Communications, vol. 11, pp. 571-576, 1990.

[172] OKANO, T., KIKUCHI, A., SAKURAI, Y., TAKEI, Y. and OGATA, N. "Temperature-Responsive Poly(N-Isopropylacrylamide) as a Modulator for

Alteration of Hydrophilic Hydrophobic Surface-Properties to Control Activation Inactivation of Platelets," Journal of Controlled Release, vol. 36, pp. 125-133, 1995.

[173] TAKEI, Y. G., AOKI, T., SANUI, K., OGATA, N., SAKURAI, Y. and OKANO, T. "Temperature-Modulated Platelet and Lymphocyte Interactions with Poly(N-Isopropylacrylamide)-Grafted Surfaces," Biomaterials, vol. 16, pp. 667-673, 1995.

[174] UCHIDA, K., SAKAI, K., ITO, E., KWON, O. H., KIKUCHI, A., YAMATO, M. and OKANO, T. "Temperature-dependent modulation of blood platelet movement and morphology on poly(N-isopropylacrylamide)-grafted surfaces," Biomaterials, vol. 21, pp. 923-929, 2000.

[175] YAKUSHIJI, T., SAKAI, K., KIKUCHI, A., AOYAGI, T., SAKURAI, Y. and OKANO, T. "Effects of cross-linked structure on temperature-responsive hydrophobic interaction of poly(N-isopropylacrylamide) hydrogel-modified surfaces with steroids," Analytical Chemistry, vol. 71, pp. 1125-1130, 1999.

[176] KITANO, H., KONDO, T., SUZUKI, H. and OHNO, K. "Temperature-responsive polymer-brush constructed on a glass substrate by atom transfer radical polymerization," Journal of Colloid and Interface Science, vol. 345, pp. 325-331, 2010.

[177] KITANO, H., KAGO, H. and MATSUURA, K. "Temperature-responsive polymer brush constructed on a colloidal gold monolayer," Journal of Colloid and Interface Science, vol. 331, pp. 343-350, 2009.

[178] BRITTAIN, W. J. and MINKO, S. "A structural definition of polymer brushes," Journal of Polymer Science Part a-Polymer Chemistry, vol. 45, pp. 3505-3512, 2007.

[179] LEMIEUX, M. C., PELESHANKO, S., ANDERSON, K. D. and TSUKRUK, V. V. "Adaptive nanomechanical response of stratified polymer brush structures," Langmuir, vol. 23, pp. 265-273, 2007.

[180] WU, K., WU, B., WANG, P., HOU, Y., ZHANG, G. Z. and ZHU, D. M. "Adsorption isotherms and dissipation of adsorbed Poly(N-isopropylacrylamide) in its swelling and collapsed states," Journal of Physical Chemistry B, vol. 111, pp. 8723-8727, 2007.

[181] ZHU, D. M., WU, K., WU, B., WANG, P., FANG, J. J., HOU, Y. and ZHANG, G. Z. "Physisorption of poly(N-isopropylacrylamide) in its swollen and collapsed states: Effects of molecular conformation and substrate interaction," Journal of Physical Chemistry C, vol. 111, pp. 18679-18686, 2007.

[182] FREITAS, R. F. S. and CUSSLER, E. L. "Temperature Sensitive Gels as Extraction Solvents," Chemical Engineering Science, vol. 42, pp. 97-103, 1987.

[183] TAKEI, Y. G., AOKI, T., SANUI, K., OGATA, N., OKANO, T. and SAKURAI, Y. "Temperature-Responsive Bioconjugates .1. Synthesis of Temperature-Responsive Oligomers with Reactive End Groups and Their Coupling to Biomolecules," Bioconjugate Chemistry, vol. 4, pp. 42-46, 1993.

[184] TAKEI, Y. G., AOKI, T., SANUI, K., OGATA, N., OKANO, T. and SAKURAI, Y. "Temperature-Responsive Bioconjugates .2. Molecular Design for Temperature-Modulated Bioseparations," Bioconjugate Chemistry, vol. 4, pp. 341-346, 1993.

[185] TAKEI, Y. G., MATSUKATA, M., AOKI, T., SANUI, K., OGATA, N., KIKUCHI, A., SAKURAI, Y. and OKANO, T. "Temperature-Responsive Bioconjugates .3. Antibody Poly(N-Isopropylacrylamide) Conjugates for Temperature-Modulated Precipitations and Affinity Bioseparations," Bioconjugate Chemistry, vol. 5, pp. 577-582, 1994.

[186] FEIL, H., BAE, Y. H., FEIJEN, J. and KIM, S. W. "Mutual Influence of Ph and Temperature on the Swelling of Ionizable and Thermosensitive Hydrogels," Macromolecules, vol. 25, pp. 5528-5530, 1992.

[187] LI, S. K. and D'EMANUELE, A. "On-off transport through a thermoresponsive hydrogel composite membrane," Journal of Controlled Release, vol. 75, pp. 55-67, 2001.

[188] SHIMIZU, T., YAMOTO, M., KIKUCHI, A. and OKANO, T. "Two-dimensional manipulation of cardiac myocyte sheets utilizing temperature-responsive culture dishes augments the pulsatile amplitude," Tissue Engineering, vol. 7, pp. 141-151, 2001.

[189] YEN, M. H. and LIN, K. F. "Atypical Transition Temperature Dependence of Poly(N-isopropylacrylamide) and Poly(N-isopropylacrylamide-co-acrylamide) Nanocomposites on the Content of Exfoliated Montmorillonites," Journal of Polymer Science Part B-Polymer Physics, vol. 47, pp. 524-530, 2009.

[190] TIAN, B. S. and YANG, C. "Temperature-Responsive Nanocomposites Based on Mesoporous SBA-15 Silica and PNIPAAm: Synthesis and Characterization," Journal of Physical Chemistry C, vol. 113, pp. 4925-4931, 2009.

[191] SUN, S. T., HU, J., TANG, H. and WU, P. Y. "Chain Collapse and Revival Thermodynamics of Poly(N-isopropylacrylamide) Hydrogel," Journal of Physical Chemistry B, vol. 114, pp. 9761-9770, 2010.

[192] VIDYASAGAR, A., SMITH, H. L., MAJEWSKI, J. and TOOMEY, R. G. "Continuous and discontinuous volume-phase transitions in surface-tethered, photo-crosslinked poly(N-isopropylacrylamide) networks," Soft Matter, vol. 5, pp. 4733-4738, 2009.

[193] SUN, B. J., LIN, Y. N., WU, P. Y. and SIESLER, H. W. "A FTIR and 2D-IR spectroscopic study on the microdynamics phase separation mechanism of the poly(N-isopropylacrylamide) aqueous solution," Macromolecules, vol. 41, pp. 1512-1520, 2008.

[194] CHENG, H., SHEN, L. and WU, C. "LLS and FTIR studies on the hysteresis in association and dissociation of poly(N-isopropylacrylamide) chains in water," Macromolecules, vol. 39, pp. 2325-2329, 2006.

[195] SCHMIDT, P., DYBAL, J. and TRCHOVA, M. "Investigations of the hydrophobic and hydrophilic interactions in polymer-water systems by AIR FTIR and Raman spectroscopy," Vibrational Spectroscopy, vol. 42, pp. 278-283, 2006.

[196] MEERSMAN, F., WANG, J., WU, Y. Q. and HEREMANS, K. "Pressure effect on the hydration properties of poly(N-isopropylacrylamide) in aqueous solution studied by FTIR spectroscopy," Macromolecules, vol. 38, pp. 8923-8928, 2005.

[197] MAEDA, Y., HIGUCHI, T. and IKEDA, I. "FTIR spectroscopic and calorimetric studies of the phase transitions of N-isopropylacrylamide copolymers in water," Langmuir, vol. 17, pp. 7535-7539, 2001.

[198] MAEDA, Y., HIGUCHI, T. and IKEDA, I. "Change in hydration state during the coil-globule transition of aqueous solutions of poly(N-isopropylacrylamide) as evidenced by FTIR spectroscopy," Langmuir, vol. 16, pp. 7503-7509, 2000.

[199] AHMED, Z., GOODING, E. A., PIMENOV, K. V., WANG, L. L. and ASHER, S. A. "UV Resonance Raman Determination of Molecular Mechanism of Poly(N-isopropylacrylamide) Volume Phase Transition," Journal of Physical Chemistry B, vol. 113, pp. 4248-4256, 2009.

[200] APPEL, R., XU, W., ZERDA, T. W. and HU, Z. B. "Direct observation of polymer network structure in macroporous N-isopropylacrylamide gel by Raman microscopy," Macromolecules, vol. 31, pp. 5071-5074, 1998.

[201] MAEDA, Y., TSUKIDA, N., KITANO, H., TERADA, T. and YAMANAKA, J. "Raman-Spectroscopic Study of Water in Aqueous Polymer-Solutions," Journal of Physical Chemistry, vol. 97, pp. 13903-13906, 1993.

[202] TERADA, T., MAEDA, Y. and KITANO, H. "Raman-Spectroscopic Study on Water in Polymer Gels," Journal of Physical Chemistry, vol. 97, pp. 3619-3622, 1993.

[203] CHO, E. C., LEE, J. and CHO, K. "Role of bound water and hydrophobic interaction in phase transition of poly(N-isopropylacrylamide) aqueous solution," Macromolecules, vol. 36, pp. 9929-9934, 2003.

[204] AFROZE, F., NIES, E. and BERGHMANS, H. "Phase transitions in the system poly(N-isopropylacrylamide)/water and swelling behaviour of the corresponding networks," Journal of Molecular Structure, vol. 554, pp. 55-68, 2000.

[205] GRINBERG, N. V., DUBOVIK, A. S., GRINBERG, V. Y., KUZNETSOV, D. V., MAKHAEVA, E. E., GROSBERG, A. Y. and TANAKA, T. "Studies of the thermal volume transition of poly(N-isopropylacrylamide) hydrogels by high-sensitivity differential scanning microcalorimetry. 1. Dynamic effects," Macromolecules, vol. 32, pp. 1471-1475, 1999.

[206] OTAKE, K., INOMATA, H., KONNO, M. and SAITO, S. "Thermal-Analysis of the Volume Phase-Transition with N-Isopropylacrylamide Gels," Macromolecules, vol. 23, pp. 283-289, 1990.

[207] WAHRMUND, J., KIM, J. W., CHU, L. Y., WANG, C. J., LI, Y., FERNANDEZ-NIEVES, A., WEITZ, D. A., KROKHIN, A. and HU, Z. B. "Swelling Kinetics of a Microgel Shell," Macromolecules, vol. 42, pp. 9357-9365, 2009.

[208] OKAJIMA, T., HARADA, I., NISHIO, K. and HIROTSU, S. "Kinetics of volume phase transition in poly(N-isopropylacrylamide) gels," J Chem Phys, vol. 116, pp. 9068-9077, 2002.

[209] WANG, J. P., GAN, D. J., LYON, L. A. and EL-SAYED, M. A. "Temperature-jump investigations of the kinetics of hydrogel nanoparticle volume phase transitions," Journal of the American Chemical Society, vol. 123, pp. 11284-11289, 2001.

[210] SHIBAYAMA, M. and NAGAI, K. "Shrinking kinetics of poly(N-isopropylacrylamide) gels T-jumped across their volume phase transition temperatures," Macromolecules, vol. 32, pp. 7461-7468, 1999.

[211] ANDERSSON, M., AXELSSON, A. and ZACCHI, G. "Swelling kinetics of poly(N-isopropylacrylamide) gel," Journal of Controlled Release, vol. 50, pp. 273-281, 1998.

[212] TANAKA, N., MATSUKAWA, S., KUROSU, H. and ANDO, I. "A study on dynamics of water in crosslinked poly(N-isopropylacrylamide) gel by nmr spectroscopy," Polymer, vol. 39, pp. 4703-4706, 1998.

[213] OHTA, H., ANDO, I., FUJISHIGE, S. and KUBOTA, K. "Molecular-Motion and H-1-Nmr Relaxation of Aqueous Poly(N-Isopropylacrylamide) Solution under High-Pressure," Journal of Polymer Science Part B-Polymer Physics, vol. 29, pp. 963-968, 1991.

[214] FERNANDES, P. A. L., SCHMIDT, S., ZEISER, M., FERY, A. and HELLWEG, T. "Swelling and mechanical properties of polymer gels with cross-linking gradient," Soft Matter, vol. 6, pp. 3455-3458, 2010.

[215] TAMAI, Y., TANAKA, H. and NAKANISHI, K. "Molecular dynamics study of water in hydrogels," Molecular Simulation, vol. 16, pp. 359-374, 1996.

[216] TONSING, T. and OLDIGES, C. "Molecular dynamic simulation study on structure of water in crosslinked poly(N-isopropylacrylamide) hydrogels," Physical Chemistry Chemical Physics, vol. 3, pp. 5542-5549, 2001.

[217] LONGHI, G., LEBON, F., ABBATE, S. and FORNILI, S. L. "Molecular dynamics simulation of a model oligomer for poly(N-isopropylamide) in water," Chemical Physics Letters, vol. 386, pp. 123-127, 2004.

[218] GANGEMI, F., LONGHI, G., ABBATE, S., LEBON, F., CORDONE, R., GHILARDI, G. P. and FORNILI, S. L. "Molecular dynamics simulation of aqueous solutions of 26-unit segments of p(NIPAAm) and of p(NIPAAm) "Doped" with amino acid based comonomers," Journal of Physical Chemistry B, vol. 112, pp. 11896-11906, 2008.

[219] MAYO, S. L., OLAFSON, B. D. and GODDARD, W. A. "Dreiding - a generic force-field for molecular simulations," Journal of Physical Chemistry, vol. 94, pp. 8897-8909, 1990.

[220] RAPPE, A. K., CASEWIT, C. J., COLWELL, K. S., GODDARD, W. A. and SKIFF, W. M. "Uff, a Full Periodic-Table Force-Field for Molecular Mechanics and Molecular-Dynamics Simulations," Journal of the American Chemical Society, vol. 114, pp. 10024-10035, 1992.

[221] BROOKS, B. R., BRUCCOLERI, R. E., OLAFSON, B. D., STATES, D. J., SWAMINATHAN, S. and KARPLUS, M. "Charmm - a Program for Macromolecular Energy, Minimization, and Dynamics Calculations," Journal of Computational Chemistry, vol. 4, pp. 187-217, 1983.

[222] WEINER, S. J., KOLLMAN, P. A., CASE, D. A., SINGH, U. C., GHIO, C., ALAGONA, G., PROFETA, S. and WEINER, P. "A New Force-Field for Molecular Mechanical Simulation of Nucleic-Acids and Proteins," Journal of the American Chemical Society, vol. 106, pp. 765-784, 1984.

[223] WEINER, S. J., KOLLMAN, P. A., NGUYEN, D. T. and CASE, D. A. "An All Atom Force-Field for Simulations of Proteins and Nucleic-Acids," Journal of Computational Chemistry, vol. 7, pp. 230-252, 1986.

[224] VERLET, L. "Computer Experiments on Classical Fluids .I. Thermodynamical Properties of Lennard-Jones Molecules," Physical Review, vol. 159, pp. 98-&, 1967.

[225] HOCKNEY, R. W. "The potential calculation and some application," Methods in Computational Physics, vol. 9, pp. 136-211, 1970.

[226] POTTER, D. E. "Computational Physics," John Wiley & Sons, New York, 1973.

[227] SWOPE, W. C., ANDERSEN, H. C., BERENS, P. H. and WILSON, K. R. "A computer-simulation method for the calculation of equilibrium-constants for the formation of physical clusters of molecules - application to small water clusters," J Chem Phys, vol. 76, pp. 637-649, 1982.

[228] DAVIS, T. P. and HUGLIN, M. B. "Some mechanical-properties of Poly(2-Hydroxyethyl Methacrylate) gels swollen in water 1,4-Dioxane mixtures," Makromolekulare Chemie-Rapid Communications, vol. 9, pp. 39-43, 1988.

[229] ALISSA, M. A., DAVIS, T. P., HUGLIN, M. B., REGO, J. M., REHAB, M. M. A. M., YIP, D. C. F. and ZAKARIA, M. B. "Observations on the swelling behavior of copolymeric hydrogels containing N-Vinyl-2-Pyrrolidone," Makromolekulare Chemie-Macromolecular Chemistry and Physics, vol. 191, pp. 321-330, 1990.

[230] LEE, J. H. and BUCKNALL, D. G. "Swelling behavior and network structure of hydrogels synthesized using controlled UV-initiated free radical polymerization," Journal of Polymer Science Part B-Polymer Physics, vol. 46, pp. 1450-1462, 2008.

[231] JANG, S. S. and GODDARD, W. A. "Structures and transport properties of hydrated water-soluble dendrimer-grafted polymer membranes for application to polymer electrolyte membrane fuel cells: Classical molecular dynamics approach," Journal of Physical Chemistry C, vol. 111, pp. 2759-2769, 2007.

[232] JANG, S. S., LIN, S. T., CAGIN, T., MOLINERO, V. and GODDARD, W. A. "Nanophase segregation and water dynamics in the dendrion diblock copolymer formed from the Frechet polyaryl ethereal dendrimer and linear PTFE," Journal of Physical Chemistry B, vol. 109, pp. 10154-10167, 2005.

[233] JANG, S. S., MOLINERO, V., CAGIN, T. and GODDARD, W. A. "Nanophase-segregation and transport in Nafion 117 from molecular dynamics simulations:

Effect of monomeric sequence," Journal of Physical Chemistry B, vol. 108, pp. 3149-3157, 2004.

[234] BRUNELLO, G., LEE, S. G., JANG, S. S. and QI, Y. "A molecular dynamics simulation study of hydrated sulfonated poly (Ether Ether Ketone) for application to polymer electrolyte membrane fuel cells: Effect of water content " Journal of Renewable and Sustainable Energy vol. 1, pp. 033101, 2009.

[235] JANG, S. S., JANG, Y. H., KIM, Y. H., GODDARD, W. A., FLOOD, A. H., LAURSEN, B. W., TSENG, H. R., STODDART, J. F., JEPPESEN, J. O., CHOI, J. W., STEUERMAN, D. W., DEIONNO, E. and HEATH, J. R. "Structures and properties of self-assembled monolayers of bistable [2]rotaxanes on Au(111) surfaces from molecular dynamics simulations validated with experiment," Journal of the American Chemical Society, vol. 127, pp. 1563-1575, 2005.

[236] JANG, Y. H., JANG, S. S. and GODDARD, W. A. "Molecular dynamics simulation study on a monolayer of half [2]rotaxane self-assembled on Au(111)," Journal of the American Chemical Society, vol. 127, pp. 4959-4964, 2005.

[237] JANG, S. S., JANG, Y. H., KIM, Y. H., GODDARD, W. A., CHOI, J. W., HEATH, J. R., LAURSEN, B. W., FLOOD, A. H., STODDART, J. F., NORGAARD, K. and BJORNHOLM, T. "Molecular dynamics simulation of amphiphilic bistable [2]rotaxane Langmuir monolayers at the air/water interface," Journal of the American Chemical Society, vol. 127, pp. 14804-14816, 2005.

[238] LEVITT, M., HIRSHBERG, M., SHARON, R., LAIDIG, K. E. and DAGGETT, V. "Calibration and testing of a water model for simulation of the molecular dynamics of proteins and nucleic acids in solution," Journal of Physical Chemistry B, vol. 101, pp. 5051-5061, 1997.

[239] HOOVER, W. G. "Canonical Dynamics - Equilibrium Phase-Space Distributions," Physical Review A, vol. 31, pp. 1695-1697, 1985.

[240] NOSE, S. "A Unified Formulation of the Constant Temperature Molecular-Dynamics Methods," J Chem Phys, vol. 81, pp. 511-519, 1984.

[241] NOSE, S. "A Molecular-Dynamics Method for Simulations in the Canonical Ensemble," Molecular Physics, vol. 52, pp. 255-268, 1984.

[242] ANDERSEN, H. C. "Molecular-Dynamics Simulations at Constant Pressure and-or Temperature," J Chem Phys, vol. 72, pp. 2384-2393, 1980.

[243] RAPPE, A. K. and GODDARD, W. A. "Charge equilibration for molecular-dynamics simulations," Journal of Physical Chemistry, vol. 95, pp. 3358-3363, 1991.

[244] HOCKNEY, R. W. and EASTWOOD, J. W. "Computer simulation using particles," McGraw-Hill International Book Co., New York, 1981.

[245] PLIMPTON, S. "Fast parallel algorithms for short-range molecular-dynamics," Journal of Computational Physics, vol. 117, pp. 1-19, 1995.

[246] PLIMPTON, S. J., POLLOCK, R. and STEVENS, M., Particle-mesh ewald and rRESPA for parallel molecular dynamics simulations. The Eighth SIAM Conference on Parallel Processing for Scientific Computing, Minneapolis, MN 1997.

[247] SOPER, A. K. "On the determination of the pair correlation-function from liquid structure factor measurements," Chemical Physics, vol. 107, pp. 61-74, 1986.

[248] SOPER, A. K. and PHILLIPS, M. G. "A new determination of the structure of water at 25-degrees-C," Chemical Physics, vol. 107, pp. 47-60, 1986.

[249] GREELEY, B. H., RUSSO, T. V., MAINZ, D. T., FRIESNER, R. A., LANGLOIS, J. M., GODDARD_III, W. A., DONNELLY, R. E. and RINGNALDA, M. N. "New pseudospectral algorithms for electronic-structure calculations - Length scale separation and analytical 2-electron integral corrections," J Chem Phys, vol. 101, pp. 4028-4041, 1994.

[250] MARTEN, B., KIM, K., CORTIS, C., FRIESNER, R. A., MURPHY, R. B., RINGNALDA, M. N., SITKOFF, D. and HONIG, B. "New model for calculation of solvation free energies: Correction of self-consistent reaction field continuum dielectric theory for short-range hydrogen-bonding effects," Journal of Physical Chemistry, vol. 100, pp. 11775-11788, 1996.

[251] TANNOR, D. J., MARTEN, B., MURPHY, R., FRIESNER, R. A., SITKOFF, D., NICHOLLS, A., RINGNALDA, M., GODDARD, W. A. and HONIG, B. "Accurate First Principles Calculation of Molecular Charge-Distributions and Solvation Energies from Ab-Initio Quantum-Mechanics and Continuum Dielectric Theory," Journal of the American Chemical Society, vol. 116, pp. 11875-11882, 1994.

[252] Jaguar. Schrödinger, LLC, New York, 2007.

[253] CRAMER, C. J. "Essentials of Computational Chemistry: Theories and Models," Wiley, West Sussex, UK, 2004.

[254] ZAMANAKOS, G., A Fast and Accurate Analytical Method for the Computation of Solvent Effects in Molecular Simulations. Physics, Vol. Ph.D., California Institute of Technology, Pasadena, CA, 2002.

[255] DITCHFIE.R, HEHRE, W. J. and POPLE, J. A. "Self-Consistent Molecular-Orbital Methods .9. Extended Gaussian-Type Basis for Molecular-Orbital Studies of Organic Molecules," J Chem Phys, vol. 54, pp. 724-&, 1971.

[256] HEHRE, W. J. and POPLE, J. A. "Self-Consistent Molecular-Orbital Methods .13. Extended Gaussian-Type Basis for Boron," J Chem Phys, vol. 56, pp. 4233-&, 1972.

[257] HEHRE, W. J., DITCHFIE.R and POPLE, J. A. "Self-Consistent Molecular-Orbital Methods .12. Further Extensions of Gaussian-Type Basis Sets for Use in Molecular-Orbital Studies of Organic-Molecules," J Chem Phys, vol. 56, pp. 2257-&, 1972.

[258] BINKLEY, J. S. and POPLE, J. A. "Self-Consistent Molecular-Orbital Methods .19. Split-Valence Gaussian-Type Basis Sets for Beryllium," J Chem Phys, vol. 66, pp. 879-880, 1977.

[259] HARIHARA.PC and POPLE, J. A. "Influence of Polarization Functions on Molecular-Orbital Hydrogenation Energies," Theoretica Chimica Acta, vol. 28, pp. 213-222, 1973.

[260] FRANCL, M. M., PIETRO, W. J., HEHRE, W. J., BINKLEY, J. S., GORDON, M. S., DEFREES, D. J. and POPLE, J. A. "Self-Consistent Molecular-Orbital Methods .23. A Polarization-Type Basis Set for 2nd-Row Elements," J Chem Phys, vol. 77, pp. 3654-3665, 1982.

[261] KOCH, W. and HOLTHAUSEN, M. C. "A chemist's guide to density functional theory," Wiley-VCH, Weinheim, Germany, 2001.

[262] STEPHENS, P. J., DEVLIN, F. J., CHABALOWSKI, C. F. and FRISCH, M. J. "Ab-Initio Calculation of Vibrational Absorption and Circular-Dichroism Spectra Using Density-Functional Force-Fields," Journal of Physical Chemistry, vol. 98, pp. 11623-11627, 1994.

[263] REGA, N., COSSI, M. and BARONE, V. "Intrinsic and environmental effects in the structure and magnetic properties of glycine radical in aqueous solution," Journal of the American Chemical Society, vol. 119, pp. 12962-12967, 1997.

[264] BARONE, V., BENCINI, A. and DIMATTEO, A. "Intrinsic and environmental effects in the structure and magnetic properties of organic molecular magnets: Bis(imino)nitroxide," Journal of the American Chemical Society, vol. 119, pp. 10831-10837, 1997.

[265] HORENSTEIN, B. A. "Quantum mechanical analysis of an alpha-carboxylate-substituted oxocarbenium ion. Isotope effects for formation of the sialyl cation

and the origin of an unusually large secondary C-14 isotope effect," Journal of the American Chemical Society, vol. 119, pp. 1101-1107, 1997.

[266] SKLENAK, S., APELOIG, Y. and RAPPOPORT, Z. "Calculated pK(Enol) values for enols of carboxylic acid derivatives HC=C(OH)X (X = OH, NH2, NMe2, OMe, OCHO, F, Cl, Br)," Journal of the American Chemical Society, vol. 120, pp. 10359-10364, 1998.

[267] KALLIES, B. and MITZNER, R. "Structural properties of protonated acyl derivatives as studied by quantum mechanics," Journal of Molecular Structure-Theochem, vol. 428, pp. 267-282, 1998.

[268] NOTARIO, R., ABBOUD, J. L. M., CATIVIELA, C., GARCIA, J. I., HERREROS, M., HOMAN, H., MAYORAL, J. A. and SALVATELLA, L. "Dramatic medium effects on reactivity. The ionization sites of pyrrole and indole carboxylic acids," Journal of the American Chemical Society, vol. 120, pp. 13224-13229, 1998.

[269] ZHAO, Y. and TRUHLAR, D. G. "The M06 suite of density functionals for main group thermochemistry, thermochemical kinetics, noncovalent interactions, excited states, and transition elements: two new functionals and systematic testing of four M06-class functionals and 12 other functionals," Theoretical Chemistry Accounts, vol. 120, pp. 215-241, 2008.

[270] CHECK, C. E. and GILBERT, T. M. "Progressive systematic underestimation of reaction energies by the B3LYP model as the number of C-C bonds increases: Why organic chemists should use multiple DFT models for calculations involving polycarbon hydrocarbons," Journal of Organic Chemistry, vol. 70, pp. 9828-9834, 2005.

[271] GRIMME, S. "Seemingly simple stereoelectronic effects in alkane isomers and the implications for Kohn-Sham density functional theory," Angewandte Chemie-International Edition, vol. 45, pp. 4460-4464, 2006.

[272] WODRICH, M. D., CORMINBOEUF, C. and SCHLEYER, P. V. "Systematic errors in computed alkane energies using B3LYP and other popular DFT functionals," Organic Letters, vol. 8, pp. 3631-3634, 2006.

[273] SCHREINER, P. R., FOKIN, A. A., PASCAL, R. A. and DE MEIJERE, A. "Many density functional theory approaches fail to give reliable large hydrocarbon isomer energy differences," Organic Letters, vol. 8, pp. 3635-3638, 2006.

[274] ZHAO, Y. and TRUHLAR, D. G. "A density functional that accounts for medium-range correlation energies in organic chemistry," Organic Letters, vol. 8, pp. 5753-5755, 2006.

[275] IZGORODINA, E. I., COOTE, M. L. and RADOM, L. "Trends in R-X bond dissociation energies (R = Me, Et, i-Pr, t-Bu; X = H, CH3, OCH3, OH, F): A surprising shortcoming of density functional theory," Journal of Physical Chemistry A, vol. 109, pp. 7558-7566, 2005.

[276] WOODCOCK, H. L., SCHAEFER, H. F. and SCHREINER, P. R. "Problematic energy differences between cumulenes and poly-ynes: Does this point to a systematic improvement of density functional theory?," Journal of Physical Chemistry A, vol. 106, pp. 11923-11931, 2002.

[277] WODRICH, M. D., CORMINBOEUF, C., SCHREINER, P. R., FOKIN, A. A. and SCHLEYER, P. V. "How accurate are DFT treatments of organic energies?," Organic Letters, vol. 9, pp. 1851-1854, 2007.

[278] TSIPIS, A. C., ORPEN, A. G. and HARVEY, J. N. "Substituent effects and the mechanism of alkene metathesis catalyzed by ruthenium dichloride catalysts," Dalton Transactions, pp. 2849-2858, 2005.

[279] ZHAO, Y. and TRUHLAR, D. G. "Attractive noncovalent interactions in the mechanism of Grubbs second-generation Ru catalysts for olefin metathesis," Organic Letters, vol. 9, pp. 1967-1970, 2007.

[280] REIHER, M., SALOMON, O. and HESS, B. A. "Reparameterization of hybrid functionals based on energy differences of states of different multiplicity," Theoretical Chemistry Accounts, vol. 107, pp. 48-55, 2001.

[281] SCHULTZ, N. E., ZHAO, Y. and TRUHLAR, D. G. "Databases for transition element bonding: Metal-metal bond energies and bond lengths and their use to test hybrid, hybrid meta, and meta density functionals and generalized gradient approximations," Journal of Physical Chemistry A, vol. 109, pp. 4388-4403, 2005.

[282] SCHULTZ, N. E., ZHAO, Y. and TRUHLAR, D. G. "Density functionals for inorganometallic and organometallic chemistry," Journal of Physical Chemistry A, vol. 109, pp. 11127-11143, 2005.

[283] HARVEY, J. N. "On the accuracy of density functional theory in transition metal chemistry," Annual Reports Section C: Physical Chemistry, vol. 102, pp. 203-226, 2006.

[284] ZHAO, Y. and TRUHLAR, D. G. "Density functionals with broad applicability in chemistry," Accounts of Chemical Research, vol. 41, pp. 157-167, 2008.

[285] TOMASI, J. and PERSICO, M. "Molecular-interactions in solution - An overview of methods based on continuous distributions of the solvent," Chemical Reviews, vol. 94, pp. 2027-2094, 1994.

[286] CRAMER, C. J. and TRUHLAR, D. G. "Implicit solvation models: Equilibria, structure, spectra, and dynamics," Chemical Reviews, vol. 99, pp. 2161-2200, 1999.

[287] SPERLING, L. H. "Introduction to physical polymer science," Wiley Interscience, Hoboken, NJ, 2006.

[288] BROSTOW, W. and KUBAT, J. "Molecular-Dynamics Simulation of Stress-Relaxation on a Triangular Lattice," Phys Rev B, vol. 47, pp. 7659-7667, 1993.

[289] Cerius2 modeling environment, v. 4.10. Accelrys Inc., San Diego, CA, 2005.

[290] LEE, S. G., BRUNELLO, G. F., JANG, S. S. and BUCKNALL, D. G. "Molecular dynamics simulation study of P (VP-co-HEMA) hydrogels: Effect of water content on equilibrium structures and mechanical properties," Biomaterials, vol. 30, pp. 6130-6141, 2009.

[291] LEE, S. G., BRUNELLO, G. F., JANG, S. S., LEE, J. H. and BUCKNALL, D. G. "Effect of monomeric sequence on mechanical properties of P(VP-co-HEMA) hydrogels at low hydration," Journal of Physical Chemistry B, vol. 113, pp. 6604-6612, 2009.

[292] TAKACSNOVAK, K. and AVDEEF, A. "Interlaboratory study of log P determination by shake-flask and potentiometric methods," Journal of Pharmaceutical and Biomedical Analysis, vol. 14, pp. 1405-1413, 1996.

[293] SANGSTER, J., LOGKOW Databank. Sangster Research Laboratories, 1994.

[294] KOU, J. H., AMIDON, G. L. and LEE, P. I. "Ph-Dependent Swelling and Solute Diffusion Characteristics of Poly(Hydroxyethyl Methacrylate-Co-Methacrylic Acid) Hydrogels," Pharmaceutical Research, vol. 5, pp. 592-597, 1988.

[295] CHOU, L. Y., BLANCH, H. W., PRAUSNITZ, J. M. and SIEGEL, R. A. "Buffer Effects on Aqueous Swelling Kinetics of Polyelectrolyte Gels," Journal of Applied Polymer Science, vol. 45, pp. 1411-1423, 1992.

[296] HARIHARAN, D. and PEPPAS, N. A. "Swelling of Ionic and Neutral Polymer Networks in Ionic-Solutions," Journal of Membrane Science, vol. 78, pp. 1-12, 1993.

[297] OGAWA, I., YAMANO, H. and MIYAGAWA, K. "Swelling of Hydrophilic Polymers .3.," Journal of Applied Polymer Science, vol. 54, pp. 1971-1975, 1994.

[298] KHARE, A. R. and PEPPAS, N. A. "Swelling Deswelling of Anionic Copolymer Gels," Biomaterials, vol. 16, pp. 559-567, 1995.

[299] PEPPAS, N. A. and WRIGHT, S. L. "Solute diffusion in poly(vinyl alcohol) poly(acrylic acid) interpenetrating networks," Macromolecules, vol. 29, pp. 8798-8804, 1996.

[300] RUSSELL, R. J., AXEL, A. C., SHIELDS, K. L. and PISHKO, M. V. "Mass transfer in rapidly photopolymerized poly(ethylene glycol) hydrogels used for chemical sensing," Polymer, vol. 42, pp. 4893-4901, 2001.

[301] GUDEMAN, L. F. and PEPPAS, N. A. "Ph-Sensitive Membranes from Poly(Vinyl Alcohol) Poly(Acrylic Acid) Interpenetrating Networks," Journal of Membrane Science, vol. 107, pp. 239-248, 1995.

[302] PEPPAS, N. A. and WRIGHT, S. L. "Drug diffusion and binding in ionizable interpenetrating networks from poly(vinyl alcohol) and poly(acrylic acid)," European Journal of Pharmaceutics and Biopharmaceutics, vol. 46, pp. 15-29, 1998.

[303] SAXTON, M. J. "Anomalous subdiffusion in fluorescence photobleaching recovery: A Monte Carlo study," Biophysical Journal, vol. 81, pp. 2226-2240, 2001.

[304] WEISS, M., ELSNER, M., KARTBERG, F. and NILSSON, T. "Anomalous subdiffusion is a measure for cytoplasmic crowding in living cells," Biophysical Journal, vol. 87, pp. 3518-3524, 2004.

[305] SCHUTZ, G. J., SCHINDLER, H. and SCHMIDT, T. "Single-molecule microscopy on model membranes reveals anomalous diffusion," Biophysical Journal, vol. 73, pp. 1073-1080, 1997.

[306] WEISS, M., HASHIMOTO, H. and NILSSON, T. "Anomalous protein diffusion in living cells as seen by fluorescence correlation spectroscopy," Biophysical Journal, vol. 84, pp. 4043-4052, 2003.

[307] AZURMENDI, H. F. and RAMIA, M. E. "Anomalous diffusion of water in a hydrogel of sucrose and diepoxide monomers," J Chem Phys, vol. 114, pp. 9657-9662, 2001.

[308] DRAZER, G. and ZANETTE, D. H. "Experimental evidence of power-law trapping-time distributions in porous media," Physical Review E, vol. 60, pp. 5858-5864, 1999.

[309] GHOSH, R. N. and WEBB, W. W. "Automated Detection and Tracking of Individual and Clustered Cell-Surface Low-Density-Lipoprotein Receptor Molecules," Biophysical Journal, vol. 66, pp. 1301-1318, 1994.

[310] SCHWILLE, P., HAUPTS, U., MAITI, S. and WEBB, W. W. "Molecular dynamics in living cells observed by fluorescence correlation spectroscopy with one- and two-photon excitation," Biophysical Journal, vol. 77, pp. 2251-2265, 1999.

[311] SCHWILLE, P., KORLACH, J. and WEBB, W. W. "Fluorescence correlation spectroscopy with single-molecule sensitivity on cell and model membranes," Cytometry, vol. 36, pp. 176-182, 1999.

[312] GALLO, P. and ROVERE, M. "Anomalous dynamics of confined water at low hydration," Journal of Physics-Condensed Matter, vol. 15, pp. 7625-7633, 2003.

[313] ROBINSON, D., ANDERSON, J. E. and LIN, J. L. "Measurement of Diffusion-Coefficients of Some Indoles and Ascorbic-Acid by Flow-Injection Analysis," Journal of Physical Chemistry, vol. 94, pp. 1003-1005, 1990.

[314] "CRC handbook of chemistry and physics " LIDE, D. R., CRC Press, Boca Raton, FL, 2005.

[315] GLADDEN, J. K. and DOLE, M. "Diffusion in Supersaturated Solutions .2. Glucose Solutions," Journal of the American Chemical Society, vol. 75, pp. 3900-3904, 1953.

[316] RIBEIRO, A. C. F., ORTONA, O., SIMOES, S. M. N., SANTOS, C. I. A. V., PRAZERES, P. M. R. A., VALENTE, A. J. M., LOBO, V. M. M. and BURROWS, H. D. "Binary mutual diffusion coefficients of aqueous solutions of sucrose, lactose, glucose, and fructose in the temperature range from (298.15 to 328.15) K," Journal of Chemical and Engineering Data, vol. 51, pp. 1836-1840, 2006.

[317] MYUNG, D., KOH, W., KO, J., NOOLANDI, J., CARRASCO, M., SMITHC, A., FRANK, C. and TA, C. "Characterization of poly(ethylene glycol)-poly(acrylic acid) (PEG-PAA) double networks designed for corneal implant applications," Investigative Ophthalmology & Visual Science, vol. 46, pp. -, 2005.

[318] GIOVAMBATTISTA, N., DEBENEDETTI, P. G. and ROSSKY, P. J. "Hydration behavior under confinement by nanoscale surfaces with patterned hydrophobicity and hydrophilicity," Journal of Physical Chemistry C, vol. 111, pp. 1323-1332, 2007.

[319] BELLISSENTFUNEL, M. C., SRIDIDORBEZ, R. and BOSIO, L. "X-ray and neutron scattering studies of the structure of water at a hydrophobic surface," J Chem Phys, vol. 104, pp. 10023-10029, 1996.

[320] STUART, M. A. C., HUCK, W. T. S., GENZER, J., MULLER, M., OBER, C., STAMM, M., SUKHORUKOV, G. B., SZLEIFER, I., TSUKRUK, V. V., URBAN, M., WINNIK, F., ZAUSCHER, S., LUZINOV, I. and MINKO, S. "Emerging applications of stimuli-responsive polymer materials," Nat Mater, vol. 9, pp. 101-113, 2010.

[321] LUZINOV, I., MINKO, S. and TSUKRUK, V. V. "Responsive brush layers: from tailored gradients to reversibly assembled nanoparticles," Soft Matter, vol. 4, pp. 714-725, 2008.

[322] YOSHIDA, R., UCHIDA, K., KANEKO, Y., SAKAI, K., KIKUCHI, A., SAKURAI, Y. and OKANO, T. "Comb-Type Grafted Hydrogels with Rapid De-Swelling Response to Temperature-Changes," Nature, vol. 374, pp. 240-242, 1995.

[323] KANAZAWA, H., YAMAMOTO, K., MATSUSHIMA, Y., TAKAI, N., KIKUCHI, A., SAKURAI, Y. and OKANO, T. "Temperature-responsive chromatography using poly(N-isopropylacrylamide)-modified silica," Analytical Chemistry, vol. 68, pp. 100-105, 1996.

[324] VIDYASAGAR, A., MAJEWSKI, J. and TOOMEY, R. "Temperature induced volume-phase transitions in surface-tethered Poly(N-isopropylacrylamide) networks," Macromolecules, vol. 41, pp. 919-924, 2008.

[325] GEWEHR, M., NAKAMURA, K., ISE, N. and KITANO, H. "Gel-Permeation Chromatography Using Porous-Glass Beads Modified with Temperature-Responsive Polymers," Makromolekulare Chemie-Macromolecular Chemistry and Physics, vol. 193, pp. 249-256, 1992.

[326] HOSOYA, K., SAWADA, E., KIMATA, K., ARAKI, T., TANAKA, N. and FRECHET, J. M. J. "In-Situ Surface-Selective Modification of Uniform Size Macroporous Polymer Particles with Temperature-Responsive Poly-N-Isopropylacrylamide," Macromolecules, vol. 27, pp. 3973-3976, 1994.

[327] KOBAYASHI, J., KIKUCHI, A., SAKAI, K. and OKANO, T. "Aqueous chromatography utilizing pH-/temperature responsive polymer stationary phases to separate ionic bioactive compounds," Analytical Chemistry, vol. 73, pp. 2027-2033, 2001.

[328] PARK, Y. S., ITO, Y. and IMANISHI, Y. "Permeation control through porous membranes immobilized with thermosensitive polymer," Langmuir, vol. 14, pp. 910-914, 1998.

[329] RAO, G. V. R., KRUG, M. E., BALAMURUGAN, S., XU, H. F., XU, Q. and LOPEZ, G. P. "Synthesis and characterization of silica-poly(N-isopropylacrylamide) hybrid membranes: Switchable molecular filters," Chemistry of Materials, vol. 14, pp. 5075-5080, 2002.

[330] YOSHIOKA, H., MIKAMI, M., NAKAI, T. and MORI, Y. "Preparation of Poly(N-Isopropylacrylamide)-Grafted Silica-Gel and Its Temperature-Dependent Interaction with Proteins," Polymers for Advanced Technologies, vol. 6, pp. 418-420, 1995.

[331] CHEN, J. H., YOSHIDA, M., MAEKAWA, Y. and TSUBOKAWA, N. "Temperature-switchable vapor sensor materials based on N-isopropylacrylamide and calcium chloride," Polymer, vol. 42, pp. 9361-9365, 2001.

[332] ABU-LAIL, N. I., KAHOLEK, M., LAMATTINA, B., CLARK, R. L. and ZAUSCHER, S. "Micro-cantilevers with end-grafted stimulus-responsive polymer brushes for actuation and sensing," Sensors and Actuators B-Chemical, vol. 114, pp. 371-378, 2006.

[333] VOIT, B., SCHMALJOHANN, D., GRAMM, S., NITSCHKE, M. and WERNER, C. "Stimuli-responsive polymer layers for advanced cell culture technologies," International Journal of Materials Research, vol. 98, pp. 646-650, 2007.

[334] YAMATO, M., KONNO, C., UTSUMI, M., KIKUCHI, A. and OKANO, T. "Thermally responsive polymer-grafted surfaces facilitate patterned cell seeding and co-culture," Biomaterials, vol. 23, pp. 561-567, 2002.

[335] OKANO, T., YAMADA, N., OKUHARA, M., SAKAI, H. and SAKURAI, Y. "Mechanism of Cell Detachment from Temperature-Modulated, Hydrophilic-Hydrophobic Polymer Surfaces," Biomaterials, vol. 16, pp. 297-303, 1995.

[336] CUNLIFFE, D., ALARCON, C. D., PETERS, V., SMITH, J. R. and ALEXANDER, C. "Thermoresponsive surface-grafted poly(N-isopropylacrylamide) copolymers: Effect of phase transitions on protein and bacterial attachment," Langmuir, vol. 19, pp. 2888-2899, 2003.

[337] AKIYAMA, Y., KIKUCHI, A., YAMATO, M. and OKANO, T. "Ultrathin poly(N-isopropylacrylamide) grafted layer on polystyrene surfaces for cell adhesion/detachment control," Langmuir, vol. 20, pp. 5506-5511, 2004.

[338] YAMATO, M., KONNO, C., KUSHIDA, A., HIROSE, M., UTSUMI, M., KIKUCHI, A. and OKANO, T. "Release of adsorbed fibronectin from temperature-responsive culture surfaces requires cellular activity," Biomaterials, vol. 21, pp. 981-986, 2000.

[339] ISTA, L. K., PEREZ-LUNA, V. H. and LOPEZ, G. P. "Surface-grafted, environmentally sensitive polymers for biofilm release," Applied and Environmental Microbiology, vol. 65, pp. 1603-1609, 1999.

[340] VON RECUM, H., OKANO, T. and KIM, S. W. "Growth factor release from thermally reversible tissue culture substrates," Journal of Controlled Release, vol. 55, pp. 121-130, 1998.

[341] DURACHER, D., ELAISSARI, A., MALLET, F. and PICHOT, C. "Adsorption of modified HIV-1 capsid p24 protein onto thermosensitive and cationic core-shell poly(styrene)-poly(N-isopropylacrylamide) particles," Langmuir, vol. 16, pp. 9002-9008, 2000.

[342] TANIGUCHI, T., DURACHER, D., DELAIR, T., ELAISSARI, A. and PICHOT, C. "Adsorption/desorption behavior and covalent grafting of an antibody onto cationic amino-functionalized poly(styrene-N-isopropylacrylamide) core-shell latex particles," Colloids and Surfaces B-Biointerfaces, vol. 29, pp. 53-65, 2003.

[343] IONOV, L., STAMM, M. and DIEZ, S. "Reversible switching of microtubule motility using thermoresponsive polymer surfaces," Nano Letters, vol. 6, pp. 1982-1987, 2006.

[344] HUBER, D. L., MANGINELL, R. P., SAMARA, M. A., KIM, B. I. and BUNKER, B. C. "Programmed adsorption and release of proteins in a microfluidic device," Science, vol. 301, pp. 352-354, 2003.

[345] NATH, N. and CHILKOTI, A. "Creating "Smart" surfaces using stimuli responsive polymers," Advanced Materials, vol. 14, pp. 1243-+, 2002.

[346] ZHU, P. W. and NAPPER, D. H. "The longer time collapse kinetics of interfacial poly(N-isopropylacrylamide) in water," J Chem Phys, vol. 106, pp. 6492-6498, 1997.

[347] ZHU, P. W. and NAPPER, D. H. "Interfacial coil-to-globule transitions: The effects of molecular weight," Colloids and Surfaces a-Physicochemical and Engineering Aspects, vol. 113, pp. 145-153, 1996.

[348] WALLDAL, C. and WALL, S. "Coil-to-globule-type transition of poly(N-isopropylacrylamide) adsorbed on colloidal silica particles," Colloid and Polymer Science, vol. 278, pp. 936-945, 2000.

[349] BALAMURUGAN, S., MENDEZ, S., BALAMURUGAN, S. S., O'BRIEN, M. J. and LOPEZ, G. P. "Thermal response of poly(N-isopropylacrylamide) brushes probed by surface plasmon resonance," Langmuir, vol. 19, pp. 2545-2549, 2003.

[350] YIM, H., KENT, M. S., HUBER, D. L., SATIJA, S., MAJEWSKI, J. and SMITH, G. S. "Conformation of end-tethered PNIPAM chains in water and in acetone by neutron reflectivity," Macromolecules, vol. 36, pp. 5244-5251, 2003.

[351] YIM, H., KENT, M. S., MENDEZ, S., BALAMURUGAN, S. S., BALAMURUGAN, S., LOPEZ, G. P. and SATIJA, S. "Temperature-dependent conformational change of PNIPAM grafted chains at high surface density in water," Macromolecules, vol. 37, pp. 1994-1997, 2004.

[352] YIM, H., KENT, M. S., MENDEZ, S., LOPEZ, G. P., SATIJA, S. and SEO, Y. "Effects of grafting density and molecular weight on the temperature-dependent conformational change of poly(N-isopropylacrylamide) grafted chains in water," Macromolecules, vol. 39, pp. 3420-3426, 2006.

[353] YIM, H., KENT, M. S., SATIJA, S., MENDEZ, S., BALAMURUGAN, S. S., BALAMURUGAN, S. and LOPEZ, C. P. "Study of the conformational change of poly(N-isopropylacrylamide)-grafted chains in water with neutron reflection: Molecular weight dependence at high grafting density," Journal of Polymer Science Part B-Polymer Physics, vol. 42, pp. 3302-3310, 2004.

[354] YIM, H., KENT, M. S., SATIJA, S., MENDEZ, S., BALAMURUGAN, S. S., BALAMURUGAN, S. and LOPEZ, G. P. "Evidence for vertical phase separation in densely grafted, high-molecular-weight poly(N-isopropylacrylamide) brushes in water," Physical Review E, vol. 72, pp. -, 2005.

[355] ZHANG, G. Z. "Study on conformation change of thermally sensitive linear grafted poly(N-isopropylacrylamide) chains by quartz crystal microbalance," Macromolecules, vol. 37, pp. 6553-6557, 2004.

[356] LIU, G. M. and ZHANG, G. Z. "Collapse and swelling of thermally sensitive Poly(N-isopropylacrylamide) brushes monitored with a quartz crystal microbalance," Journal of Physical Chemistry B, vol. 109, pp. 743-747, 2005.

[357] LIU, G. M., CHENG, H., YAN, L. F. and ZHANG, G. Z. "Study of the kinetics of the pancake-to-brush transition of poly(N-isopropylacrylamide) chains," Journal of Physical Chemistry B, vol. 109, pp. 22603-22607, 2005.

[358] ANNAKA, M., YAHIRO, C., NAGASE, K., KIKUCHI, A. and OKANO, T. "Real-time observation of coil-to-globule transition in thermosensitive poly (N-isopropylacrylamide) brushes by quartz crystal microbalance," Polymer, vol. 48, pp. 5713-5720, 2007.

[359] PLUNKETT, M. A., WANG, Z. H., RUTLAND, M. W. and JOHANNSMANN, D. "Adsorption of pNIPAM layers on hydrophobic gold surfaces, measured in situ by QCM and SPR," Langmuir, vol. 19, pp. 6837-6844, 2003.

[360] ISHIDA, N. and BIGGS, S. "Effect of Grafting Density on Phase Transition Behavior for Poly(N-isopropylacryamide) Brushes in Aqueous Solutions Studied by AFM and QCM-D," Macromolecules, vol. 43, pp. 7269-7276, 2010.

[361] KIDOAKI, S., OHYA, S., NAKAYAMA, Y. and MATSUDA, T. "Thermoresponsive structural change of a poly(N-isopropylacrylamide) graft layer measured with an atomic force microscope," Langmuir, vol. 17, pp. 2402-2407, 2001.

[362] ISHIDA, N. and KOBAYASHI, M. "Interaction forces measured between poly(N-isopropylacrylamide) grafted surface and hydrophobic particle," Journal of Colloid and Interface Science, vol. 297, pp. 513-519, 2006.

[363] JONES, D. M., SMITH, J. R., HUCK, W. T. S. and ALEXANDER, C. "Variable adhesion of micropatterned thermoresponsive polymer brushes: AFM investigations of poly (N-isopropylacrylamide) brushes prepared by surface-initiated polymerizations," Advanced Materials, vol. 14, pp. 1130-1134, 2002.

[364] PLUNKETT, K. N., ZHU, X., MOORE, J. S. and LECKBAND, D. E. "PNIPAM chain collapse depends on the molecular weight and grafting density," Langmuir, vol. 22, pp. 4259-4266, 2006.

[365] ZHU, X., YAN, C., WINNIK, F. M. and LECKBAND, D. "End-grafted low-molecular-weight PNIPAM does not collapse above the LCST," Langmuir, vol. 23, pp. 162-169, 2007.

[366] MALHAM, I. B. and BUREAU, L. "Density Effects on Collapse, Compression, and Adhesion of Thermoresponsive Polymer Brushes," Langmuir, vol. 26, pp. 4762-4768, 2010.

[367] TAKEI, Y. G., AOKI, T., SANUI, K., OGATA, N., SAKURAI, Y. and OKANO, T. "Dynamic Contact-Angle Measurement of Temperature-Responsive Surface-Properties for Poly(N-Isopropylacrylamide) Grafted Surfaces," Macromolecules, vol. 27, pp. 6163-6166, 1994.

[368] YAKUSHIJI, T., SAKAI, K., KIKUCHI, A., AOYAGI, T., SAKURAI, Y. and OKANO, T. "Graft architectural effects on thermoresponsive wettability changes of poly(N-isopropylacrylamide)-Modified surfaces," Langmuir, vol. 14, pp. 4657-4662, 1998.

[369] FOMENKO, A., POSPISIL, H., SEDLAKOVA, Z., PLESTIL, J. and ILAVSKY, M. "Phase transition in swollen gels - Part 32. Temperature transition in charged poly(N-isopropylmethacrylamide) hydrogels in water and aqueous NaCl solutions," Physical Chemistry Chemical Physics, vol. 4, pp. 4360-4367, 2002.

[370] SILBERBERG, A., ELIASSAF, J. and KATCHALSKY, A. "Temperature-Dependence of Light Scattering and Intrinsic Viscosity of Hydrogen Bonding Polymers," Journal of Polymer Science, vol. 23, pp. 259-284, 1957.

[371] LUZAR, A. and CHANDLER, D. "Structure and Hydrogen-Bond Dynamics of Water-Dimethyl Sulfoxide Mixtures by Computer-Simulations," J Chem Phys, vol. 98, pp. 8160-8173, 1993.